25X1

C009φ1

(Unclassified Title)

INTERIM REPORT
IMAGE ANALYSIS STUDY

TO-B 67-1

January 1967

25X1

25X1

NOTICE

This document contains proprietary information of [ ] reserves all its rights thereto. It is sub-mitted in confidence solely for study and evaluation. Any application of any of the information herein contained, or reproduction of this document, except with prior written permission of [ ] is prohibited.

25X1

25X1

25X1

25X1

This Document Consists of _2256_ Pages.

Copy No. ____2__ of __6__ Copies.

(Unclassified Title)

INTERIM REPORT
IMAGE ANALYSIS STUDY

TO-B 67-1

January 1967

25X1

This document contains information affecting the national defense of the United States within the meaning of the Espionage Laws, Title 18, U.S.C., sections 793 and 794. Its transmission or the revelation of its contents in any manner to an unauthorized person is prohibited by law.

25X1

SECRET

ABSTRACT

In this semiannual report on Image Evaluation, we present a summary of the principal experimental and theoretical work performed by the three contractors* in the interim July-December 1966. Overall goals of this program are to investigate existing image quality theory, to derive new and superior image quality methods, and in so doing to address ourselves to both short-term and long-term problems of the Sponsor's task.

This report will show that a successful start on our program in the following four main fields has been accomplished and, already, new results that will serve to guide our future studies have appeared.

1. Preparation of Controlled Experimental Model Emulsion Films

   Experimental emulsions of known grain size distribution (GSD) and thickness have been made by [   ] The relationship between undeveloped and developed GSD is under study as a function of emulsion parameters and developers. This will lead to a study of the relationship between emulsion parameters, developed silver, and existing image quality criteria. These emulsions will serve for experimental tests of existing and new image quality parameters, at [   ] and also by the subcontractors.

2. Study of the Limits of Imaging Systems

   [   ] has also carried out theoretical and experimental studies of imaging with partially coherent light. The intensity distribution in the image of a variety of test targets has been determined theoretically, and these results have been compared to the appropriate experimental measurements. This comparison has shown both the necessity for and the validity of the use of the nonlinear theory.

   The effects of coherence in microdensitometry have also been studied. The assumptions of incoherently illuminated preslit and incoherent illumination of the sample have been investigated and found not to be valid. The operation of the microdensitometer without these assumptions is being modeled.

3. Evaluation of Existing Linear Analysis (MTF) Theory

   [   ] has concerned itself with a careful experimental analysis of existing linear analysis theory. By the imposition of sine-wave targets of known contrast, on films of interest to the Sponsor, and by careful microdensitometric analysis of the developed images, they have established some limits on the validity of existing MTF theory. This work may serve as a basis for the establishment of a new, more sophisticated and experimentally valid nonlinear image quality theory.

4. Establishment of a Theory of Image Formation in Film

   [   ] has started the study of an image theory of film that searches for valid linear relationships between measurable image quality parameters. A relationship of this type between GSD and density is presently under study, and experimental tests are being done on the model emulsion prepared under [   ] Item 1.

In conclusion, the program represents an integrated pragmatic approach to the problem in which the basic preliminary experimental and theoretical studies have been well initiated in this first semiannual reporting period.

25X1

25X1

25X1

25X1

25X1

25X1

25X1

ii

SECRET

TABLE OF CONTENTS

LIST OF ILLUSTRATIONS

25X1

LIST OF ILLUSTRATIONS (Cont'd.)

25X1

v   25X1

LIST OF ILLUSTRATIONS (Cont'd.)

LIST OF TABLES

SECRET

25X1

TABLE OF CONTENTS (Cont'd.)

LIST OF ILLUSTRATIONS

SECRET

LIST OF ILLUSTRATIONS (Cont'd.)

SECRET

25X1

TABLE OF CONTENTS (Cont'd.)

Page Denied

25X1

CHAPTER 1

CHEMISTRY

25X1

25X1

Page Denied

25X1

CHAPTER 1

CHEMISTRY

TASKS 2B AND 5

MODEL EMULSIONS

Commercial film coatings not being suitable for most aspects of this program necessitated our preparing emulsions that were designed to meet the following requirements:

1. A wide range of coating thicknesses not accommodated in commercial films

2. A well-defined grain shape which is the same for all of the grains so that one parameter defines all grain shapes

3. Monodispersity of grains (Originally, this was considered to be important in order to simplify the theory which was going to be tested by these systems. Recently, however, the grain size distribution has been accommodated in the theory with no problems and so this condition has become less important.)

4. A mean grain size at least 3μ or, preferably, larger for those studies where optical microscopy is the sole means of observation or where the microdensitometric measurements are more difficult to interpret at very small slit widths (in granularity studies), and if any granularity is to be recorded at large slit widths, it must be a large grained emulsion under study.

The work for this period, therefore, includes emulsion preparation, a coating study and the design of a small coater that will meet these requirements, processing procedures, and grain studies. During this time we have also obtained data on existing films of interest and performed electron microscopic experimentation.

1-1   25X1

Page Denied

Next 4 Page(s) In Document Denied

25X1
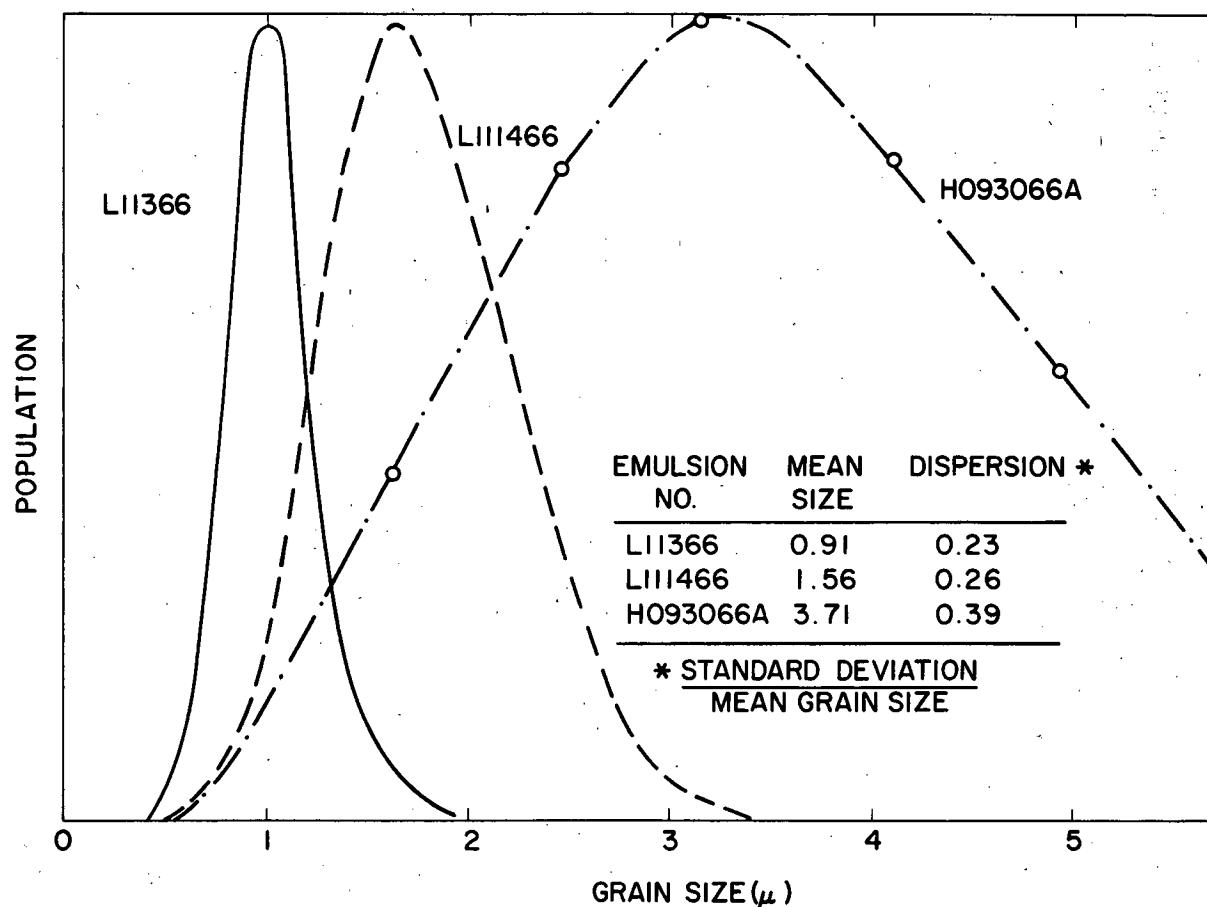
Figure 1. Grain Size Distributions of Emulsions of Interest
(Distributions have been normalized to give same peak height.)

The chart shows POPULATION vs GRAIN SIZE (μ), with curves labeled L11366, L111466, and H093066A.

EMULSION NO.	MEAN SIZE	DISPERSION *
L11366	0.91	0.23
L111466	1.56	0.26
H093066A	3.71	0.39

$$* \frac{\text{STANDARD DEVIATION}}{\text{MEAN GRAIN SIZE}}$$

Coating Studies

It is well known that one of the important parameters affecting image quality
is the thickness and silver coverage of a particular emulsion. The two major re-
quirements of coating for this program, therefore, are that (1) emulsion thick-
nesses (and silver content) be produced in a controlled manner, and (2) the coatings
be even. The several coating facilities available do not fulfill either one of these
requirements. Three coaters at   ranging from the large pilot plant type 25X1
to the small laboratory-scale type, have coating heads of the same general principle
and come under the heading of trought or kiss coaters. In both of these systems,
the film base is in contact with an excess of emulsion, and the amount of pick-up
depends almost entirely on the viscosity of the emulsion. Since this relationship

1-7   25X1
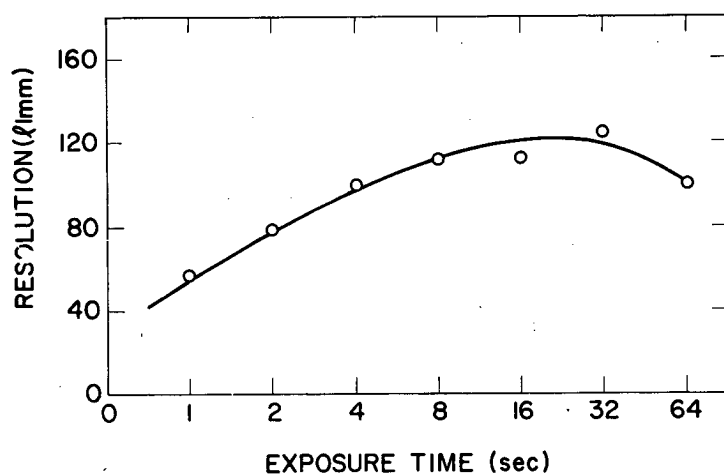
SECRET
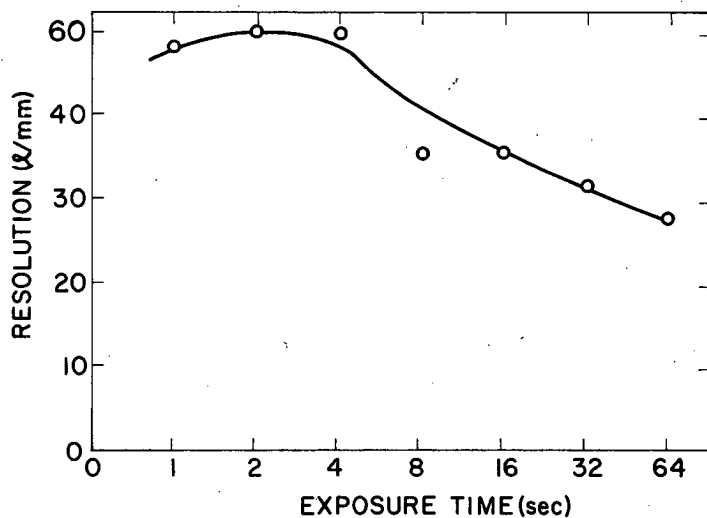
(a) Emulsion L11366
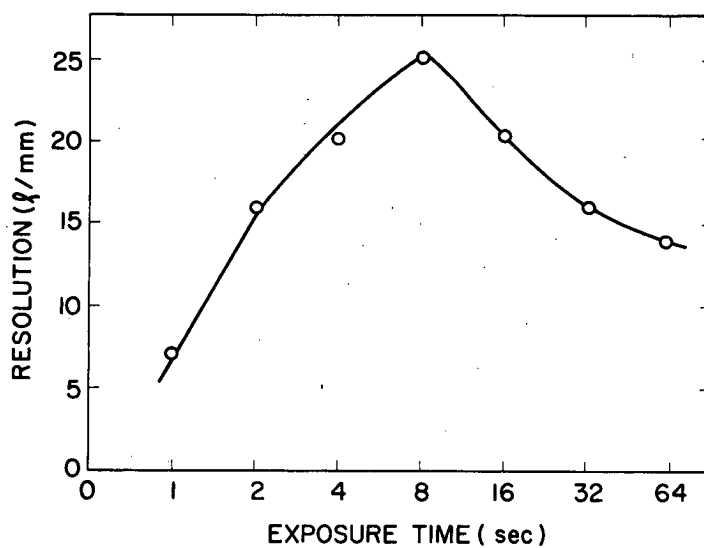
(b) Emulsion 111466

(c) Emulsion H093066A

Figure 2. Resolution of Emulsions L11366, L11466, and
H093066A as a Function of Exposure

1-8
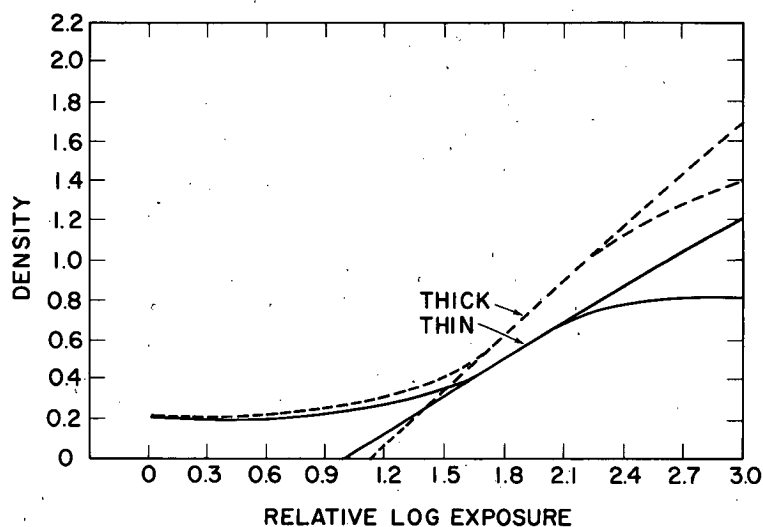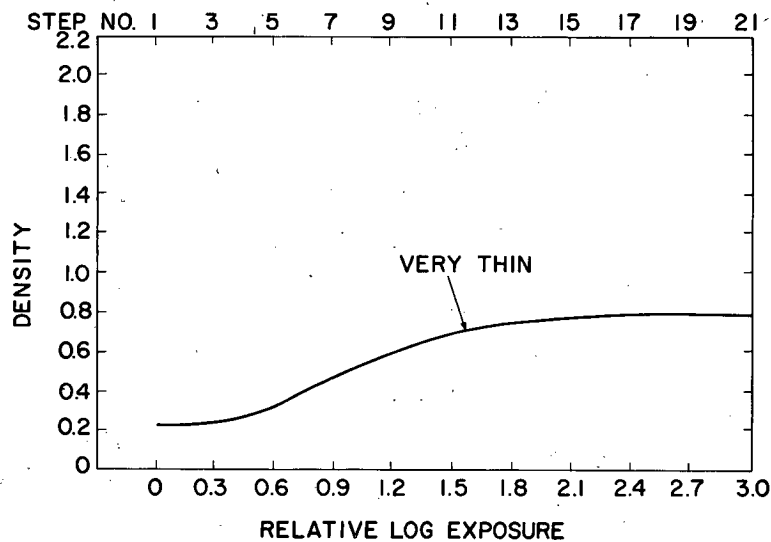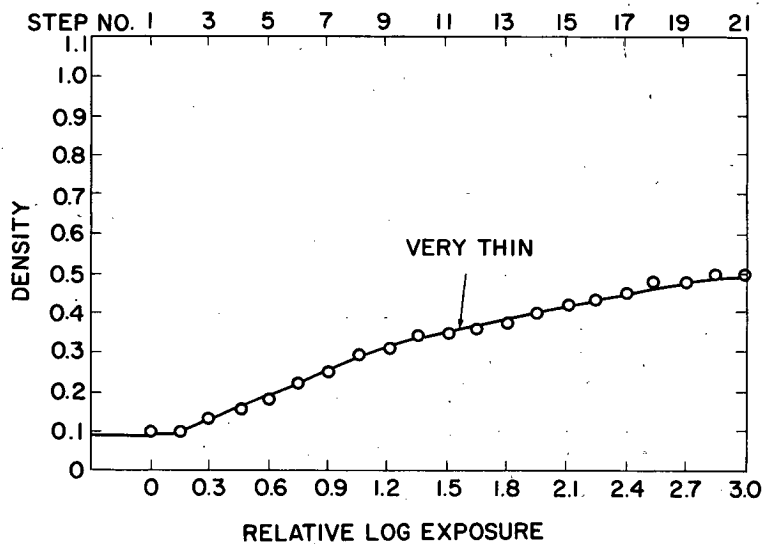
SECRET

Figure 3. Characteristic Curves of Emulsions L11366 (a), L111466 (b), and H093066A (c) Coated at Various Thicknesses.
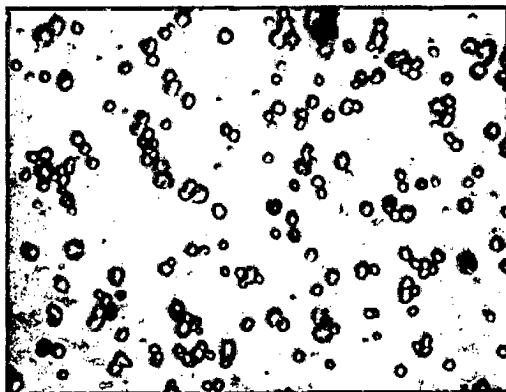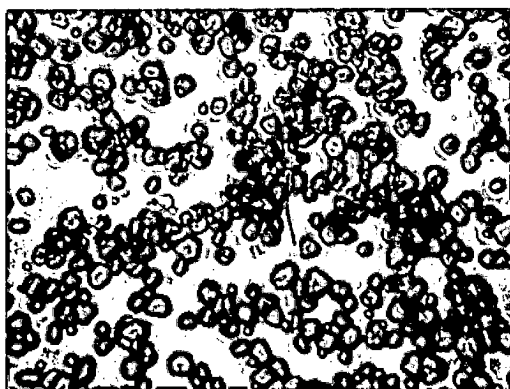
(a) Emulsion L11366

(b) Emulsion L111466

(c) Emulsion H093066A

Figure 4.   Photomicrographs of Emulsions L11366, L111466,
and H093066A

1-10

25X1

SECRET

between viscosity and pick-up is so complex (indeed, viscosity itself is a variable in a system containing gelatin), it is extremely difficult to produce a coating of pre-arranged thickness. Of course a preliminary series of coatings can be made to cover the desired thickness, and then by interpolation of these conditions, derive the correct requirements for that particular system, but this consumes time and emulsions, and is then only approximate. For example, for the laboratory-scale coater small coating aliquots are mandatory if all are to be coated from one pre-paration. Unfortunately, the coating quality here is comparatively poor (see Figure 5). The quality is better from the larger coaters (see Figure 6), but the consumption of emulsion is such that two preparations are necessary.

The coating system that appears to satisfy the preceding requirements has been designed, and should be operational in January 1967. It is an injection coater with an output of 7 ft of 70 mm film per loop. It is anticipated that less than 100 ml of emulsion per loop will be required and that coatings can be made at the rate of 5 min per loop. Because the emulsion is injected onto the film base with no wastage, the deposition can be calculated exactly from a knowledge of the rate of delivery for the coating head slot and the speed of the film base past the slot. The viscosity plays a minor role so long as it is sufficiently high to maintain a meniscus between slot and film base.

Coating Thickness

Various techniques for measuring thin film thickness have been examined. The interferometric technique, although extremely accurate, suffers from the dis-advantage that it cannot measure absolute thickness; it measures only change in thickness. Standardization is difficult since the composition of the emulsions varies sufficiently to affect the refractive index and, therefore, a standard must be used with each emulsion type. Moreover, the system is expensive.

At automated caliper gauge is on the market which records the thickness of a material on a chart with a ten-fold longitudinal magnification. After overall measurement, the emulsion can be washed off and the film base thickness re-recorded on the same chart. While this provides an attractive presentation of the data, the accuracy is only $\pm 2.5\,\mu$. (Since the average film thickness is only of the order of $10-20\,\mu$, the accuracy is poor.) The technique involving microscopic

SECRET

SECRET
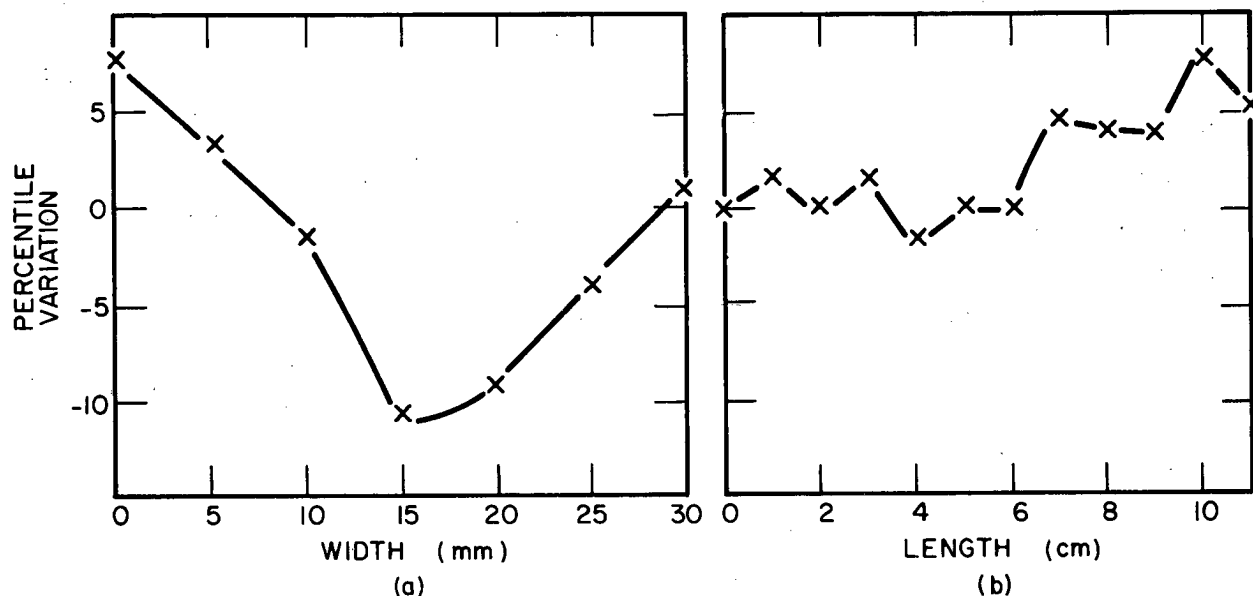
Figure 5. Percentile Variation of Coating a Small Coater (35 mm) Sample Taken (a) Across the Web, and (b) Down the Web
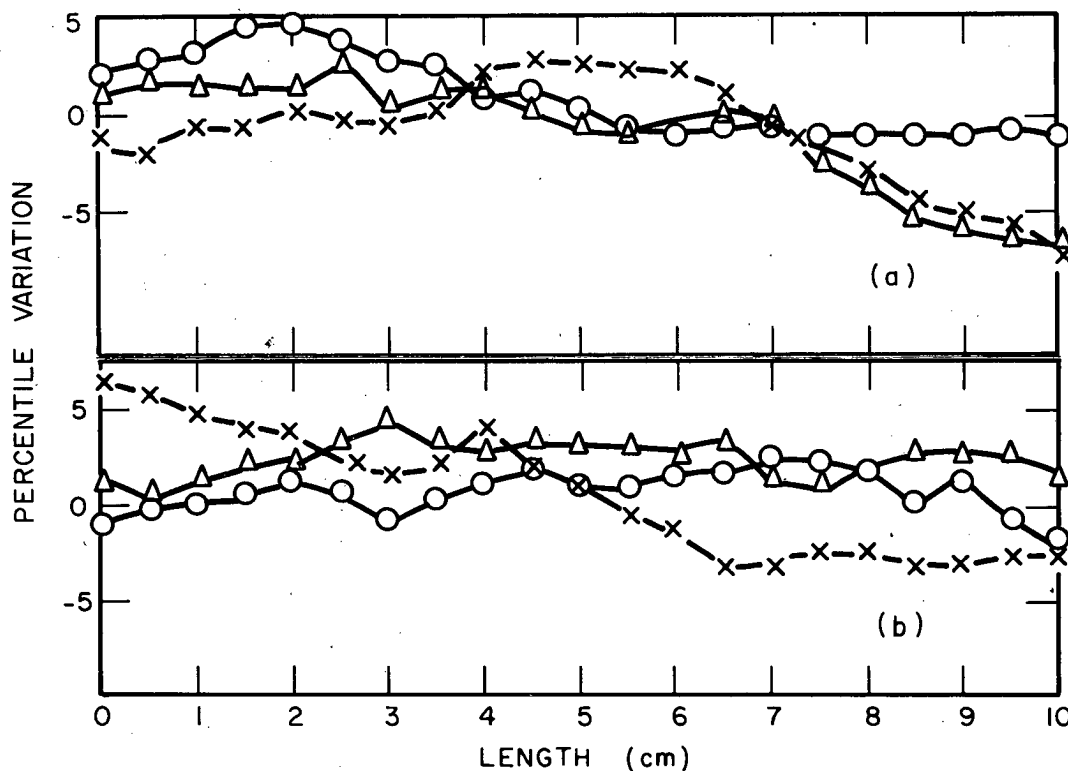
Figure 6. Percentile Variation of Coating of Large Coater Sample Taken (a) Across the Web and (b) Down the Web. (Parallel Control experiments both along and across the web on a Kodak coating (EK 8430) showed a variation in density of ± 0.01 density units (± 0.33%). Such a variation cannot be considered as significant since the limits of the densitometer have been reached.)

SECRET

25X1

examination of microtomed film samples is also of low accuracy because of limitations with respect to the wavelength of the light used. The air gauge technique is still to be considered.

Coating Weight Determination

The conventional technique is done by taking a known weight of emulsion (or known film area) and dissolving it in excess silver complexing agent. This agent may be the cyanide ion, such as potassium cyanide, or a sulfur compound, such as thioacetamide. The solution is then back-titrated with standard silver nitrate solution, and the equivalence point is made manifest by use of a dye (color change) or by sudden change in potentiometric data. Silver complexing agent strength is determined by a blank titration. This technique is operable, but there is an obvious hazard with cyanide present in a permanent installation (although the HCN vapors can be minimized by addition of ammonia to elevate the pH), and if a thio compound is substituted for cyanide, the instability of this compound makes it imperative that new solutions be prepared every few days, thereby increasing the time for the operation. Another disadvantage is the time consumed in making the potentiometric runs. At the present, however, it would appear that the conventional procedure, using thioacetamide, will be used for analyzing liquid emulsions. (It may also be used for film analysis should the x-ray technique* prove too costly.)

Developer Studies

During development the shape of an exposed grain often changes from the near spherical to an irregular filamental structure. It is known that developer type markedly affects developed grain morphology (see Figure 7). In this figure, grains developed in three developers are compared. The physical developer is the pre-fixation type where the film is treated with an iodide sulfite solution before being

---

* A very fast and convenient alternative for film analysis lies in x-ray fluorescence analysis. In this method, a film sample is irradiated with x rays and the resultant fluorescent intensity is read on a meter which can be calibrated as a direct function of the silver content. The problem here lies in the cost of the instruments. No further action on the choice between these two approaches will be made until the manufacturers of such instruments have returned a cost estimate of the basic unit, stripped of all refinements.

SECRET

Original Undeveloped
Grains
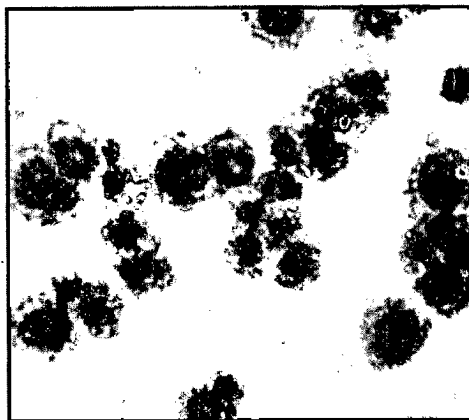
Physical Developer
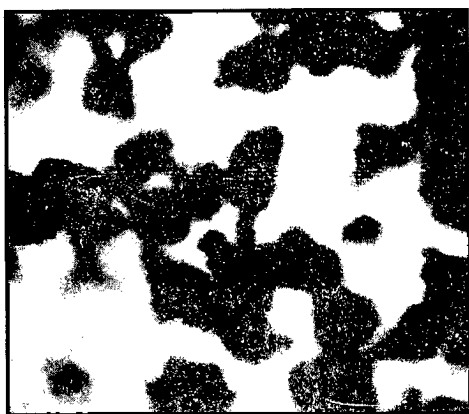
Inorganic Developer

D-76

Figure 7. Comparison of Undeveloped and Developed
Grain Morphology

SECRET

SECRET

developed in silver nitrate in the presence of a sulfite, thiosulfate, and amidol solution; development time is 30 min at $68^{\circ}F$ (see Handbook of Photography,[*] p. 374). The inorganic developer is a sodium hydrosulfite, bisulfite, and bromide solution; development time is 3 min at $68^{\circ}F$ (see Handbook of Photography,[*] p. 316). The third developer is D-76; development time is 8 min at $68^{\circ}F$.

Experiments were conducted which, we believed, would lead to a factor, unique for each developer, relating the projected area of the original grain system to the projected area of the developed grains. An analysis of the changes occurring in the grain size distribution would allow the determination of the developing grain in the absence of light. Coatings prepared such that the coverage was much less than a complete monolayer[†] would prevent any developed grain from fusing with any neighboring grain, and would remain distinguishable and individual throughout. A description of the experiments follows.

A partially exposed film was developed in D-19 for the recommended time (5 min) and stopped in dilute acetic acid but was not fixed. The grain size distribution of the undeveloped fraction of grains was then determined and subtracted from the parent grain size distribution for that emulsion. This yielded the grain size distribution of those grains which finally developed. The total projected area of the developed grains was now measured. The average number of grains per field was known by taking at least 20 pictures of each system, and since the average of residual undeveloped grains was also known, the developed projected area could be related to a mean developed grain size. The comparison between this number and the original distribution obtained for the grains to be developed yields the factor relating original grain size to developed grain size.

---

[*] K. Henney, ed., "Handbook of Photography" (New York, N.Y.: McGraw-Hill Book Company, 1939).

[†] Initial studies showed that the monolayer coatings supplied to [ ] were too thick for studying the developed grains in isolation. 25X1 25X1

1-15 25X1
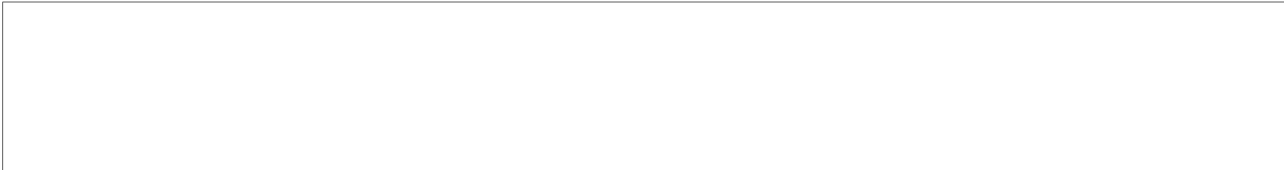
SECRET

Several interesting facts have been revealed. The first is that under conditions of partial exposure, only the largest grains are exposed so that the emulsion is behaving as an emulsion of greater grain size than the mean. With increasing exposure, the active emulsion grains approach the mean (see Figure 8). This may offer partial explanation for the increase in resolution with exposures over and above the contrast consideration. It has also been found that the factor relating exposed undeveloped grain area and developed grain area is not a constant, but increases with exposure (see Figure 9). Thus under conditions of high exposure, this may be the phenomenon responsible for the observed loss in resolution under conditions of overexposure. The effect had hitherto been believed to be caused by excessive light scattering, increasing depth of image, and perhaps infectious development; this effect, however, has been observed in films less than a complete monolayer thick in which the light scatter is minimal and the intergrain distance is large. It is believed that the root of the phenomenon may be in the number of sensitivity centers present prior to development and is to be the subject of further study. It has also been observed that while gradient exposure is selective in rendering only the larger grains developable, the fog which is created in the manufacture of the emulsion has a similar grain size distribution to the unexposed undeveloped film indicating nonselectivity.

Film Data

We have also obtained during this period image quality data on films EK-5427 and EK-8430. The modulation transfer functions (MTF) of EK-5427 and EK-8430 are shown in Figure 10. Their characteristic curves are given in Figures 11 and 12.*

Data on SO-132 (3404) is still not available because of delays in MTF instrumentation.

1
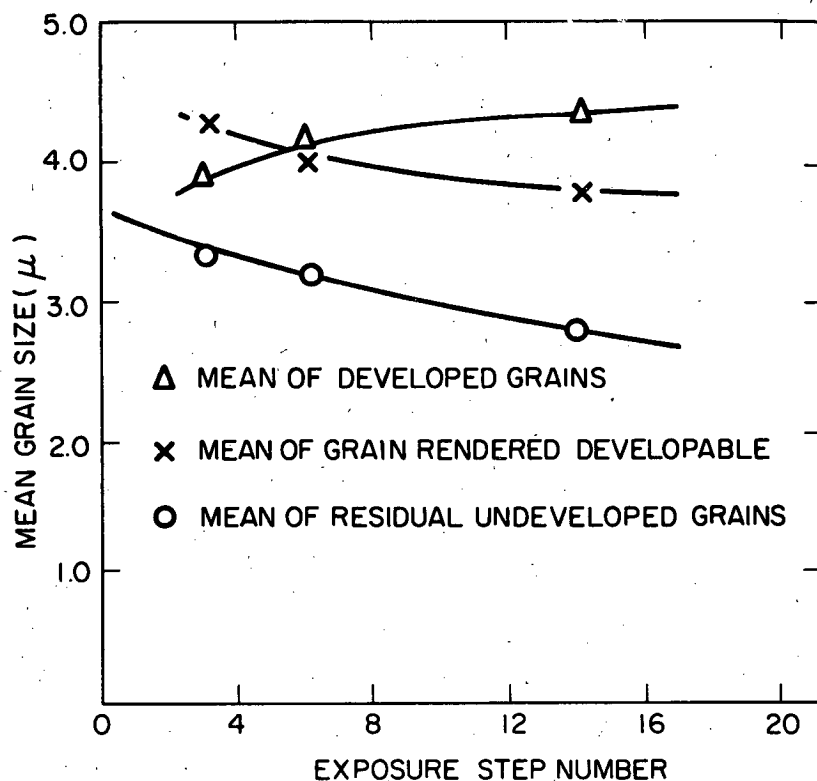
25X1

Figure 8. Mean Size of Various Grain Components as a Function of Exposure
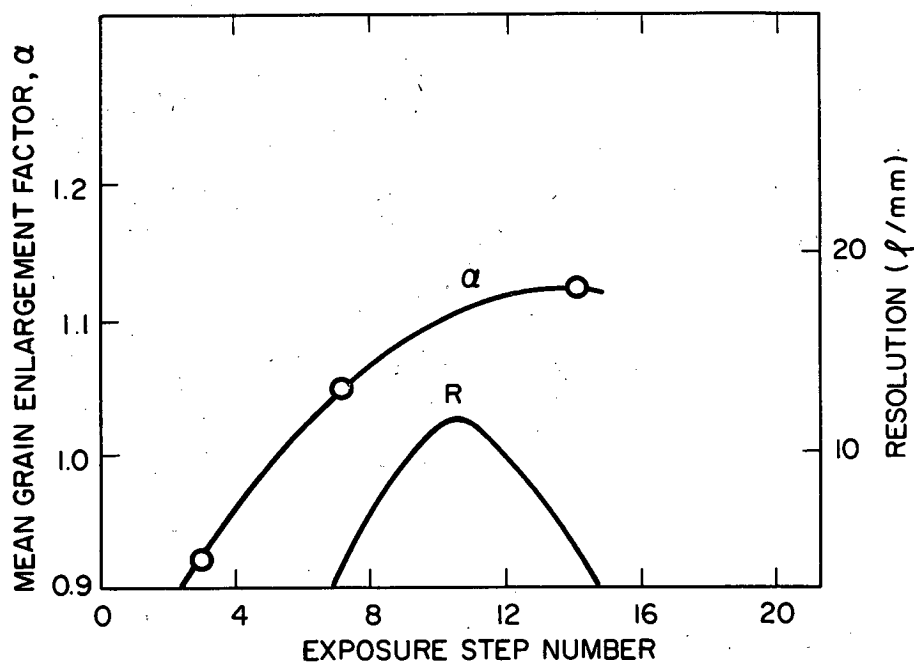
Figure 9. Mean Grain Enlargement Factor (α) as a Function of Exposure

1-17   25X1
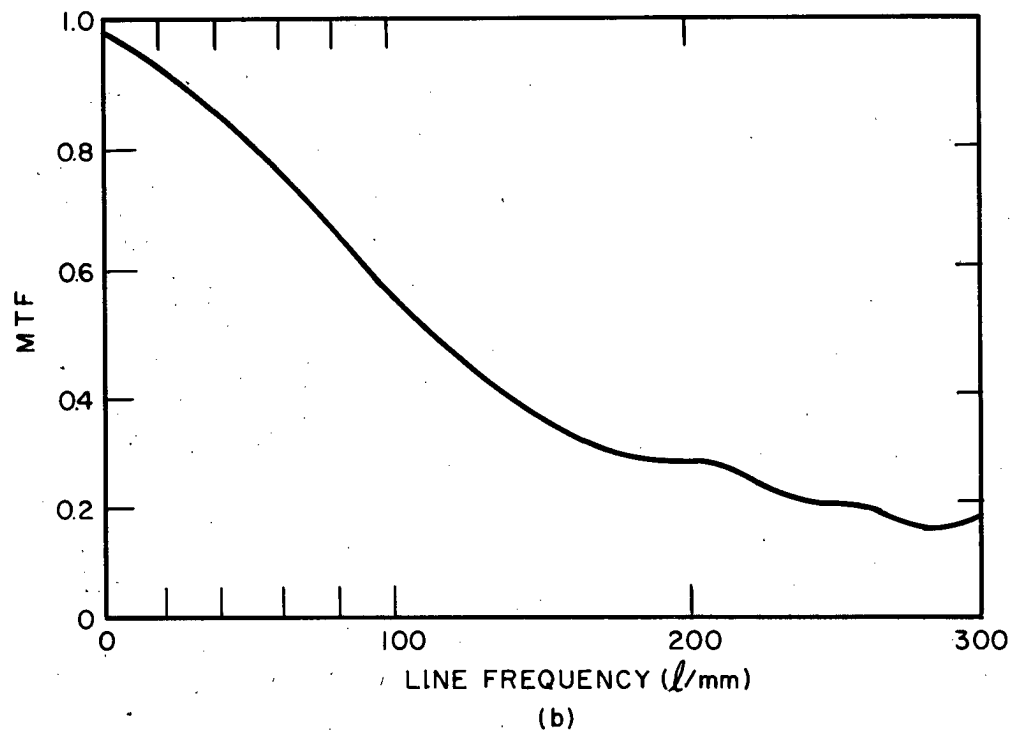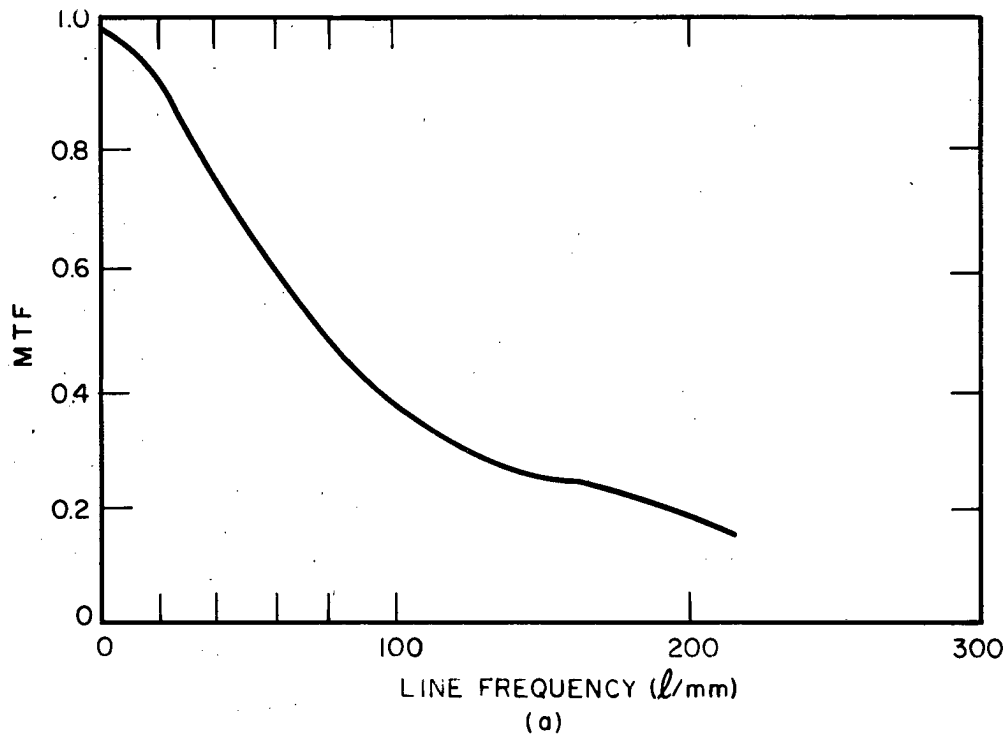
Figure 10.   MTF of (a) EK-5427 and (b) EK-8430
Developed in D-19

25X1

DATE __9-65__
U P NUMBER ____
PREPARED BY ____
TYPE __Dupe__
CLASS __Blue Sensitive__
MANUFACTURER __EK__
EXPIRATION DATE ____
EMULSION NUMBER __5427__
LAMP __III (2800°K)__
EXPOSURE TIME __1/10 sec__
WEDGE NUMBER __6464__
DEVELOPER __D-19__
TIME __Various__
TEMPERATURE __70__ °F

TOTAL DENSITIES

F ___	11 ___
1 ___	12 ___
2 ___	13 ___
3 ___	14 ___
4 ___	15 ___
5 ___	16 ___
6 ___	17 ___
7 ___	18 ___
8 ___	19 ___
9 ___	20 ___
10 ___	21 ___

BASE DENSITY ____

SENSITOMETRIC PROPERTIES

SPEED ____
GAMMA ____
FILTER ____
FILTER FACTOR ____

Figure 11. Characteristic Curves for EK-5427 Developed in D-19 at 70°F for Various Times

Films were processed in the Vane Agitator Sensitometric Processing Machine using 22 stroke/min agitation

ABSOLUTE LOG E __8.72-10__

RELATIVE LOG EXPOSURE
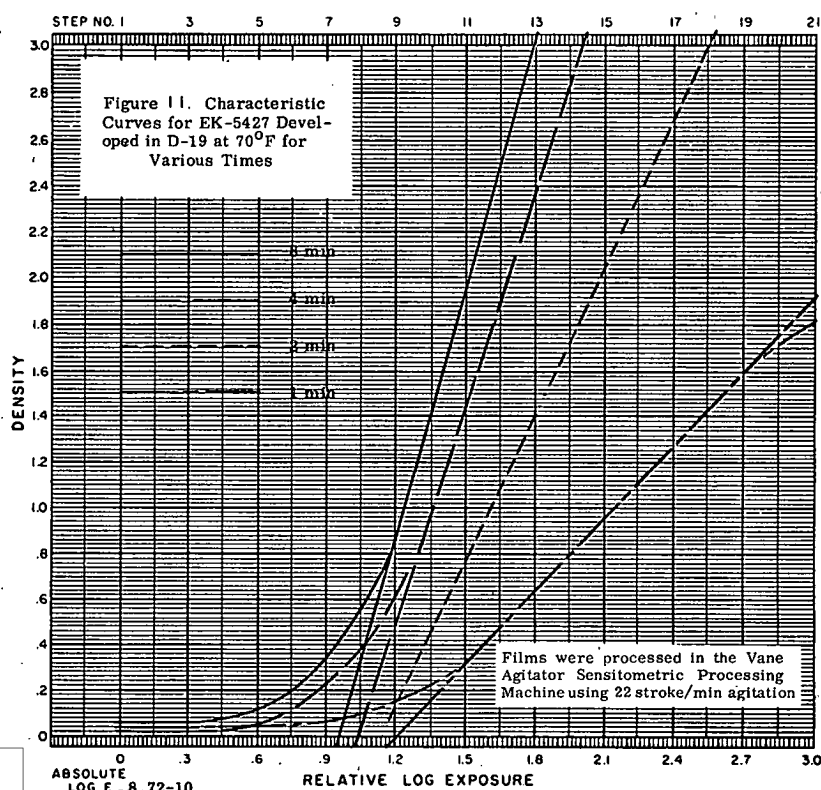
DENSITY

25X1

DATE __9-65__
U P NUMBER ____
PREPARED BY ____
TYPE __Dupe__
CLASS __Blue Sensitive__
MANUFACTURER __EK__
EXPIRATION DATE ____
EMULSION NUMBER __8430__
LAMP __III (2800°K)__
EXPOSURE TIME __2 sec__
WEDGE NUMBER __6464__
DEVELOPER __D-19__
TIME __Various__
TEMPERATURE __70__ °F

TOTAL DENSITIES

F ___	11 ___
1 ___	12 ___
2 ___	13 ___
3 ___	14 ___
4 ___	15 ___
5 ___	16 ___
6 ___	17 ___
7 ___	18 ___
8 ___	19 ___
9 ___	20 ___
10 ___	21 ___

BASE DENSITY ____

SENSITOMETRIC PROPERTIES

SPEED ____
GAMMA ____
FILTER ____
FILTER FACTOR ____

Figure 12. Characteristic Curves for EK-8430 Developed in D-19 at 70°F for Various Times

Films were processed in the Vane Agitator Sensitometric Processing Machine using 22 stroke/min agitation

ABSOLUTE LOG E __9.97-10__

RELATIVE LOG EXPOSURE

DENSITY

1-19
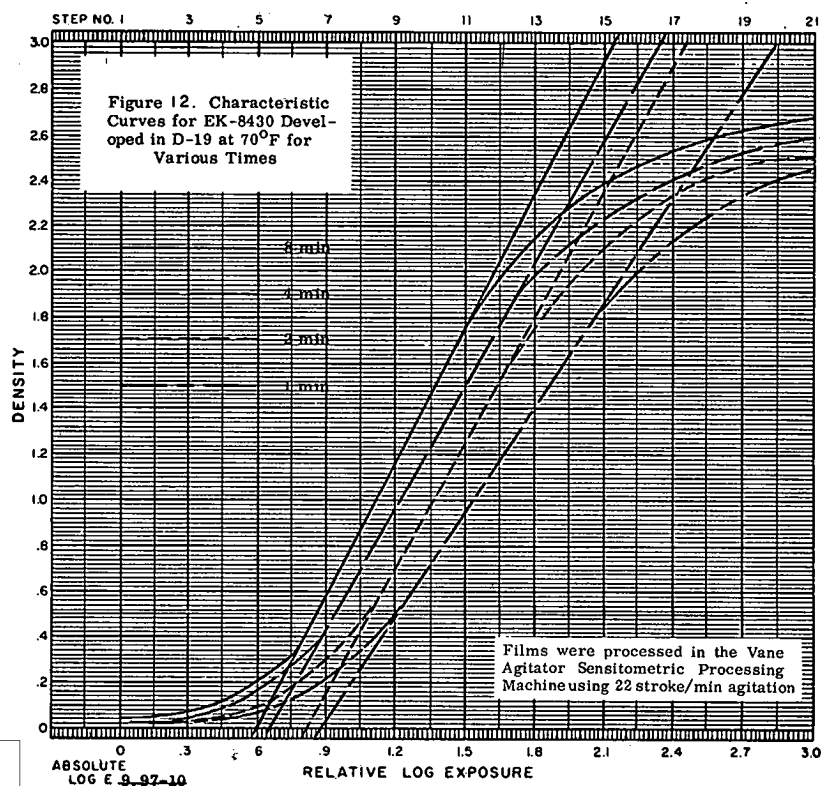
25X1

The Electron Microscope

The electron microscope was installed in the first week of December in accordance with Phase II of Task 2B work statement, and the special techniques of specimen preparation which are necessary in order to examine emulsions by electron microscopy are being developed. An outline of such procedures is as follows:

1. A glass slide is coated with collodion or formvar.

2. Dilute emulsion is coated on the formvar.

3. The gelatin is destroyed by alkaline solution of trypsin.

4. The grains are shadowed with carbon or gold.

5. The grains are then dissolved away with sodium thiosulfate solution.

6. The replica on the formvar is floated off and picked up on a grid.

The special characteristics are: (1) Unless the tenaciously held gelatin skin is removed before shadowing, the definition will be extremely poor. (2) Unless the silver halide crystal is removed before electron microscopic observation, the electron beam will rapidly convert it to amorphous silver metal. The alternative to crystal dissolution is to freeze the specimen with liquid nitrogen. This immobilizes the interstitial silver ions and thus arrests silver conversion.

SUMMARY

The model emulsion preparations have been completed as far as is required for this stage of the program. Of course, after the electron microscope has become fully operational and has been used to examine the back-log of emulsions, new emulsion formulations of fine grain type (scheduled for Phase III) will be developed. In the developer studies, several interesting facts relating to the developed grain size have been found. Of particular interest is the dependence of developed grain size on exposure time. Work will continue on these developer studies of submonolayer films. Having examined the system as a function of exposure for a given developer time, we now plan to study it as a function of developer time for a given exposure.

25X1

Coater construction is on schedule and will be operational in January 1967. Test coaters will be made. Installation of the chosen coating weight system and emulsion thickness system will commence. The electron microscope has been installed, and preliminary electron micrographs will be made. Final data on film 3404, delayed because of modifications in the MTF apparatus, will be obtained.

25X1

Page Denied

SECRET

CHAPTER 2

OPTICS

SECRET

Page Denied

CHAPTER 2

OPTICS

TASKS 2AA, 2AB, AND 2C

This chapter presents the results obtained to date under tasks 2AA, 2AB, and 2C of the Image Analysis program.

STUDIES OF IMAGING WITH PARTIALLY COHERENT LIGHT

Tasks 2AA and 2AB are concerned with theoretical and experimental studies of imaging with partially coherent light. The work performed under these two tasks is designed to determine the validity and the necessity of the theory of partial coherence in image analysis. For this purpose the intensity distribution in the image of certain commonly used test targets is calculated using both the theory of partial coherence and the simpler incoherent theory. The image intensity distribution predicted by both of these theories is then compared directly with the appropriate experimental image intensity distribution. This determines the validity of and the necessity for recourse to the theory of partial coherence in many imaging problems.

Theory (Task 2AA)

The general theory of partial coherence as applied to image analysis was presented in Proposal No. TO-B 100-65. The result of this theory which forms the basis for the present investigations of quasi-monochromatic imaging is the relation

$$I_i(\underline{x}) = \int\int \Gamma_o\left(\underline{\xi}_1 - \underline{\xi}_2\right) t\left(\underline{\xi}_1\right) t^*\left(\underline{\xi}_2\right) K\left(\underline{x} - \underline{\xi}_1\right) K^*\left(\underline{x} - \underline{\xi}_2\right) d\underline{\xi}_1 \, d\underline{\xi}_2 \, , \quad (1)$$

which expresses the image intensity distribution $I_i(\underline{x})$ in terms of the mutual intensity of the object illumination $\Gamma_o(\underline{\xi}_1 - \underline{\xi}_2)$, the complex amplitude transmittance of the object $t(\underline{\xi})$, and the complex amplitude impulse response of the imaging system $K(\underline{x} - \underline{\xi})$. In Eq. (1) we have taken the mutual intensity of the object illumination to be spatially stationary and assumed that we are dealing with transilluminated objects. These two conditions apply to the investigations being reported here.

Since the results of the theoretical calculations of $I_i(\underline{x})$ are to be compared with the results of experimental work, the form of the object illumination mutual intensity $\Gamma_o(\underline{\xi}_1 - \underline{\xi}_2)$ is chosen to be that associated with a uniform incoherent circular source, so that by the van Cittert-Zernike theorem

$$\Gamma_o\left(\underline{\xi}_1 - \underline{\xi}_2\right) = \frac{2J_1\left(\text{const}\,|\underline{\xi}_1 - \underline{\xi}_2|\right)}{\text{const}\,|\underline{\xi}_1 - \underline{\xi}_2|} \quad . \tag{2}$$

For the same reason, the amplitude impulse response $K(\underline{x} - \underline{\xi})$ chosen is that for a circularly symmetric diffraction limited imaging system; here,

$$K(\underline{x} - \underline{\xi}) = \frac{2J_1\,(\text{const}\,|\underline{x} - \underline{\xi}|)}{\text{const}\,|\underline{x} - \underline{\xi}|} \quad . \tag{3}$$

These functions, Eqs. (2) and (3), represent accurately the experimental conditions used in the experimental optical bench investigations discussed later.

The remaining factor in Eq. (1) which has not yet been specified is $t(\underline{\xi})$, the amplitude transmittance of the object. (The objects selected for theoretical and experimental investigation are commonly used test objects, i.e., edges, square waves, three-bar targets, and sine waves.) The complexity of the calculations of the image intensity $I_i(\underline{x})$ for these objects, $t(\underline{\xi})$, and the conditions represented by Eqs. (2) and (3) have required the use of a digital computer. Equation (1) has therefore been programmed for the IBM 360. The details of the computer program will not be covered here, but one consideration which has been found to play an important role in computing reliable image intensity distributions will be mentioned.

The fundamental operation performed on a given object distribution, $t(\underline{\xi})$, to put it in a form acceptable to a digital machine, is <u>sampling</u>. The Shannon Sampling theorem for band-limited objects is well known, but for objects which are not band limited or for which, for practical reasons, the sampling is not frequent enough, the situation is somewhat more involved. The sampling operation for equispaced

SECRET

samples may be regarded as a multiplication of the object distribution by a Dirac comb with spacing Δ between the samples. The convolution theorem then shows that the Fourier transforms of this product distribution is a convolution of the individual transforms. Since the transform of a Dirac comb with spacing Δ is another Dirac comb with spacing $1/\Delta$, the transform of the product is then the Dirac comb of spacing $1/\Delta$ with the Fourier transform of the original object distribution convolved about each spike of this comb. If the original object distribution is not band limited, the situation is as shown in (a) of Figure 1. This is to be compared with the Fourier transform of the object which appears in the actual optical imaging system as shown in Figure 1(b). In the analog operation performed by the optical system (Figure 1(b)) the optical passband determined by the lens aperture rejects those frequencies above some critical value and effectively band limits the object. However, in the digital operation (Figure 1(a)) the replication of the original object transform about each spike separated by $1/\Delta$ produces some troublesome effects. The high frequencies from the replica just to the right or just to left of center come through the optical passband. The inverse Fourier transform of the distribution that appears within the optical passband of Figure 1(a) is now not simply a bandlimited image of the original object, as it would be in the optical imaging system. In cases where the transforms overlap considerably, the image calculated by transforming the distribution within the passband of Figure 1(a) can be expected to bear little, if any, resemblance to the original object. This effect of sampling at too low a rate is known as "aliasing." The solution to the problem of aliasing is to
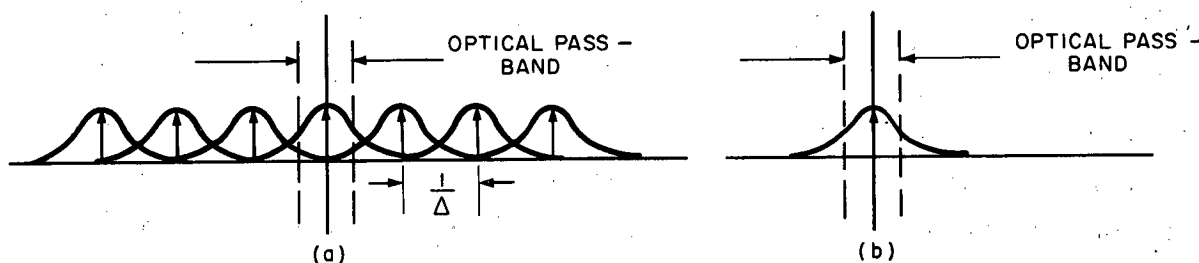
Figure 1. Fourier Transform of Sampled Object Distribution (a), and
Fourier Transform of Object Distribution in Optical System (b)

SECRET

band limit the original distribution $t(\xi)$ <u>prior</u> to sampling. If the distribution $t(\underline{\xi})$ has been band limited to the region of the spectrum between $\pm 1/2\Delta$ (where Δ is the distance between samples), then the spectra will not overlap in transform space and reliable image intensity distributions can be calculated. This band–limiting operation prior to sampling is an important consideration in the digital calculation of image intensity distributions.

The significant parameter in the calculations of the images of partially coherent objects has been found to be the ratio R of the coherence interval of the object illumination to the radius of the diffraction pattern produced in the object plane by the imaging system. For a unit magnification system such as we are using in these studies the diffraction pattern or impulse response is of the same size in both the object and the image plane. The coherence interval of interest, therefore, is the characteristic width of the function Eq. (2) and the size of the diffraction pattern is the characteristic width of the function Eq. (3). Since Eqs. (2) and (3) have the same form it is useful to define this ratio R as unity when the two functions (2) and (3) have the same size, and as (2) becomes wider than (3) the value of R increases. One would then expect coherence effects to become more pronounced as R increases and, indeed, this is the case.

The theoretical image intensity distribution $I_i(\underline{x})$ has been calculated digitally using Eq. (1) for the following objects and R values:

1. A pure amplitude <u>edge</u> object of intensity contrast 3.5:1 for R = 1, 4, and 8.

2. A pure amplitude <u>square wave</u> object of fundamental frequency 3.16 cycles/mm and of infinite contrast for R = 0, 4, and ∞. The values R = 0 and ∞ represent the incoherent and coherent limits respectively.

In these calculations the constant in Eq. (3) is chosen so that the coherent cutoff frequency of the imaging system is 7.25 cycles/mm. Figures 2 and 3 show the theoretical intensity distributions. In Figure 2 the theoretical results for the edges are plotted on the same graph with experimental results to facilitate comparison.
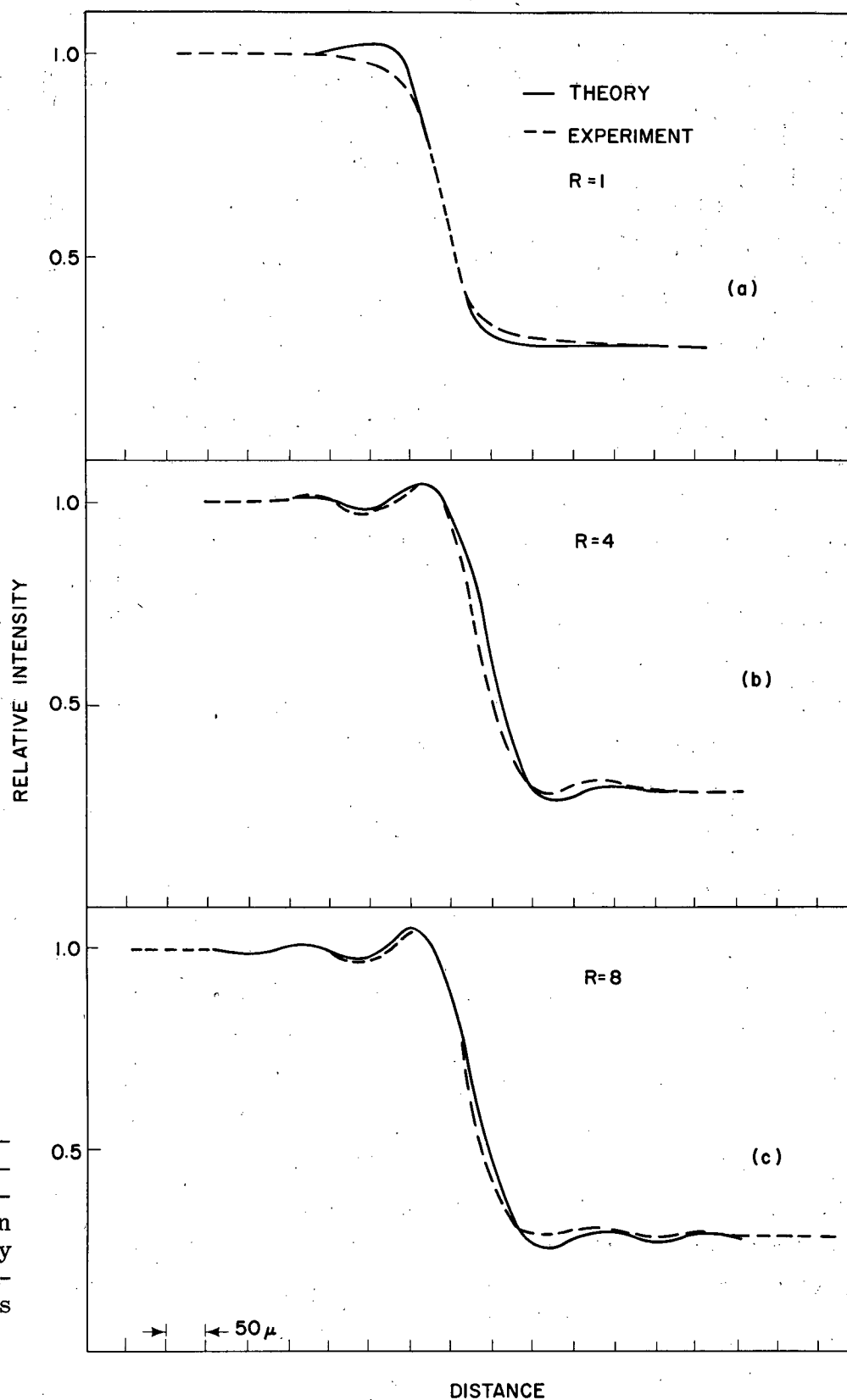
25X1

Figure 2. Theoretical and Experimental Image Intensity Distribution for 3.5:1 Intensity Contrast Edge Object and Various Values of R

2-5   25X1
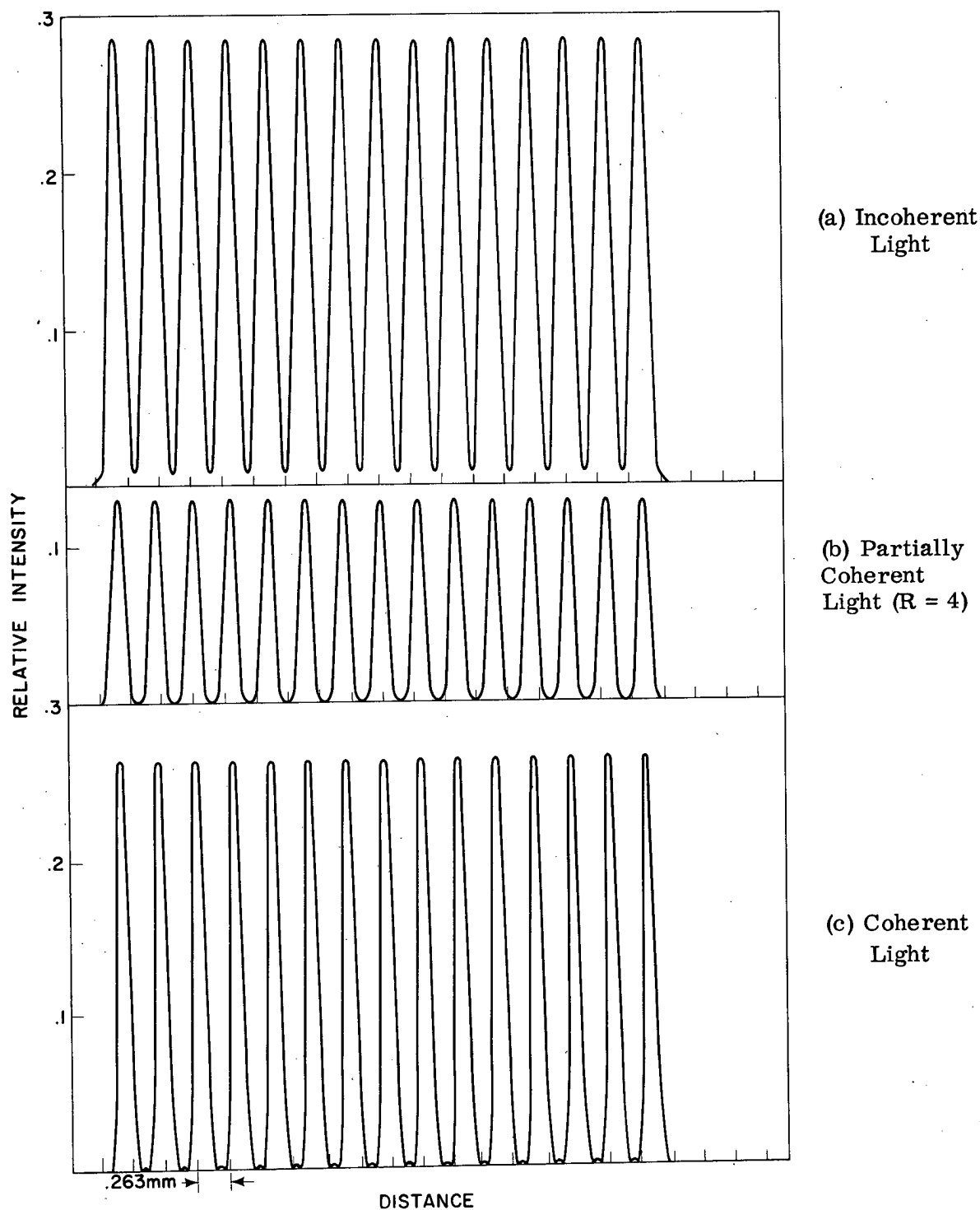
Figure 3. Theoretical Image Intensity Distribution for Infinite Contrast Square Wave Object of Fundamental Frequency 3.16 Cycles/mm and Optical System of 7.25 Cycles/mm Coherent Cutoff Frequency

25X1
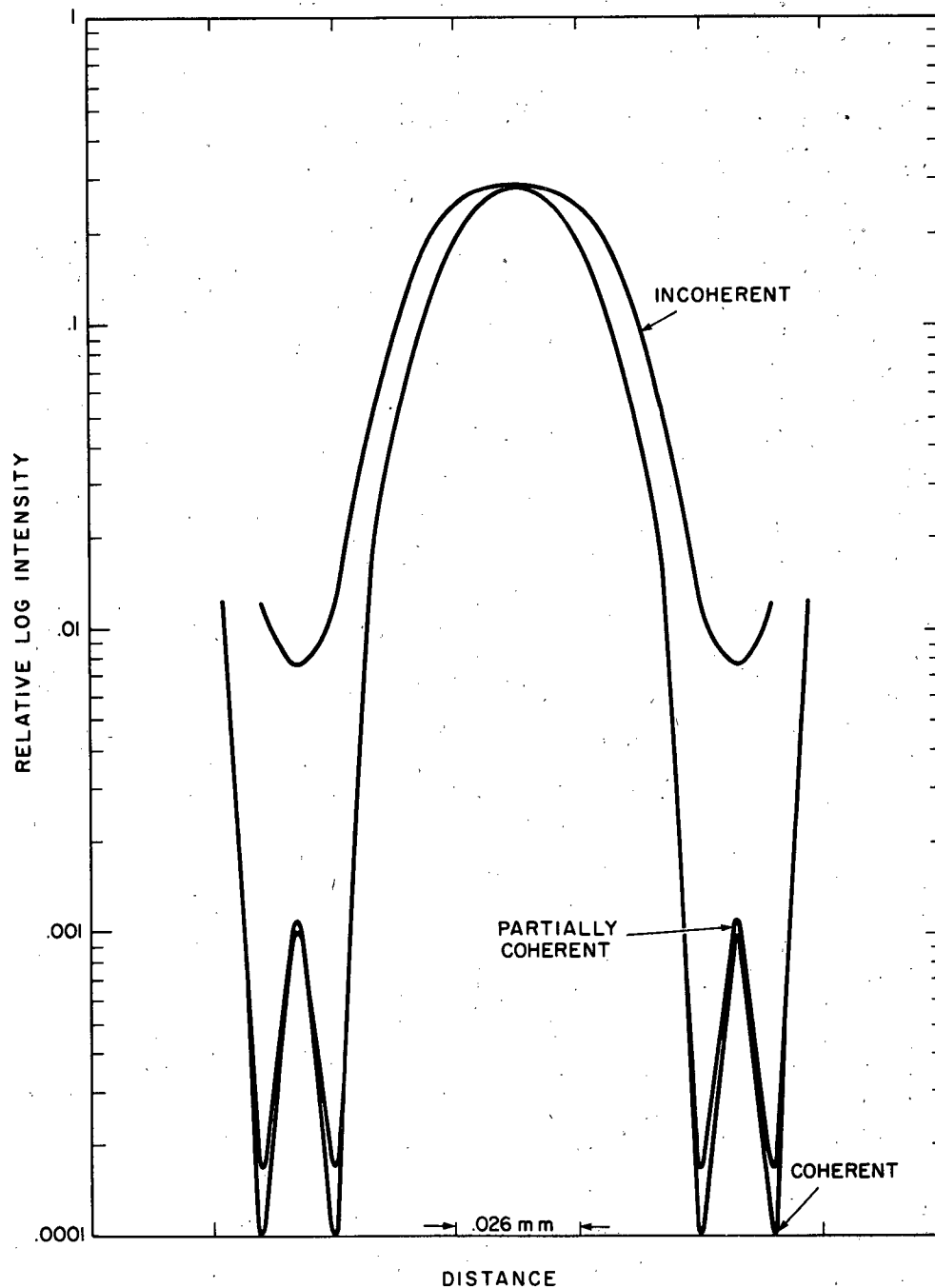
(d) Expanded Comparison of One Bar of (a), (b), and (c) on
Logarithmic Scale

Figure 3 (Continued). Theoretical Image Intensity Distribution for
Infinite Contrast Square Wave Object of Fundamental Frequency
3.16 Cycles/mm and Optical System of 7.25 Cycles/mm Coherent
Cutoff Frequency

2-7   25X1

25X1

The intensity distribution in one bar of the square wave image in expanded form is presented in Figure 3(d) for comparison of the different degrees of coherence. A discussion of these results follows in the next section.

Experiments (Task 2AB)

Two imaging systems are used in experimentally studying partially coherent imaging. One of these is an optical bench arrangement; the other is a photographic enlarger. The basic difference between these two systems is the form of the mutual intensity of the illumination in the object plane; for the bench setup this function is a Bessinc, for the enlarger, a gaussian. The experiments performed on the optical bench correspond to the theoretical work described in the preceding section. The theoretical work corresponding to the experiments performed on the enlarger was done during an earlier program for which the enlarger was evaluated   25X1 In both cases, the experiments were carried out at   25X1 low spatial frequencies to facilitate analysis.

In these systems the images are recorded on SO-243 film and are processed under sensitometric conditions along with step-wedge exposures. The images and step wedges are traced with a microdensitometer under identical settings, and the intensity distributions in the images are then recovered from the D log E curve of the step wedge. SO-243 film is an exceptionally fine grain film with a resolution limit of about 500 ℓ/mm. The maximum frequency we are asking the film to record in these experiments is 30 ℓ/mm. The transfer function of the film should therefore have a negligible effect on the images at these frequencies. When the images are traced with the microdensitometer, the scanning slit is chosen such that its transfer function remains above 0.80 at the maximum frequency of interest. This allows virtually all the grain noise to be integrated out with negligible effect on the trace. The calibration of the ratio arms of the microdensitometer is periodically checked to insure that the scale of the images is correct.

Optical Bench

Figure 4 shows a schematic of the optical bench imaging system. The sample is illuminated by a collimated beam and then imaged by a telescope of unit magnification. The aperture in the transform plane determines the cutoff frequency of the

25X1
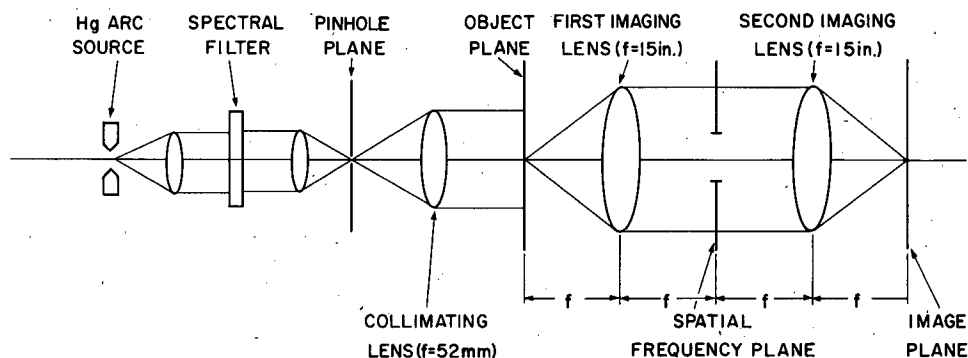
Figure 4. Optical Bench Imaging System

system. In studying the images of pure amplitude objects, the object is held in a liquid gate to eliminate phase effects.

The imaging system was designed to work at a maximum aperture of f/65. The on-axis incoherent transfer function of the system was measured by imaging sine waves of known frequency and modulation through the system and measuring the resultant modulation. An Aristo source with a peak wavelength of 5480 Å was used to provide effectively incoherent illumination for these measurements. This is very close to the peak wavelength (5461 Å) of the Hg green line. Figure 5 shows the
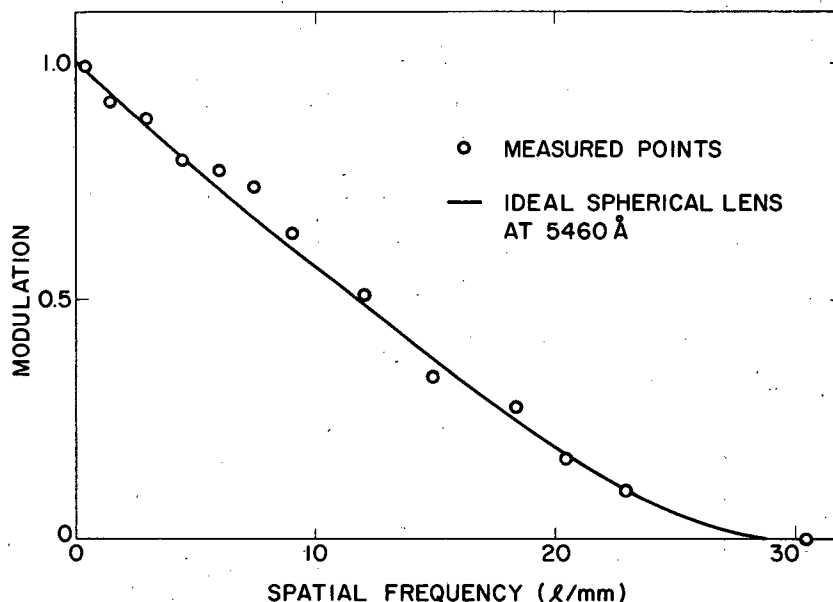
Figure 5. Comparison of Measured Transfer Function of Optical Bench Imaging System at f/65 and Theoretical Curve for a   at f/65 in 5460 Å Incoherent Light

25X1

25X1

25X1

measured results compared to the transfer function of a diffraction limited system. The agreement is very good and it is reasonable to assume that the impulse response of this imaging system at f/65 and smaller apertures is that of a diffraction limited system on axis.

The coherence in the collimated beam which illuminates the object can be predicted by the van Cittert-Zernike theorem if the pinhole is incoherently and uniformly illuminated. The pinhole diameters range from 25 to 400 μ, and it is reasonable to assume that the coherence interval of the illumination in each pinhole is much smaller than the pinhole size itself. However, the size of the Hg arc is 300μ, and if the pinholes are placed at the image of this arc, the larger pinholes will not be uniformly illuminated.

In order to definitively establish the form of the coherence function in the object plane, direct two pinhole measurements of $\gamma_{12}(0)$ were made. Double pinhole sets with spacings as small as 50 μ were used. The diameter of the individual pinholes in these sets was one fifth of the separation. The fringe patterns formed in the far field of these pinhole sets were photographed and the visibility of the patterns measured. This gave a measure of $|\gamma_{12}(0)|$. The phase of $\gamma_{12}(0)$ was measured by observing whether the central fringe was an intensity maximum or minimum.

When the arc was directly imaged on the 400 μ pinhole, the measurements made in this way differed greatly from what would be expected from the van Cittert-Zernike theorem assuming uniform illumination across the pinhole. In order to attain uniform illumination, several layers of Kodak Diffusion Sheeting were placed between the condenser and pinhole. Figure 6 shows the results of measurements made when eight layers of sheeting were used. The agreement of the measured results with the prediction of the van Cittert-Zernike theorem is very good in this case. The point at which $|\gamma_{12}(0)|$ first goes to zero is quite sensitive to the actual intensity distribution across the pinhole (when only six layers of sheeting were used this point shifted to between 100 and 200 μ). Inasmuch as this result showed that the illumination was uniform over 400 μ with eight layers of sheeting, we are justified in assuming that under the same conditions the smaller pinholes will be uniformly illuminated and that the van Cittert-Zernike theorem applies.

2-10

25X1
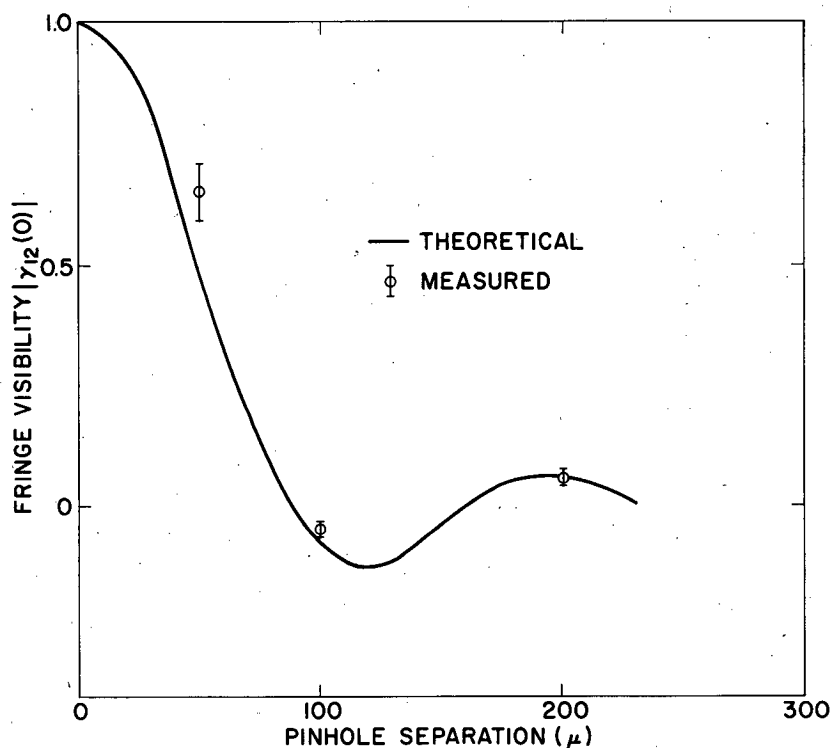
Figure 6. Measured Fringe Visibility in Object
Plane vs Pinhole Separation for 400μ Source
Pinhole with 52 mm Focal Length Collimating
Lens Compared to Theoretical Curve Assuming
Uniform Incoherent Source

We take the coherence interval r to be the distance from the origin to the first
zero of the Bessinc given by Eq. (2), i.e.

$$r = \frac{1.22\ f\lambda}{D}\quad,$$

where f is the focal length of collimating lens; D, the pinhole diameter; and r, the
mean wavelength.   For f = 52 mm, D = 400μ, and λ = 0.56μ, we have r = 87μ. The
radius of the spot size of the system is defined similarly to be

$$s.s. = 1.22\ \lambda f/No.$$

At f/130, s.s. = 87 μ. Thus, for this case

$$R = \frac{r}{s.s.} = 1 \ ,$$

where R here is the same R as that defined in the theoretical section. The smaller pinholes vary from 400 μ by factors of 2. Thus, values of R = 1, 2, 4, 8, and 16 are obtained with this system.

The imaging studies to date have involved pure amplitude objects corresponding to objects which have been studied or will be studied theoretically. Images have been formed of the following three objects:

1. A 3.5:1 intensity contrast edge

2. An infinite contrast long-line three-bar target

3. A 5:1 intensity contrast sine wave.

For each object except the edge, a variety of groups at different spatial frequencies were present. In each case, a particular group at some frequency within the resolution limit of the optics was chosen for analysis.

Comparisons between experimental measurements and theoretical calculations for images of the 3.5:1 contrast edge for three values of R are shown in Figure 2. For the two more coherent cases (R = 4, 8) the agreement between the theoretical and experimental results is much better in the high intensity region of the images than in the low intensity regions and for the R = 1 image. Figure 7 shows experimental images of a three-bar target group at 8 ℓ/mm. This frequency is slightly higher than the coherent cutoff frequency (7.25 ℓ/mm) of the imaging system but still well below the incoherent cutoff. As can be seen, the images show considerable variations over the range of R-values used. Microdensitometer traces of images of a 9 ℓ/mm group in the sine wave target are presented in Figure 8. Again, the quantitative differences in the images are considerable over the range of R values. Comparisons of these experimental image intensity distributions with corresponding theoretical results are being made as the theoretical results become available.

2-12

Declassified in Part - Sanitized Copy Approved for Release 2012/11/01 : CIA-RDP79B00873A000100010159-8

Enlarger

The second imaging system being used to perform experiments is an enlarger
(see Figure 9). Evaluating this enlarger we found that the imaging system was
diffraction limited on axis at f/3.5 and that the form of the mutual intensity func-
tion in the object illumination was gaussian (i.e., the mutual intensity in the object
plane could be described by assuming that the laser beam striking the rotating dif-
fuser acted as an incoherent source, and by applying the van Cittert-Zernike theo-
rem, the scale of the mutual intensity could then be varied by varying the size of
the beam on the diffuser). Figure 10 shows the forms of the impulse response and
mutual intensity. The important coherence parameter is the ratio of the scale of
the mutual intensity function to the impulse response function. If we define D as

$$D = \frac{\beta}{\alpha} \, ,$$

where α and β are the widths of the respective curves at the 0.88 points, D in-
creases as the system becomes more coherent. The smallest value of β is ob-
tained for the largest beam size on the diffuser. A negative lens was used as the
condenser to cause the beam to cover the entire usable area of the diffuser, giving
a value of $\beta = 20 \, \mu$. In order to vary D, it was generally more convenient to vary
α than than β. This was done with a series of apertures in the transform plane.
These apertures gave values of $\alpha = 20$, 10, and 5 μ. The minimum obtainable
value of D is thus one, and D could be varied up from this by factors of two both
by decreasing α and increasing β.

Calculations of edge images for D = 2, 4, and 8 were done for this system
under Contract ⬚ Task Order No. 3, and under the present program
experimental images corresponding to these values were measured. Figure 11
presents the experimental and theoretical results. Comparison of the data shows
that agreement is generally quite good. Microdensitometer traces of images of
groups of a three-bar target for various values of D are shown in Figure 12. As
the transform plane aperture is varied, the cutoff frequency of the imaging system

25X1
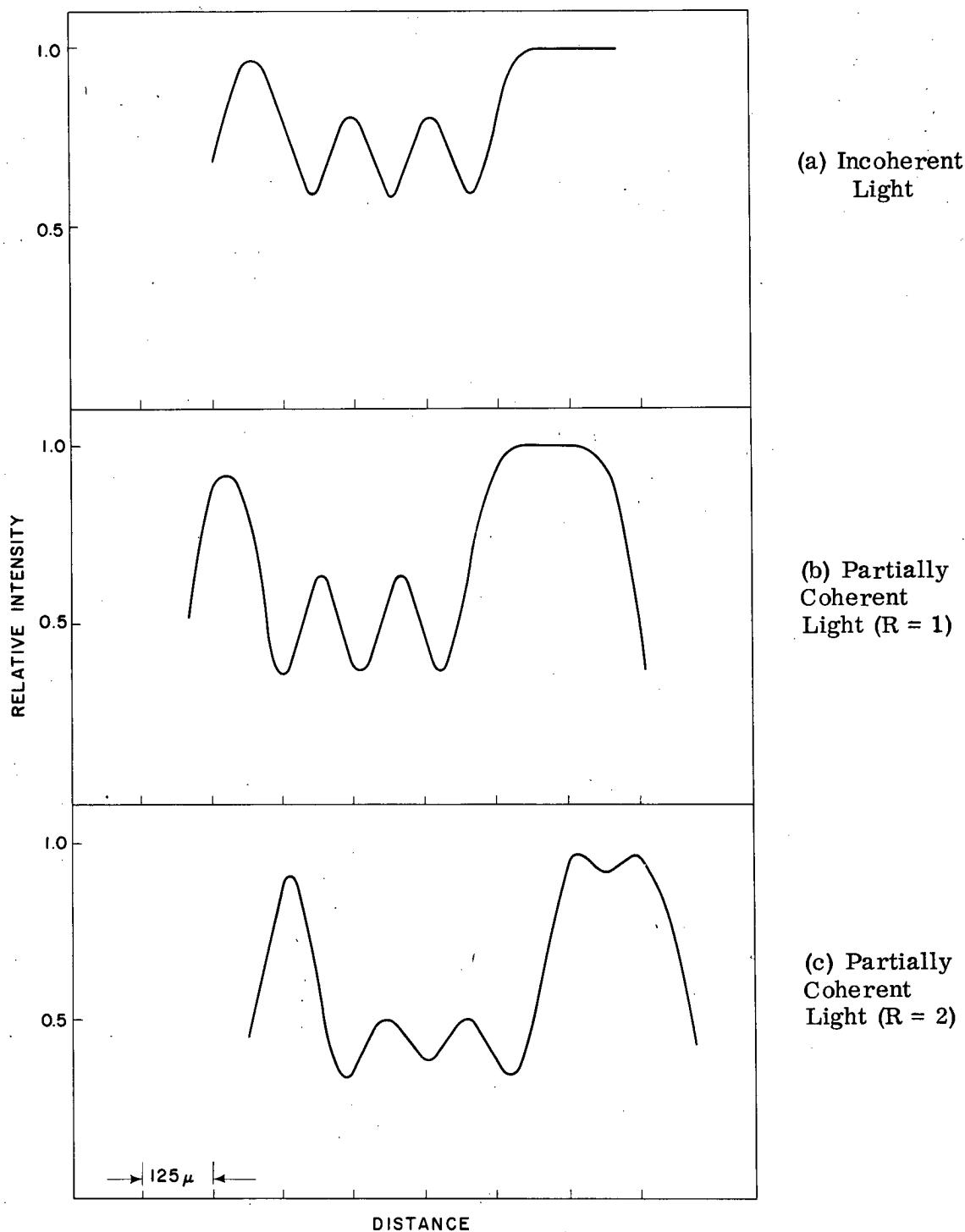
Figure 7. Experimental Images of a Long-Line Three-Bar Target
Group at 8 ℓ/mm Made with Imaging System of 7.25 Cycles/mm
Coherent Cutoff Frequency

2-14

25X1

SECRET

25X1

(d) Partially
Coherent
Light (R = 4)

(e) Partially
Coherent
Light (R = 16)
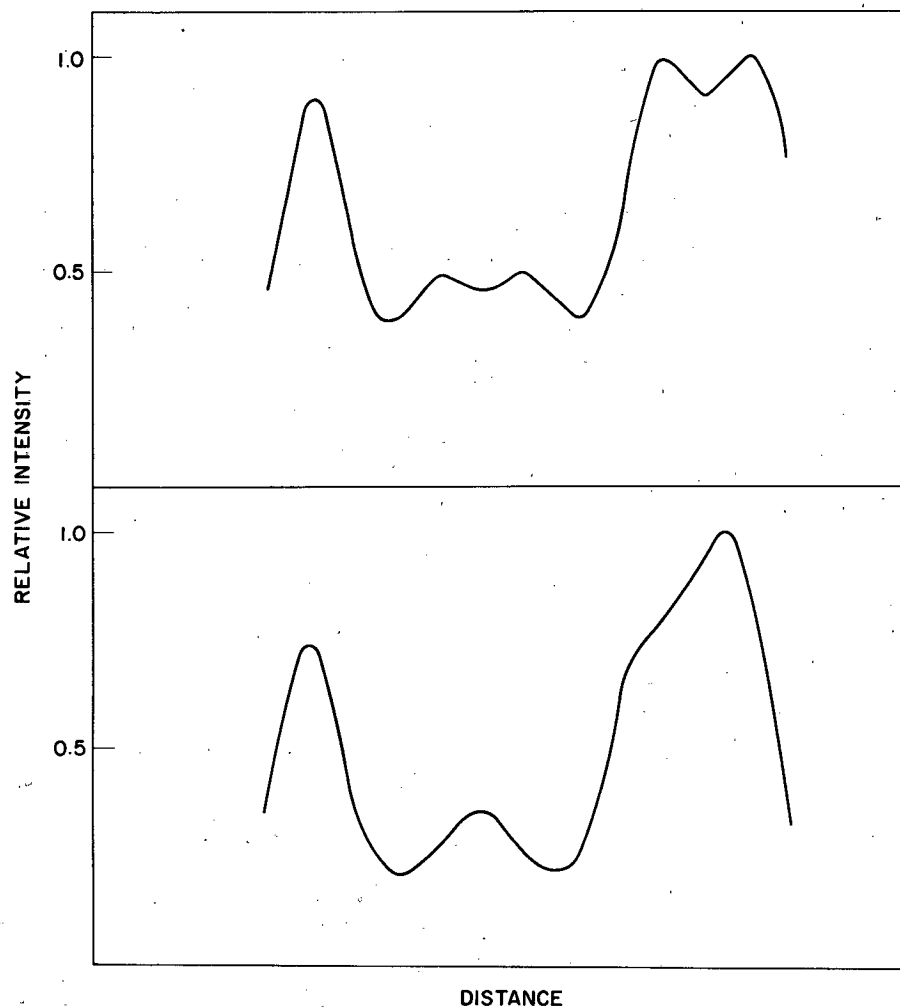
Figure 7 (Continued). Experimental Images of a Long-Line Three-Bar
Target Group at 8 ℓ/mm Made with Imaging System of 7.25 Cycles/mm
Coherent Cutoff Frequency

SECRET

SECRET

(a) INCOHERENT LIGHT

(b) PARTIALLY COHERENT LIGHT(R=1)

(c) PARTIALLY COHERENT LIGHT(R=2)

(d) PARTIALLY COHERENT LIGHT(R=4)

(e) PARTIALLY COHERENT LIGHT(R=8)

DISTANCE

RELATIVE DENSITY
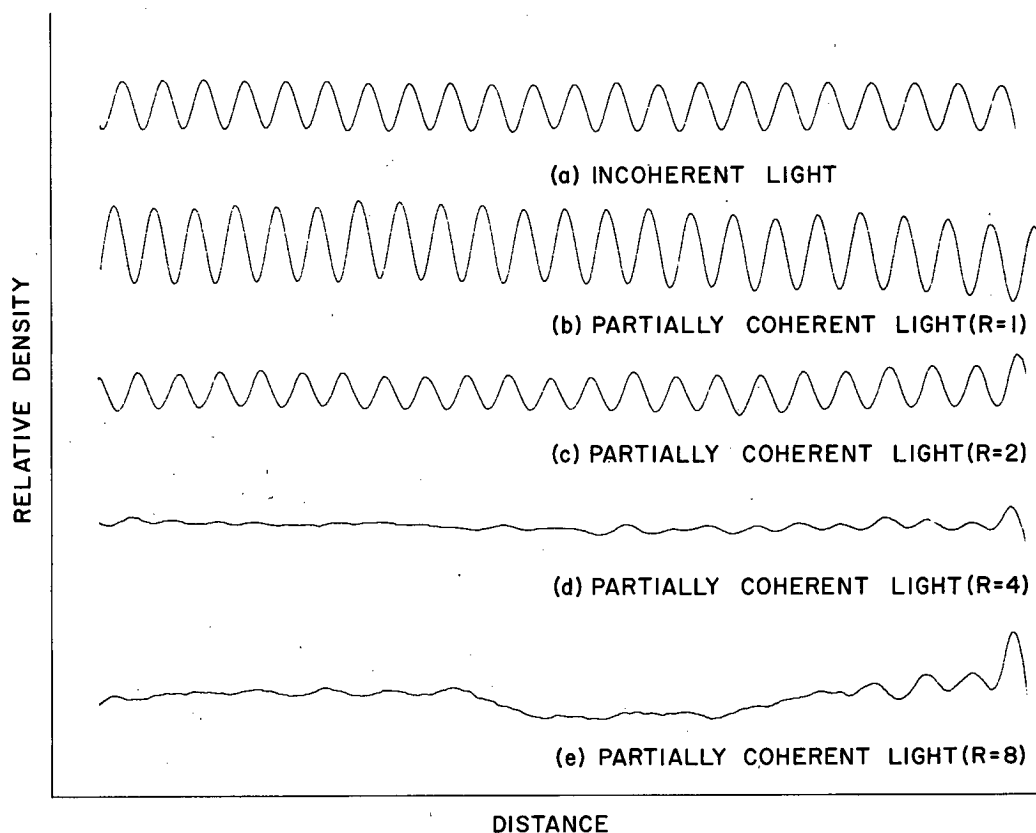
Figure 8. Microdensitometer Traces of Experimental Images
of a Sinusoidal Intensity Transmittance Target at 9 Cycles/mm
Made with Imaging System of 7.25 Cycles/mm Coherent
Cutoff Frequency
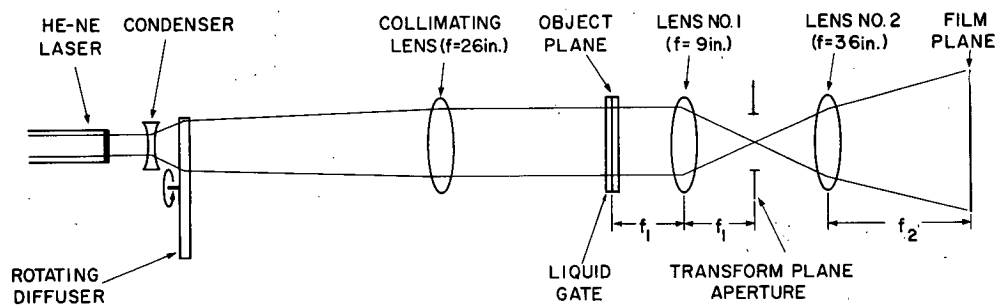
Figure 9. Enlarger Optical System Schematic

SECRET

IMPULSE RESPONSE
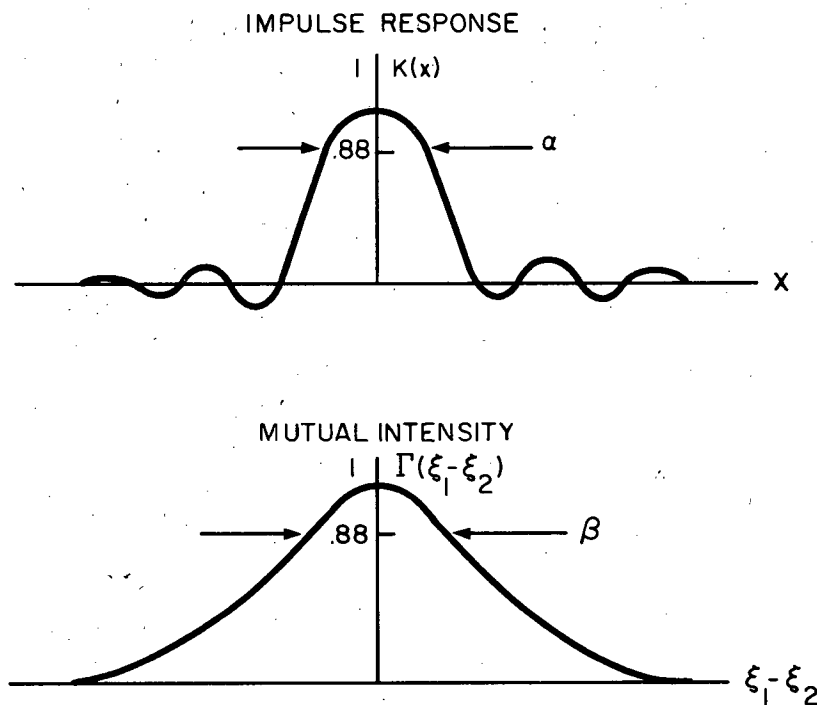
MUTUAL INTENSITY

Figure 10.   Impulse Response and Object Plane Mutual
Intensity Function of Enlarger

also varies; therefore, we must look at different groups in the object to look at
corresponding imaging conditions. In all the images in Figure 12 the frequency
of the three-bar group exceeded the coherent cutoff frequency by a factor of 1.10.
The images are, however, all drawn to the same scale. Although theoretical
image intensity distributions for these three-bar targets under the condition of
a gaussian mutual intensity function have not been calculated, we will compare
the experimental data with the theoretical results obtained, using a Bessinc
mutual intensity function. This comparison will provide information about the
dependence of the image structure on the particular functional form of the
object illumination mutual intensity.
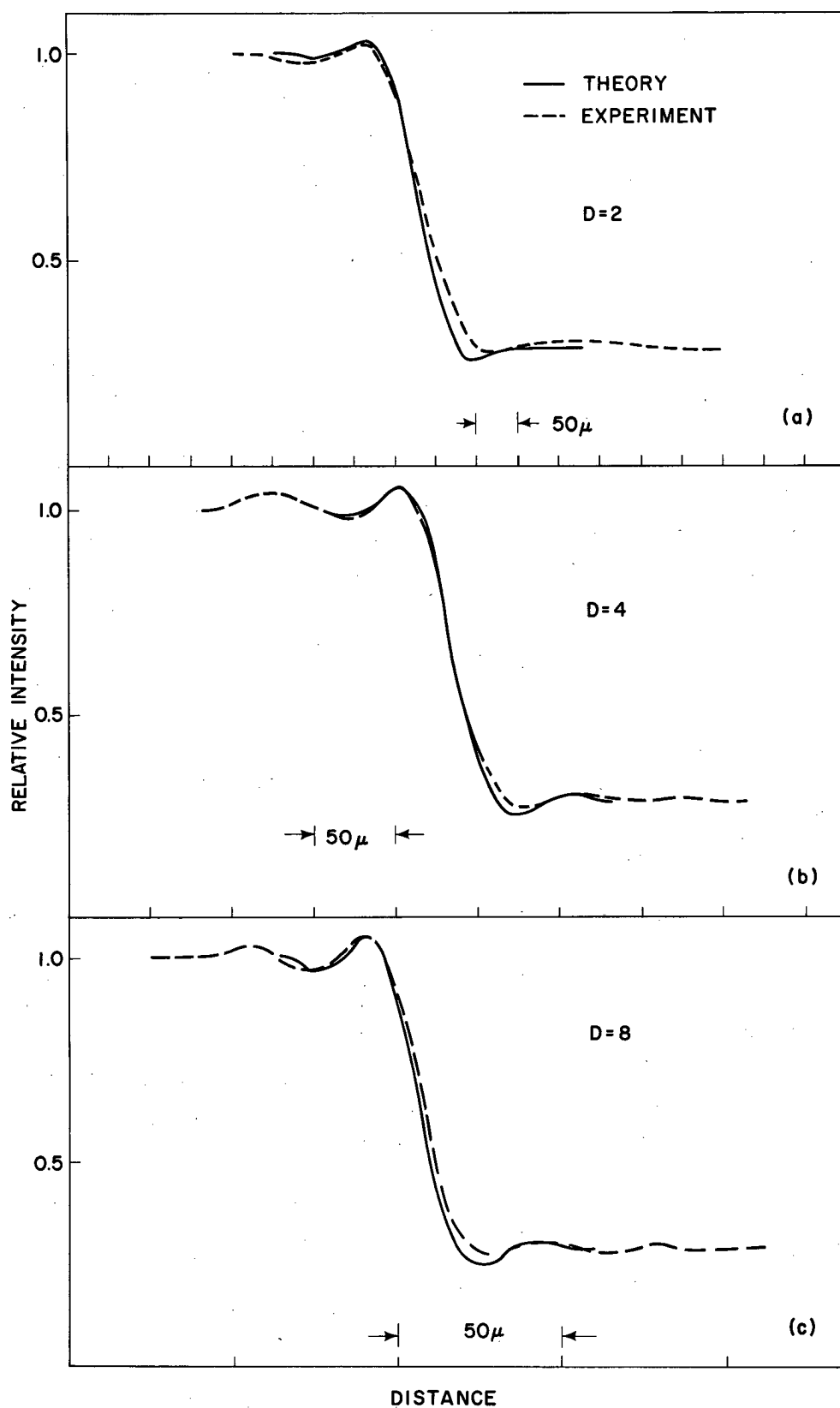
25X1

Figure 11. Theoretical and Experimental Edge Image Intensity Distributions for Enlarger Imaging System in Partially Coherent Light for Various Values of D

2-18

25X1

SECRET

STUDIES OF THE DEGREE OF COHERENCE OF MICRODENSITOM- ETER ILLUMINATION (Task 2C)

Task 2C is concerned with deter- mining the extent to which two basic assumptions made in microdensito- metric image evaluation are justified, namely that (1) the illumination in the preslit (primary slit) of a microden- sitometer may be regarded as in- coherent, and (2) the illumination in the object plane (sample plane, film plane) of a microdensitometer may be regarded as incoherent. In these in- vestigations the validity of the theory of partial coherence is assumed.

These two assumptions could be tested by a direct measurement of the complex degree of coherence $(\gamma_{12}(0))$ in the preslit and sample planes. However, since the smallest pinhole separation available for performing two-pinhole interference measure- ments is $50\,\mu$, and in microdensitom- etry coherence effects can become important for much smaller coherence intervals due to the high resolutions involved, we approached these prob- lems in a somewhat indirect manner.

Our experiments were performed using a Joyce-Loebl microdensitom- eter. A schematic of the optical sys- tem is illustrated in Figure 13.
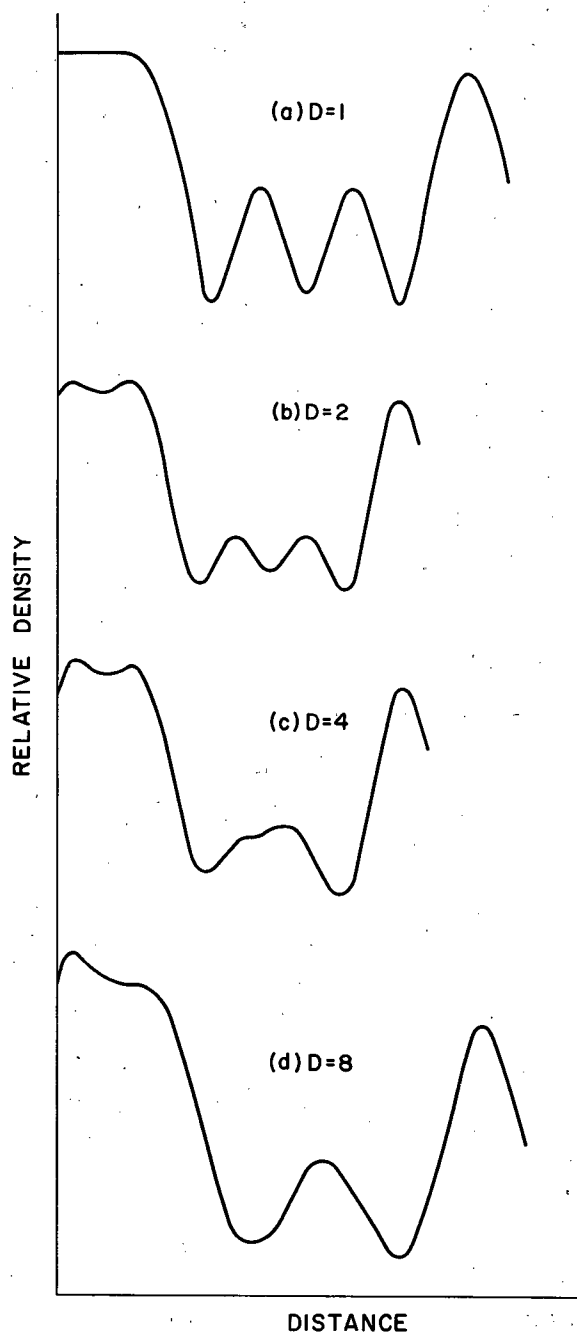
Figure 12. Microdensitometer Traces of Experimental Images of Long-Line Three-Bar Target of Spatial Frequency 1.1 Times the Coherent Cutoff Fre- quency of Enlarger Imaging System in Partially Coherent Light for Various Values of D

SECRET
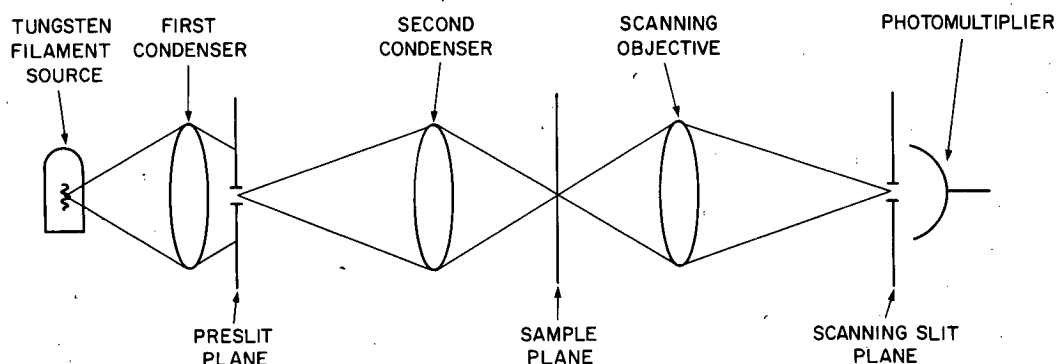
Figure 13. Schematic of Microdensitometer Optical System

Although there are also several prisms in the optical system to bend the beam along a path within the instrument itself, the prisms were not included in these experiments. The additional optical path they introduce, however, was compensated for. A No. 57 Wratten filter with a bandpass of about 800 Å centered at 5200 Å was used so that the spatial coherence measurements could be separated from temporal coherence effects. The fringe patterns, recorded in the far-field of the pinholes, were traced with a microdensitometer and the maxima and minima in the centers of the traces were reduced to relative intensities through a step-wedge exposure. The fringe visibilities, equal to $\left|\gamma_{12}(0)\right|$, were then found by

$$V = \frac{I_{max} - I_{min}}{I_{max} + I_{min}} .$$

With the ultimate aim of characterizing the coherence in the preslit and sample planes, two pinhole coherence measurements (at pinhole widths of 1.43 mm and 140 μ) were made in the plane of the second condenser (Figure 13). A knowledge of the coherence function in this plane allows the coherence function to be calculated in the preslit and sample planes. There are three special cases of interest which can arise:

1. If the illumination in the condenser is coherent, the illumination in the sample plane will be coherent.

25X1

2.   If the illumination in the condenser is incoherent, the coherence in the sample plane can be found using the van Cittert-Zernike theorem.

3.   If the illumination in the preslit is incoherent, the coherence in the condenser will arise from the van Cittert-Zernike theorem, and the measurements in the condenser can be related to the predictions of this theorem.

Measurements were first made for a preslit of width 1.43 mm, the results of which are shown in Figure 14, together with the results predicted by the van Cittert-Zernike theorem under the assumption that the preslit is uniformly, incoherently illuminated.   From this figure we note that the data are in good agreement.   The van Cittert-Zernike theorem also predicts that the coherence should be a function of coordinate differences only, and not of the position in the field.   In order to check this prediction, measurements at nine positions in the field, from the center to the edges, were made with the 100-μ pinhole separation.   The values of fringe visibility at all nine positions were equal within experimental error.   We can thus conclude that at preslit widths of 1.43 mm or larger it is a good assumption to consider the illumination in the preslit as incoherent.

Measurements of $\left|\gamma_{12}(0)\right|$ in the plane of the second condenser were then made for a preslit width of $140\,\mu$.   The results of these measurements are shown in Figure 15, again compared to what would be expected if the preslit was incoherently illuminated.   There is no particular correlation between this theoretical curve and the experimentally measured points.   Although more measurements are necessary before the coherence in the plane of the condenser can be characterized for this preslit width, we may conclude that at preslit widths of $140\,\mu$ or smaller the assumption that the preslit is incoherently illuminated is not a good one.

By applying to the microdensitometer the results obtained in the imaging calculations presented in Proposal No. TO-B 100-65, we have theoretically determined that the second basic assumption made in microdensitometric image evaluation, i.e., that the illumination in the object (or film) plane of a microdensitometer may be regarded as incoherent, is not justified.   Those calculations were done for a unit magnification imaging system.   By generalizing this result to imaging systems of other than unit magnification it has been found that the significant parameter in determining the importance of coherence effects may be written as the ratio of the

2-21   25X1

25X1

Figure 15. Measured Fringe Visibility in
Entrance Pupil of Second Condenser vs
Pinhole Separation for 140μ Width Preslit
Compared to Theoretical Curve for Inco-
herent Preslit Illumination

Figure 14. Measured Fringe Visibility in Entrance Pupil of
Second Condenser vs Pinhole Separation for 1.43 mm Width
Preslit Compared to Theoretical Curve for Incoherent
Preslit Illumination

2-22

25X1

numerical apertures of the imaging objective and the incoherent source which illuminates the object.

Now it is common practice in microdensitometric image evaluation to match the numerical apertures of the illuminating and imaging objectives of the microdensitometer. When the aperture of the illuminating objective may be regarded as incoherently illuminated, this corresponds to the situation represented by $a/b = 1$ in the results of the imaging calculations. Examination of the apparent transfer function curves for this situation shows that for both sine waves and edges the system is nonlinear in intensity, i.e., there are pronounced coherence effects. When the aperture of the illuminating objective cannot be regarded as incoherently illuminated and must be regarded as partially coherently illuminated, then the degree of coherence existing between the two typical points in the film plane can be expected to increase.

While the calculations presented in the proposal were for a one-dimensional imaging system (a system with slit sources, slit apertures, and one-dimensional object variations), it is known from past experience that the results in a two-dimensional situation can be expected to be qualitatively similar. Indeed, the above mentioned situation of matching numerical apertures in a microdensitometer corresponds to the case $R = 1$ in the imaging calculations presented previously. The degree of coherence can therefore not be expected to be less than that which exists for $R = 1$ and, as mentioned earlier, may be greater.

CONCLUSIONS

The theoretical and experimental imaging studies conducted to date show clearly that for a given object significant differences in the image intensity distribution are to be expected as the degree of coherence (mutual intensity) of the object illumination is varied. Using the theory of partial coherence, we have calculated the images of pure amplitude edges (Figure 2) and pure amplitude square wave targets (Figure 3) at the various degrees of coherence of object illumination represented by the various R values. Experimentally, we have found the images of pure amplitude edges (Figure 2), pure amplitude long-line three-bar targets (Figure 7), and a pure amplitude object which is an intensity sine wave (Figure 8). These experiments

have also been performed for the various degrees of coherence of object illumination represented by the various R values. At this point in the program the edge object is the only one for which theoretical and experimental results can be compared directly. It can be seen from Figure 2 that the agreement between theory and experiment is qualitatively excellent and quantitatively fairly good, being somewhat better in the more coherent cases. It can be concluded on the basis of the comparisons which are now possible that the theory of partial coherence provides an adequate and necessary description of the imaging process under the conditions of these investigations (i.e., scaled-up imaging systems). As more comparisons become available it will, of course, be possible to make more definite statements about the accuracy of the theory and to compare its predictions with that of the simpler incoherent theory.

The studies of the coherence of microdensitometer illumination have shown that the assumption of an incoherently illuminated preslit is a good assumption when the preslit width is 1.43 mm. (This corresponds roughly to the preslit width which would be used with a 10X condenser when a microdensitometer resolution of about 10 ℓ/mm is desired.) On the other hand when the preslit width is reduced by approximately a factor of 10 to 140 μ, the assumption of incoherent illumination in the preslit is not a good assumption. (This 140-μ preslit width can be said to correspond roughly to the preslit width which would be used with a 10X condenser when a microdensitometer resolution of about 100 ℓ/mm is desired.) It is not possible to state on the basis of these measurements the functional form or the characteristic width of the coherence function (mutual intensity) in the film plane. However, it can be concluded that at the smaller preslit width (140 μ) the assumption of an incoherently illuminated film plane is not a good one (this is also substantiated by the theory). In addition, since the determination of the degree of coherence (mutual intensity) in the preslit plane provides the boundary condition for the determination of the degree of coherence (mutual intensity) in the film plane, further work will employ the results of these measurements to ascertain the degree of coherence (mutual intensity) in the film plane.

SECRET
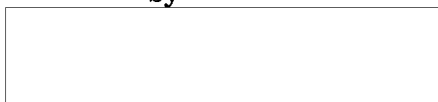
SIX MONTH TECHNICAL REPORT

TASK 8

PROJECT JS-492

January 13, 1967

by

25X1

25X1

SECRET

SECRET

I. EFFECTIVE EXPOSURE ANALYSIS

A. INTRODUCTION

The effective exposure concept has been used extensively in the analysis of performance of photographic systems. Basically, the concept is that the exposure that caused a particular density on film can be found by using the $D \log E$ curve for the film, and determining the exposure as given by the curve at that particular point. While this is certainly true for the static case, the evaluation of photographic system is based on measurements of system performance at relatively high spatial frequencies. Since the film itself becomes a degrading element in the total system it is obvious that the effective exposure concept cannot be valid at the higher spatial frequencies. The important question is the degree of error involved when using the hypothesis at the higher spatial frequencies. As far as can be determined, no quantitative investigation has been made of the relative validity of effective exposure, although the concept is used widely in image assessment research.

The effective exposure concept can be expressed as

$$D = f(E)$$

where D is density

E is exposure

and the functional relationship of the $D \log E$ curve is indicated by f .

This relationship is completely valid for the static case; indeed, this is how the curve is defined. However, at higher spatial frequencies, characteristics of film are not adequately defined. In an attempt to use conventional communication theory methods or photographic systems, a transfer function for film was introduced. The definition and method of determining this transfer function is described by Lamberts[*] and others. However, the main point to be made is that the effective exposure concept is used to determine the modulation transfer function of film. The advantage of this ap-

---

[*]   Lamberts, Robert L. "Measurement of Sine-Wave Response of a Photographic Emulsion", Journal of the Optical Society of America, May, 1959

1

SECRET

proach is that photographic system evaluation can be done by a simple cascading of transfer functions. This can be shown as :

$$E_0(f) = T_f(f) \times T_s(f) \times E_i(f)$$

where $E_i(f)$ is the Fourier transform of the input stimulus

           $T_s(f)$ is the transfer function of the system exclusive of the film

           $T_f(f)$ is the transfer function of the film

           $E_0(f)$ is the Fourier transform of the resultant image <u>after</u> con-

                  version to exposure units through use of the effective ex-

                  posure concept.

It is of interest to examine the model that this cascading of transfer functions implies.

We have: $D = f(E)$

           Defined by the sensitometric curve.

or $D(x) = f[E(x)]$ where a one-dimensional representation of distance,

           x , is used.

Now, $E_0(x) = f^{-1}[D(x)]$ where $E_0(x)$ is the exposure value determined

                  using effective exposure.

Now, $D(x) = f[\int_{-\infty}^{\infty} E_i(\tau)\, \omega\,(x-\tau)\, d\tau]$

where $\omega(x) \longleftrightarrow T_f(f)$

        $\longleftrightarrow$ indicates Fourier transform pairs

        $E_i(x)$ is the input exposure at the surface of the film

or $E_0(x) = f^{-1}[f(\int_{-\infty}^{\infty} E_i(\tau)\, \omega\,(x-\tau)\, d\tau)]$

                 $E_0(x) = \int_{-\infty}^{\infty} E_i(\tau)\, \omega\,(x-\tau)\, d\tau$

The model for this is shown in Figure 1.

SECRET
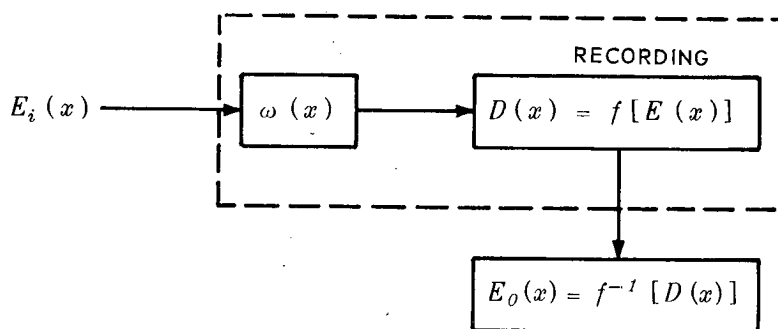
Figure 1.

The problem is that the degradation and recording steps are not separable operations, as the effective exposure concept implied, but rather are one operation which may or may not be approximated by a linear convolution and a nonlinear recording operation.

B. EXPERIMENTAL PROCEDURE

In general the $D \log E$ curve, or the static response of film is used in research work. However, to investigate the properties of film imaging at higher spatial frequencies, a test signal or input stimulus is required. The most convenient one to use from the standpoint of analysis of results is a sine wave. For photographic work this should be a sine wave linear in intensity.

To generate such a waveform the technique described by Swing and Shin[*] is used. The technique will not be described here since it is adequately explained in the original paper.

The aerial image intensity is given by

$$h^2(z, j) = C[1 + m \cos(j \omega_0 z)]$$

where
$$C = A^2(0) + A^2(j \omega_0)$$

---

[*] Swing, R.E. and Shin, M.C.H., "The Determination of Modulation Transfer Characteristics of Photographic Emulsions in a Coherent Optical System", Photographic Science and Engineering, November-December, 1963.

3

SECRET

and

$$M = \frac{2 A (j \omega_0) A(O)}{A^2 (O) + A^2 (j \omega_0)}$$

and $A(j \omega_0)$ is the complex amplitude function of the first order, and $A(O)$ is the amplitude function of the zero order z is the distance function, and $\omega_0 = 2\pi f_0$ where f_0 is the fundamental line spacing of the diffraction grating. C is the average intensity, and M is the modulation.

If we let

$$B^2 = \frac{A^2 (j \omega_0)}{A^2 (O)} \quad ,$$

then

$$M = \frac{2 \sqrt{B^2}}{1 + B^2} \quad ,$$

so the modulation is simply a function of the ratio of the intensities of the two orders.

The average light intensity is the sum of the intensities of the orders.

Of course a diffraction grating generates all odd harmonies of the fundamental frequency. To generate a sine wave intensity, all except the two orders desired are blocked at the transform plane. It might be noted that frequencies other than the fundamental can be generated by using combinations of orders other than zero and one. The resultant frequency in this case is the sum of the spatial frequencies of the orders used.

The coherent light is generated by using a mercury arc lamp and passing the light through a narrow band interference filter and a pinhole aperture. The pass band of the interference filter is shown in Figure 2.

The modulation is determined in practice by using neutral density filters in the transform plane to modify the light available in a particular order. The average intensity is modified by a combination of neutral density filters and exposure times.

C.   DATA ANALYSIS PROCEDURE

Several properties of film can be investigated with the experimental apparatus available. A primary property to be determined is the absence or presence of harmonic distortion when data is analyzed in effective exposure. If significant harmonics are generated by using this procedure, then certainly the effective exposure concept is not

4

SECRET

25X1

DATE 9/16/66

INSTRUMENT Cary 14

CALIBRATION

FULL SCALE 100%

AMBIENT TEMP 73°F

5700Å   5580Å

5461Å

5400Å   5300Å

FIGURE 2. PASSBAND OF INTERFERENCE FILTER
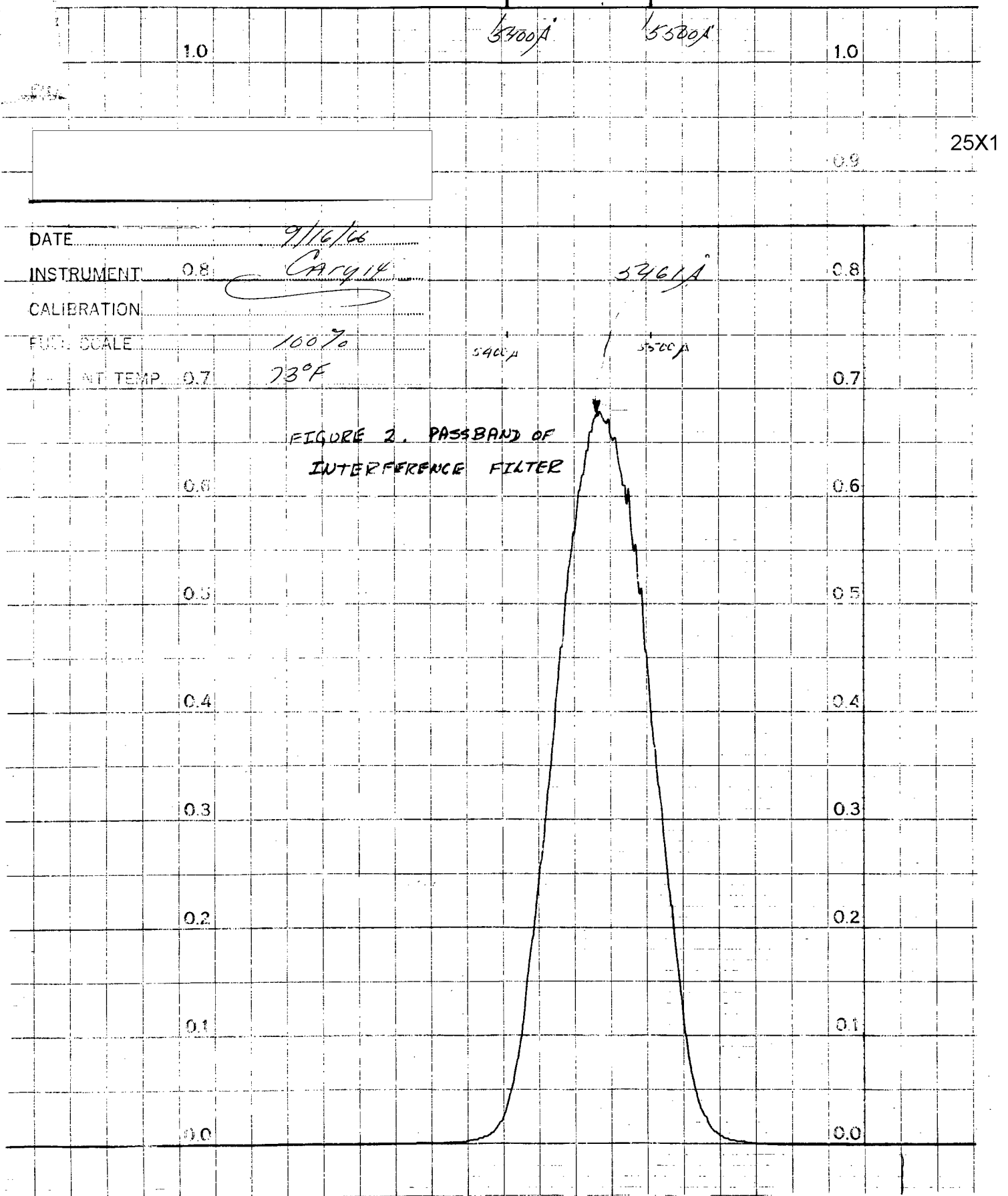
SECRET

valid. As long as the density obtained is not on the toe or shoulder of the $D \log E$ curve, the average density level and input modulation should not be a factor in the analysis. That is, if the effective exposure concept is valid (or a reasonably good approximation) then distortion should be zero when exposure units are used, regardless of density level or modulation, as long as the total range of variation is on the reasonably straight portion of the $D \log E$ curve.

When a sine wave input is used, total distortion is defined by:

$$D = \frac{[a_2{}^2 + a_3{}^2 + a_4{}^2 - - -]^{1/2}}{a_1}$$

where

$$a_n{}^2 = a_n{}^2 + b_n{}^2$$

where a_n and b_n are the Fourier series coefficients.

That is:

$$a_n = \frac{1}{T} \int_{-T/2}^{T/2} f(x) \cos \frac{2\pi n x}{T} \; dx$$

$$b_n = \frac{1}{T} \int_{-T/2}^{T/2} f(x) \sin \frac{2\pi n x}{T} \; dx$$

Where T is the period of the function under investigation, and $f(x)$ is the function itself.

Because of the grain noise, the procedure used to compute distortion is modified by tracing long records of data rather than one cycle of the fundamental. The power spectral density of the record is computed, using the relationship:

$$P(f) = \frac{1}{X} \left[\left(\int_0^X f(x) \cos \omega x \; dx \right)^2 + \left(\int_0^X f(x) \sin \omega x \; dx \right)^2 \right]$$

The coefficients of the Fourier series of a periodic function are related to the power spectral density by:

$$a_n{}^2 + b_n{}^2 = \frac{P(n f_0)}{X}$$

where X is the total length of the record, and f_0 is the fundamental frequency.

The distortion associated with each harmonic can be expressed as:

6

SECRET

$$D_n = \sqrt{\frac{a_n{}^2 + b_n{}^2}{a_1{}^2 + b_1{}^2}} = \sqrt{\frac{P(n\,f_0)}{P(f_0)}}$$

Identical computations are carried out in exposure and density units. One would certainly expect to see more distortion in density units if the effective exposure hypothesis is a good approximation. The resultant modulation is also computed by determining the maximum and minimum in terms of exposure units. This is computed by:

$$M_0 = \frac{E_{max} - E_{min}}{E_{max} + E_{min}}$$

The necessary calibration data is generated by placing on the same strip of film a step wedge using the same spectral properties for the source as that used in making the test material. The step wedge is then scanned with the microdensitometer at the same calibration settings that are used in taking the sample data. In this way the micro-densitometer is used only as a function generator, and the actual calibration is done in the computer.

The computations are done by a high speed digital computer, utilizing an algorithm to compute the necessary sine and cosine terms.

D. RESULTS AND CONCLUSIONS

Test samples were generated and analyzed for spatial frequencies of 40, 80, 120, 160, and 240 cycles/mm. These samples were at different input modulations and various average density levels. The results of the analysis can be used to examine both the effects of different modulations at a given density, and the effect of holding input modulation constant and moving up and down the $D \log E$ curve. Figure 3 shows the sensitometric data for the test material.

The data was generated by setting the modulation by the use of filters, and varying the exposure time to obtain different average density levels. Three different average densities were obtained for each modulation. Figure 4 shows the second harmonics obtained for each modulation level as a function of average density. These are the harmonic distortions when computed in effective exposure. Figure 5 shows the results when density units are used in the computation.

7

SECRET

FIGURE 3. SENSITOMETRIC DATA

FOR TEST MATERIAL - 3404 FILM

VERSOMAT PROCESSING

"MX" CHEMISTRY

GREEN INTERFERENCE FILTER

GAMMA = 2.0

SECRET

FIGURE 4   SECOND HARMONIC DISTORTION
AS A FUNCTION OF AVERAGE
DENSITY
(EFFECTIVE EXPOSURE)
40 cycles/mm 2v. 4 FILM

4 INPUT MODULATIONS

$m_1 = .92$
$m_2 = .87$
$m_3 = .75$
$m_4 = .56$

$\overline{D}$ - AVERAGE DENSITY

FIGURE 5

SECOND HARMONIC DISTORTION
AS A FUNCTION OF
AVERAGE DENSITY
(DENSITY UNITS)

40 CYCLES/mm - 3409 FILM

4 INPUT MODULATIONS

$M_1 = .92$
$M_2 = .67$
$M_3 = .75$
$M_4 = .56$

SECOND HARMONIC DISTORTION (%)

D - AVERAGE DENSITY
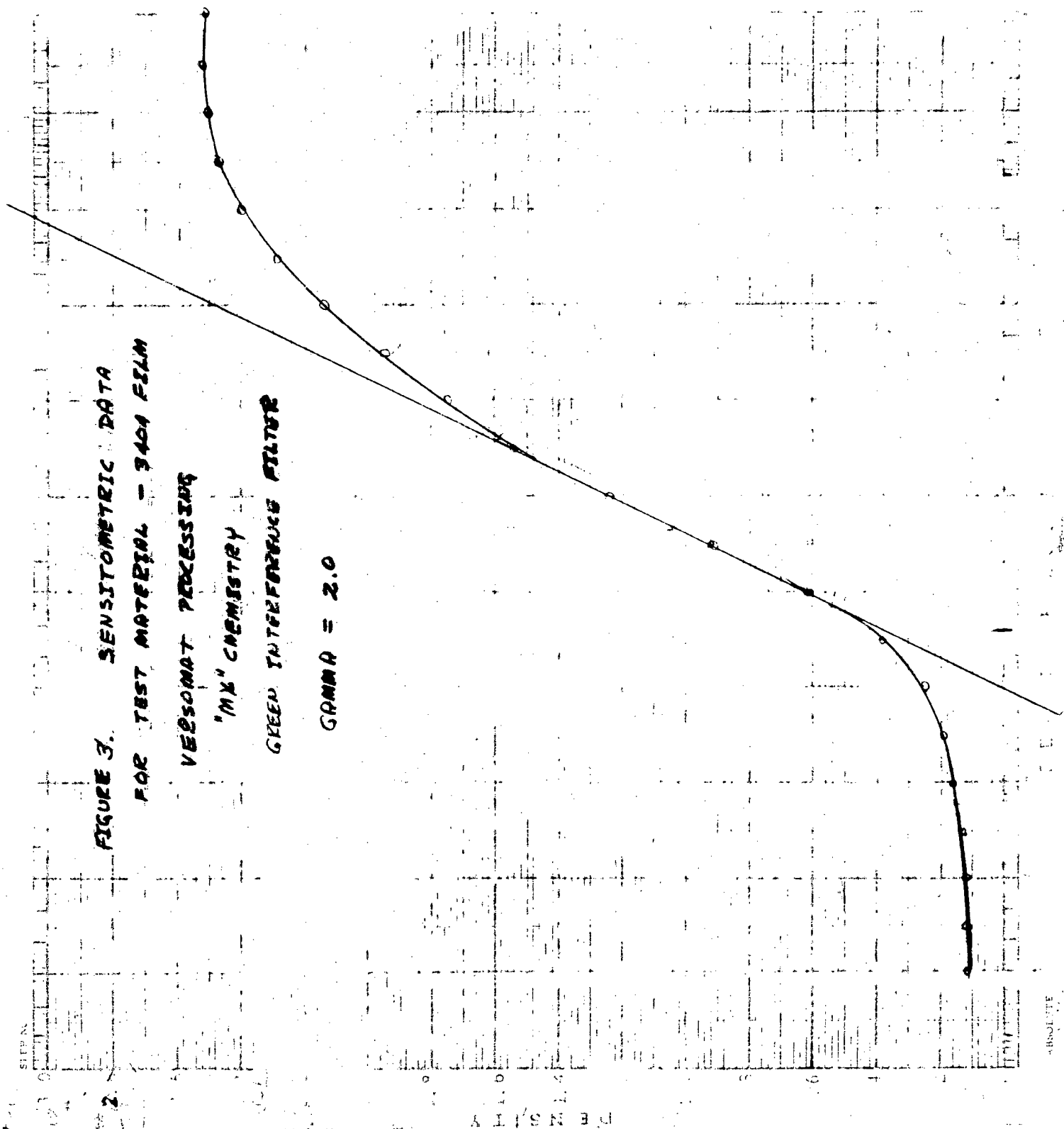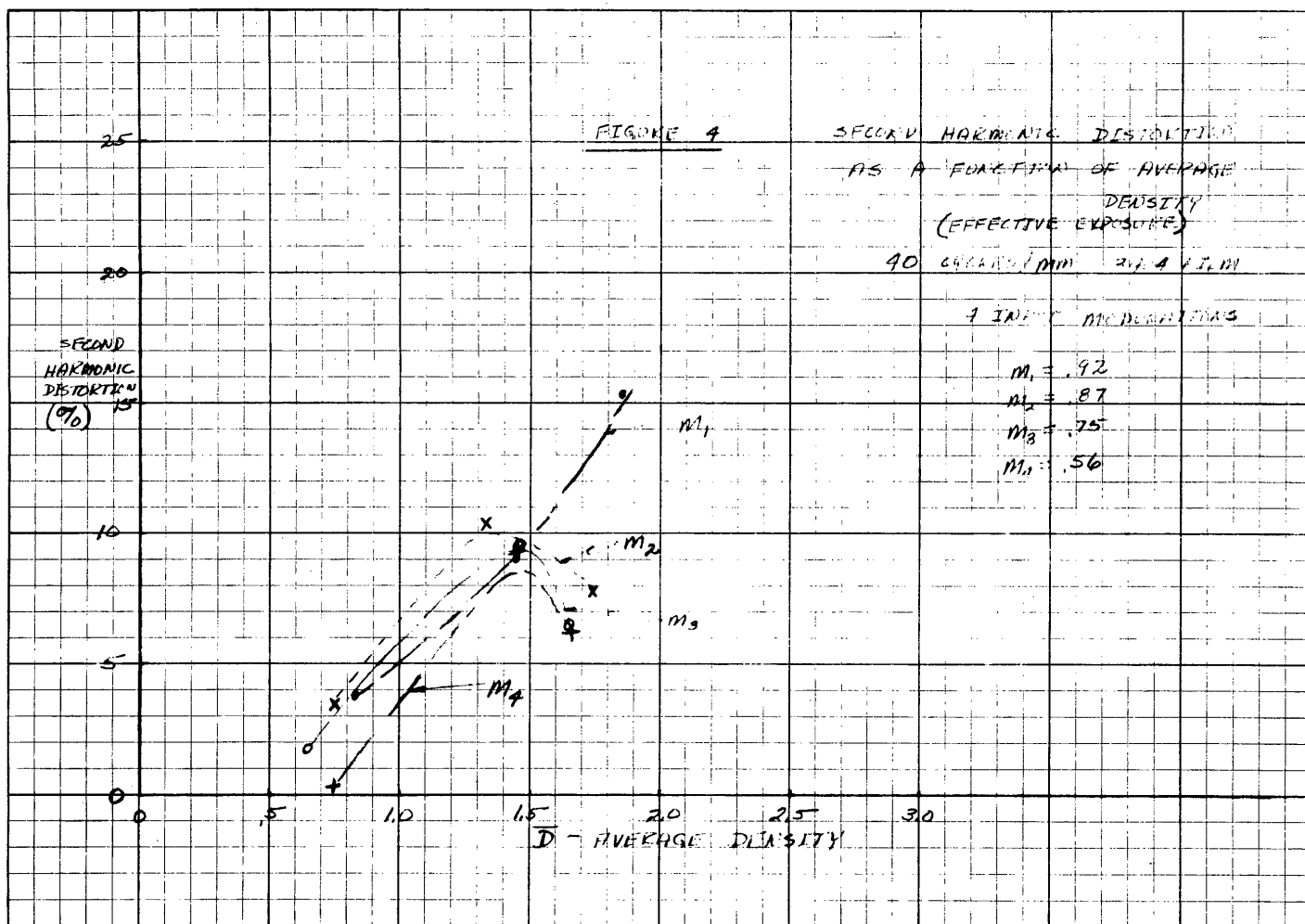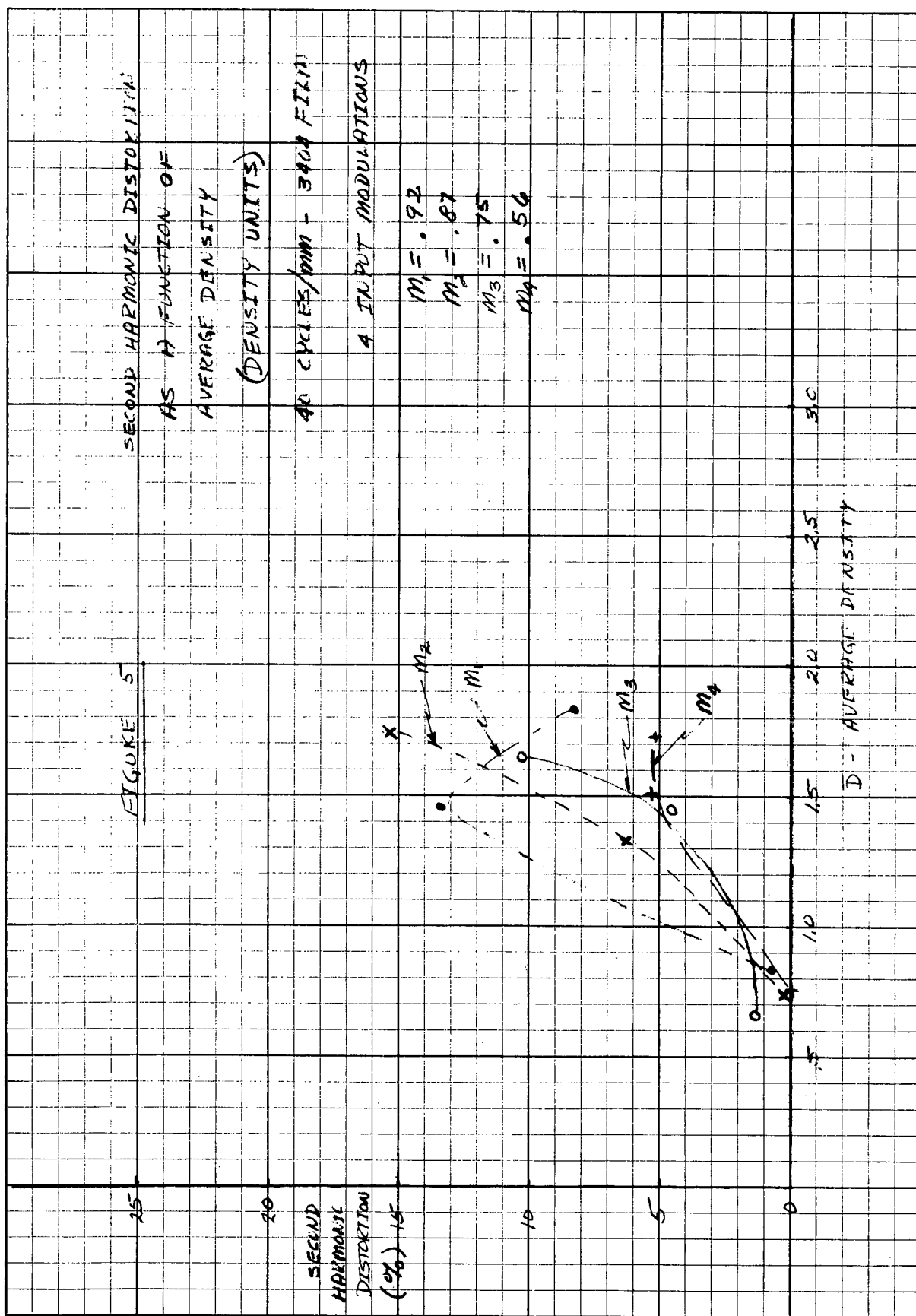
SECRET

One can see that in all cases the harmonic distortions are significant when exposure units are used, and are generally the same magnitude or higher than corresponding distortions computed in density. It is also apparent that the percent distortion increases significantly as the average density goes higher. This means, of course, that the response characteristics of the film change with density level and the specification of film properties becomes difficult and practically impossible in a relatively simple way.

Figures 6 and 7 show the data for 80 cycles per millimeter presented in the same format. The same trends are indicated by this data. It should be noted that the magnitude of the distortion is considerably less than that in the lower frequency case.

In all cases, the third and fourth harmonics were computed and the distortions were always less than 1.5%, which is relatively insignificant compared to that obtained for the second harmonic distortions.

Data for 160 and 240 cycles per millimeter was generated and analyzed. The trends of this data were all consistent with the results reported, although the distortions were always under 2 percent. The exposure times were so long for these frequencies that reciprocity law failure in the film becomes an important factor and calibration data becomes difficult to generate. Figures 8 and 9 show the results obtained from the 120 cycles per millimeter material.

It can be seen that as the modulation is decreased, the harmonic distortion decreases. This is to be expected, since the small signal case can generally be well approximated by a linear system.

The output modulations for all the data were also computed by using peak-to-peak measurements in exposure units. That is, the modulation was computed as:

$$M_0 = \frac{E_{max} - E_{min}}{E_{max} + E_{min}}$$

This is the standard way output modulation are computed in the determination of modulation transfer functions for film. Of course, this approach ignores the harmonic content of the signal. The results of these measurements are shown in Figure 10, which is a plot of the computed output modulation as a function of the average density, with the

11

SECRET

SECRET

SECOND HARMONIC DISTORTION

AS A FUNCTION OF DENSITY

(EFFECTIVE EXPOSURE)

30 CYCLES/MM - 3404 FILM

3 EXPOSURE MAGNIFICATIONS

$M_1 = .96$

$M_2 = 8.2$

$M_3 = 65$

FIGURE 9

SECOND HARMONIC DISTORTION (%)

10   7.5   5   2.5   0

D - AVERAGE DENSITY

0   .5   1.0   1.5   2.0   2.5   3.0

M_1 M_3 M_2

SECRET

SECRET

FIGURE 7

SECOND HARMONIC DISTORTION
AS A FUNCTION OF AVERAGE
DENSITY

(DENSITY UNITS)

80 CYCLES/MM — 3404 FILM

3 INPUT MODULATIONS

$M_1 = .96$

$M_2 = .82$

$M_3 = .65$

SECOND HARMONIC DISTORTION (%)

$\bar{D}$ = AVERAGE DENSITY

13

SECRET

SECRET

SECOND HARMONIC DISTORTION
AS A FUNCTION OF
AVERAGE DENSITY

(EFFECTIVE EXPOSURE)

120 CYCLES/MM — 3404 FILM

3 INPUT MODULATIONS

$M_1 =$

$M_2 =$

$M_3 =$

FIGURE 6

14

SECRET

SECRET

SECOND HARMONIC DISTORTION
AS A FUNCTION OF
AVERAGE DENSITY
(DENSITY UNITS)

120 CYCLES/MM 3404 FILM

3 INPUT MODULATIONS

$M_1 = .94$

$M_2 = .80$

$M_3 = .63$

FIGURE 9

SECOND HARMONIC DISTORTION (%)

$\bar{D}$ - AVERAGE DENSITY

SECRET

SECRET

FIGURE 10

MEASURED OUTPUT MODULATION

AS A FUNCTION OF AVERAGE DENSITY (INPUT MODULATION HELD CONSTANT)

3404 FILM

$M_1 = .92$
$M_2 = .87$
$M_3 = .75$
$M_4 = .56$
$M_5 = .96$
$M_6 = .82$
$M_7 = .65$
$M_8 = .94$
$M_9 = .80$
$M_{10} = .63$

$\overline{D}$ - AVERAGE DENSITY

16

SECRET

input modulation held constant. Various input modulations were used, with the values of each given input modulation indicated.

As one can see from the data, the value of modulation transfer function is not single valued (for a given frequency) but rather is a function of the operating point in density. Indeed, the harmonic analysis shows that a true modulation transfer function cannot exist, since the output of a linear system when a sine wave input is used is a distortion-free sine wave of the same frequency with only the amplitude and/or phase angle modified.

In order to present a better physical picture of the difference in waveforms of the images, Figures 11 through 19 are microdensitometer traces of the test material with spatial frequencies varying from 11.9 through 240 cycles per millimeter.

If one examines the waveforms of the traces as the spatial frequency goes up, the different shapes are readily apparent. At a relatively low frequency, the distortion of the waveform from a true sine wave is apparent, which is to be expected, since the units on the chart are density. However, at a higher frequency such as 80 or 120 cycles per millimeter the density trace more closely resembles a sine wave, which means that converting to effective exposure, which is approximately a logarithmic transformation would introduce distortion.

The experiments that have been run were utilizing a stylized input stimulus. Since the effective exposure concept is not a good approximation, the properties of small-scale images are very difficult, and perhaps impossible to predict. However, it may be possible to construct a good model of film response by utilizing a nonlinear representation. The data available from these experiments will be useful in studying the approach to the problem, and verifying any model that is developed.

The data generated must be qualified to some extent, as is true of most photographic experiments. Because of the method used, there is no doubt that the input stimuli is a true sine wave in intensity. However, the light is coherent, and whether there is any significant difference of film response between coherent and incoherent or partially coherent light has not been determined. The exposure times used to generate the material were considerably longer than generally used for 3404 film, which introduces the factor of reciprocity law failure. The exposure times used were on the order

17

SECRET

FIGURE 11

11.9 cyc/mm

INPUT MODULATION = .94

EXPOSURE TIME = 20 sec.

DENSITY

3.0

2.0

1.0

0

#6

18
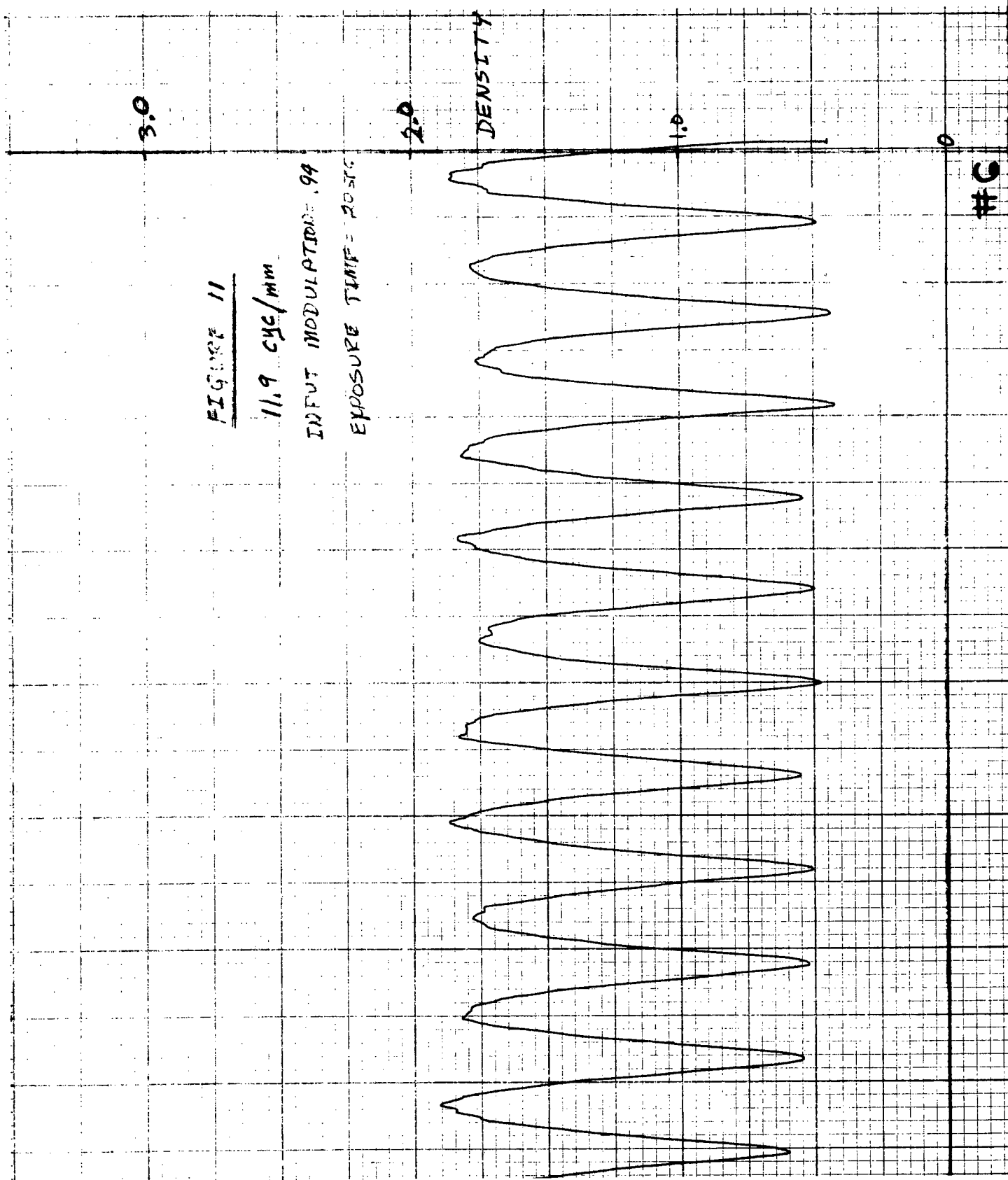
SECRET

FIGURE 12

20 CYC/MM

EXPOSURE TIME 60 SEC.

INPUT MODULATION = .90
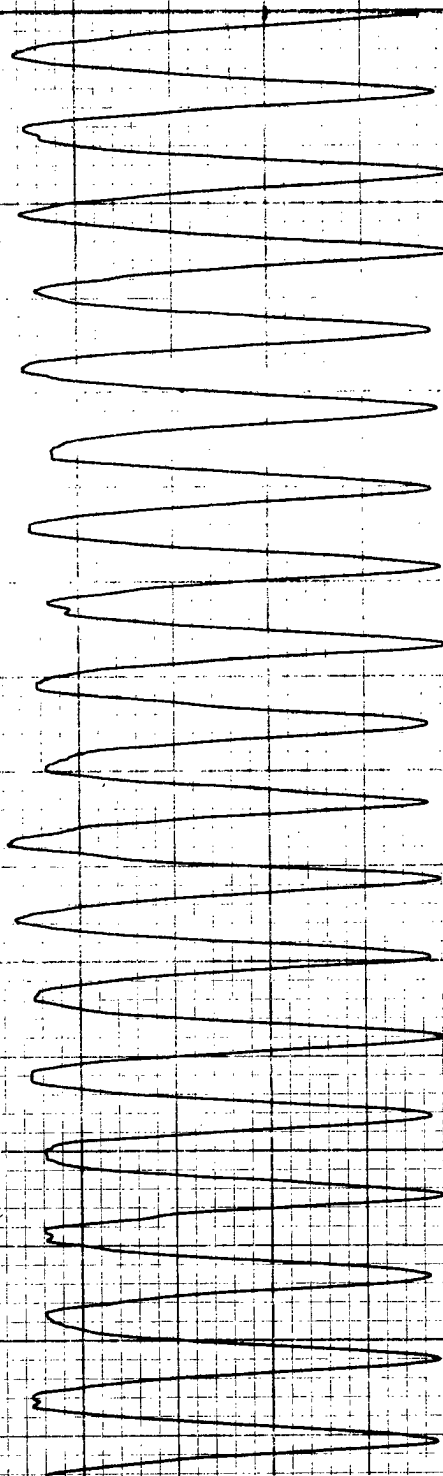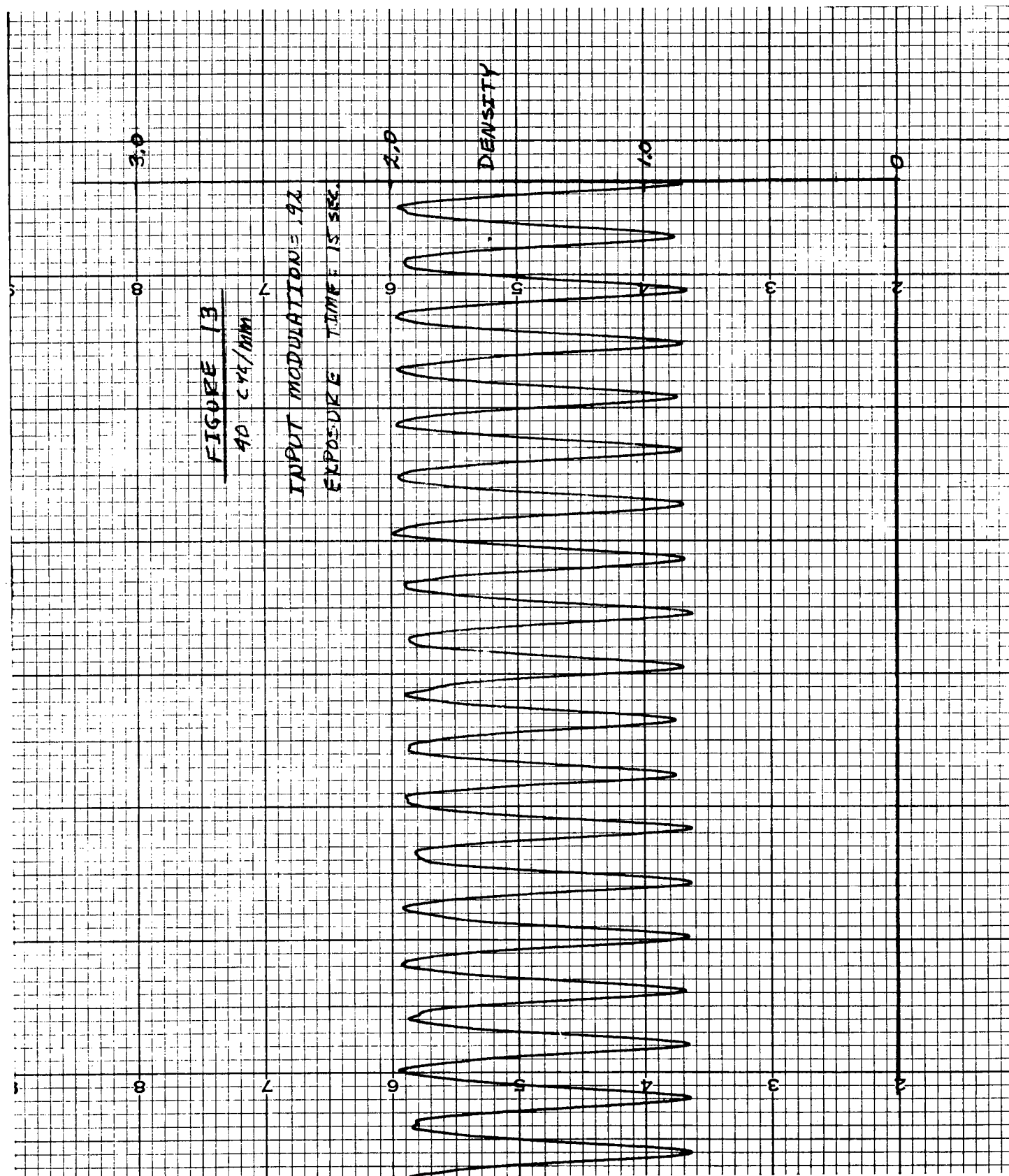
FIGURE 13
40 cy/mm

INPUT MODULATION = .94
EXPOSURE TIME = 15 SEC.

DENSITY

FIGURE 14

40 CYC/MM

INPUT MODULATION = .56

EXPOSURE TIME = 15 SEC

FIGURE 15

80 CYC/MM

INPUT MODULATION = .96

EXPOSURE TIME = 40 SEC

SECRET

FIGURE 16
80 CYC/MM
INPUT MODULATION = .65
EXPOSURE TIME =

DENSITY

23

SECRET

FIGURE 17

120 CYC/MM

INPUT MODULATION = .94

EXPOSURE TIME = 20 MIN

DENSITY

SECRET

FIGURE 18

160 cyc/mm

INPUT MODULATION = .90

EXPOSURE TIME = 15 MIN

SECRET

FIGURE 19

240 CYC/MM
INPUT MODULATION = .95
EXPOSURE TIME = 15 MIN.
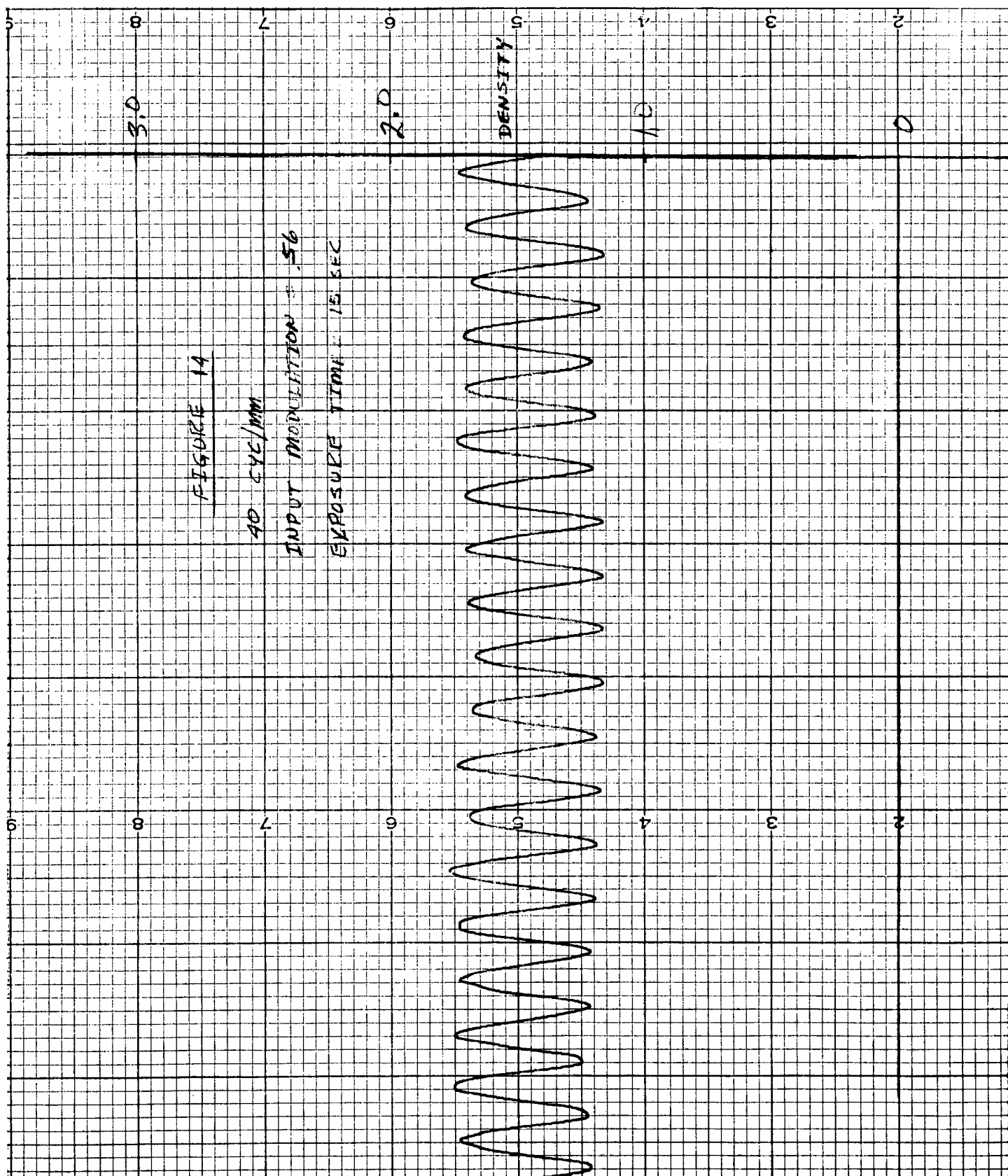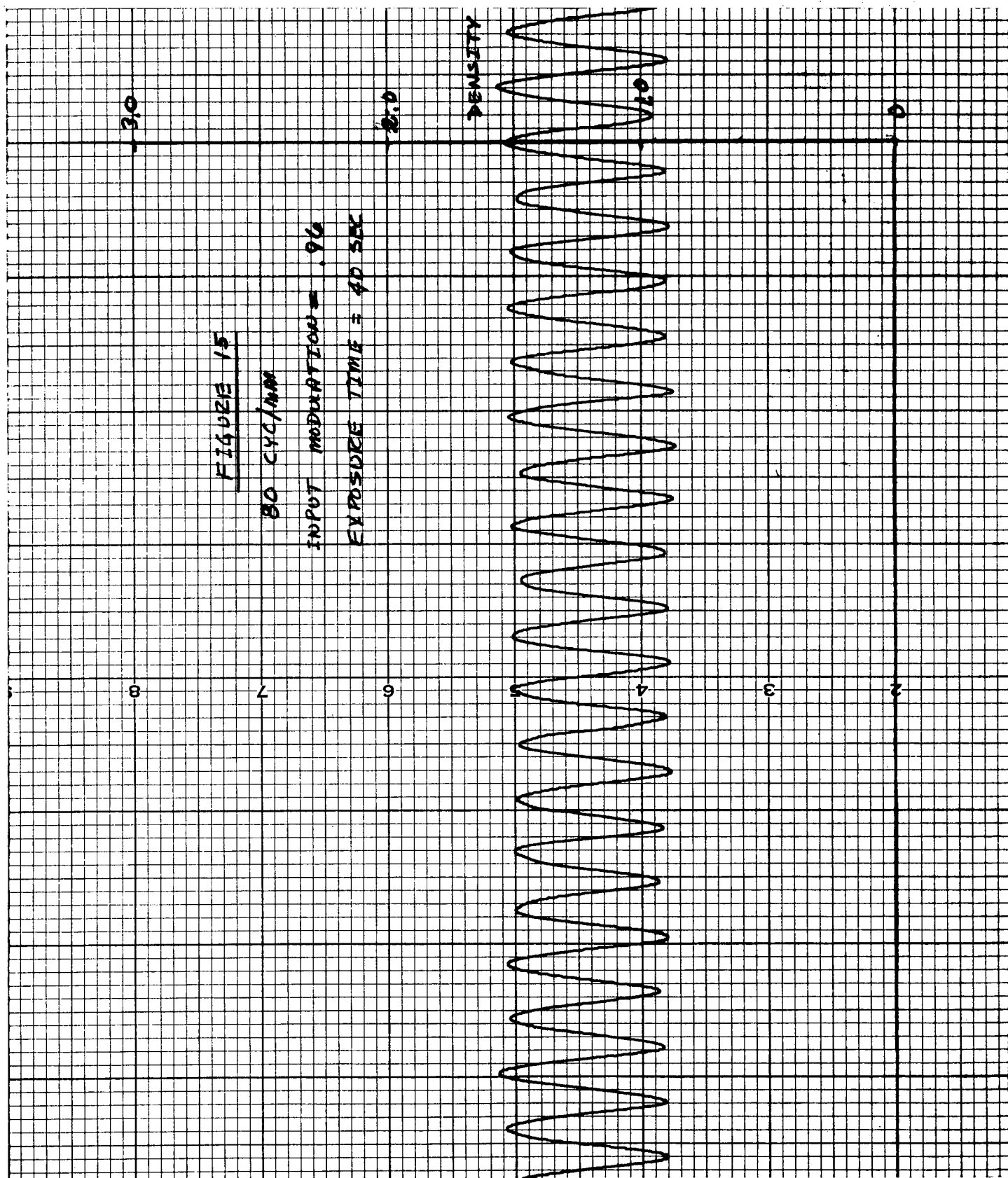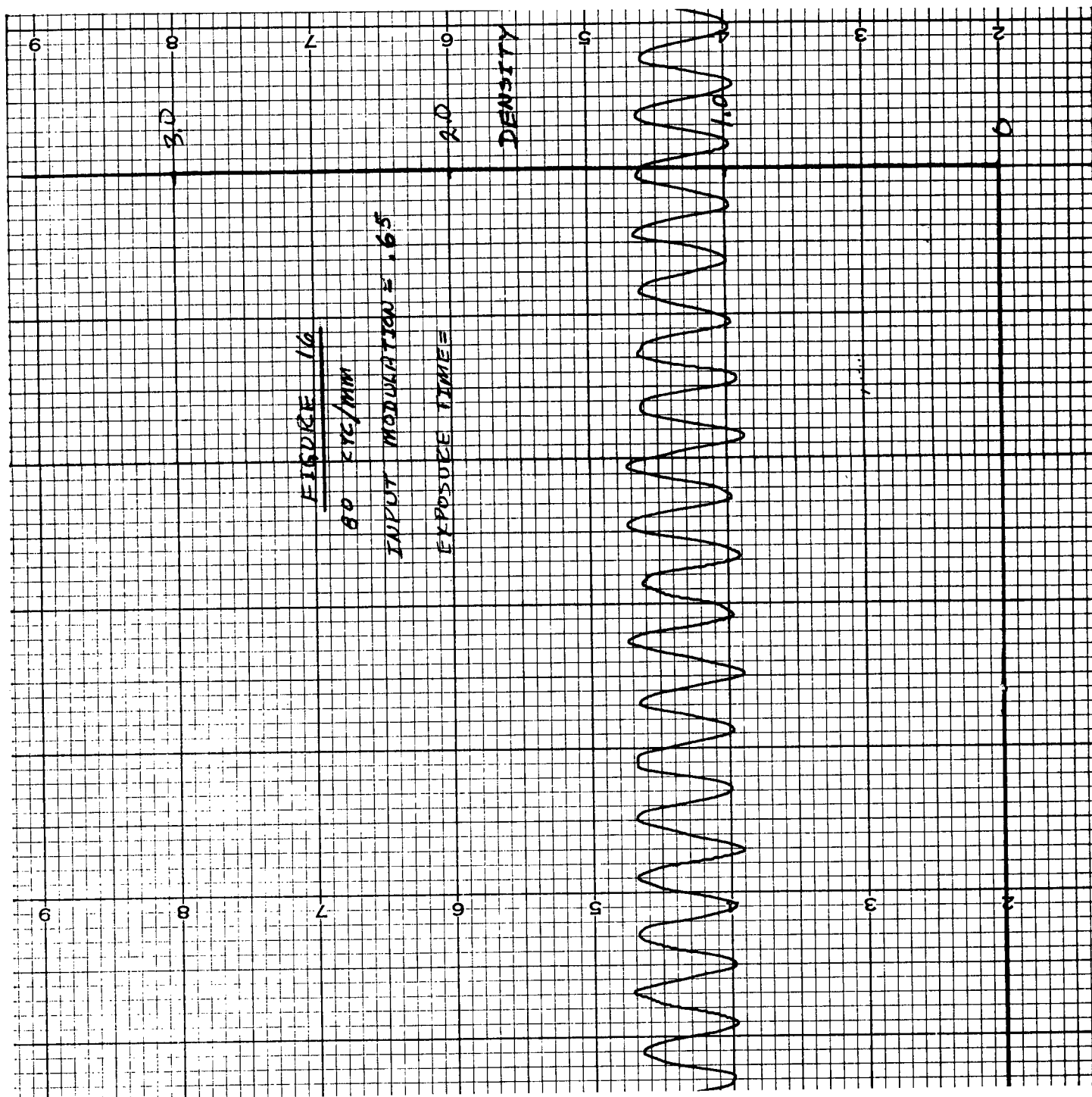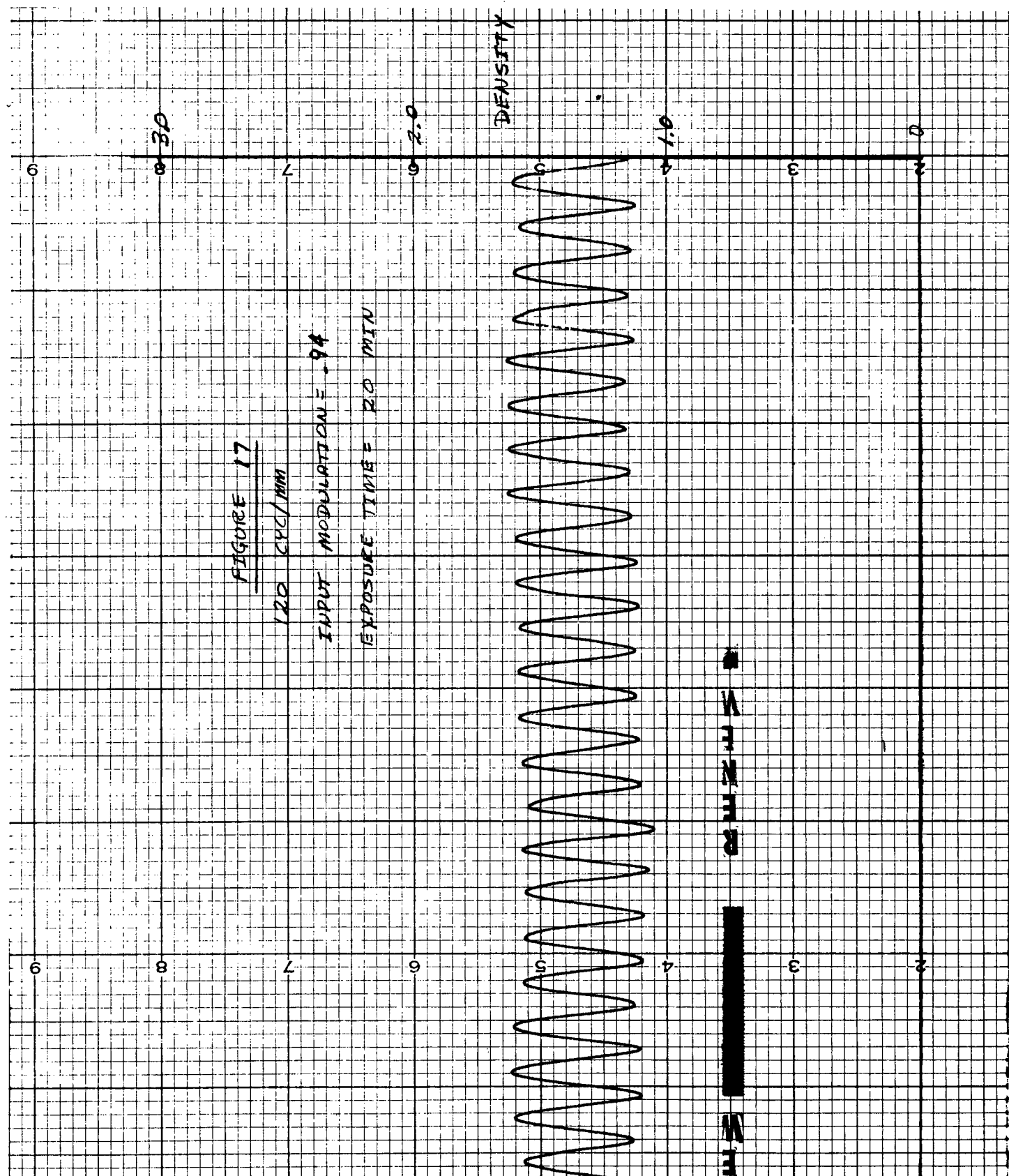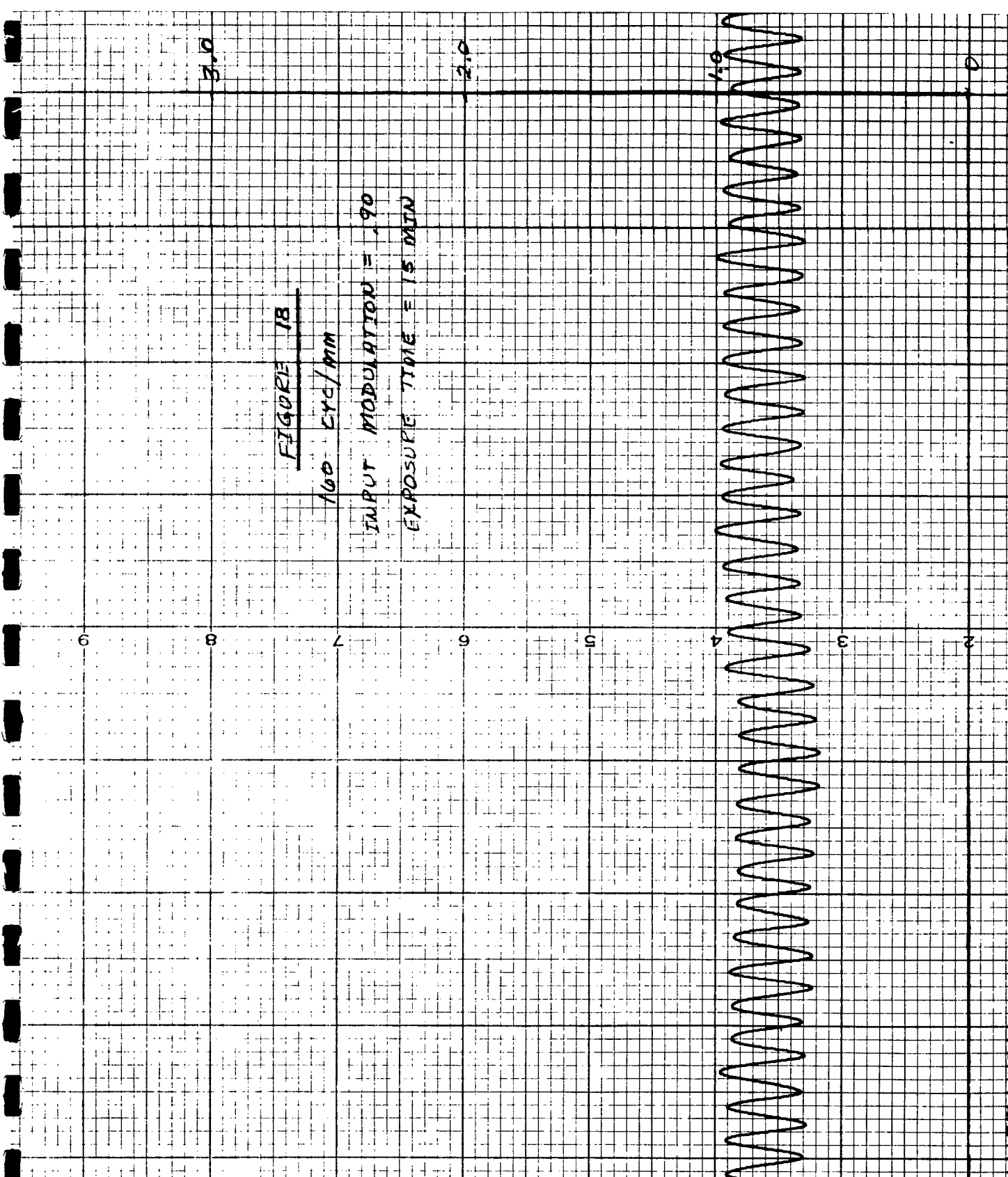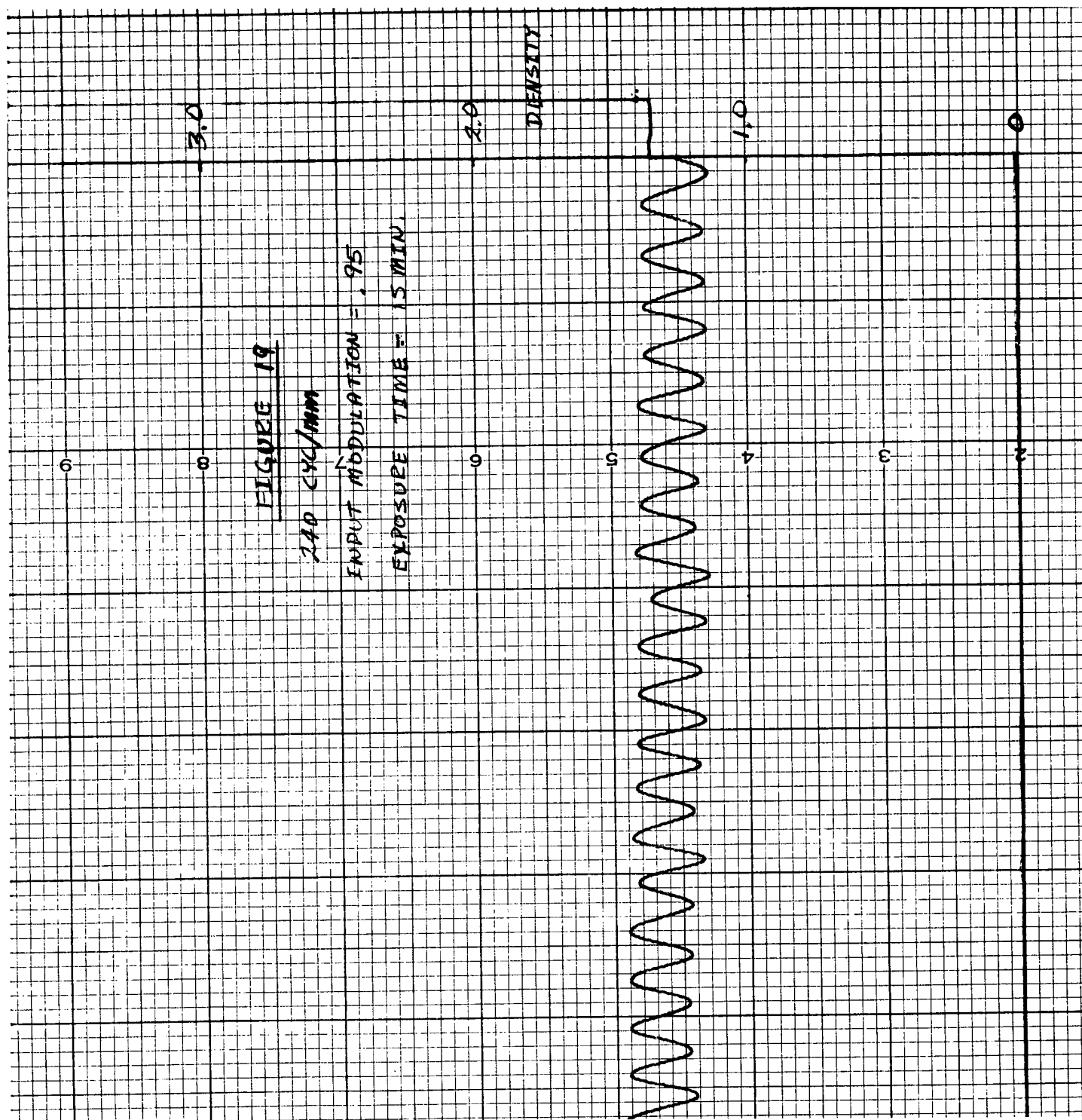
SECRET

of 10 to 200 seconds for the frequencies up to 80 cycles per millimeter, with longer times required for the higher spatial frequencies. This means that the calibration data in terms of exposure can be in error. Experimental tests have been run by generating calibration data over a wide range of exposure times and for the film processing conditions used, the change in gamma has been small, which means that the only significant change is a speed shift, which is equivalent to multiplying exposure data by a constant. However, all the data is normalized so this factor is not as important. One must also realize that the measuring instrument, in this case the microdensitometer, is a part of the overall process. Undoubtedly, the microdensitometer attenuates the higher harmonics, but the question of whether this attenuation can be approximated by a constant or is image dependent is still open. All the data was traced using a 1 x 80 micron slit size.

Considerable effort has been expended in improving the optical system of the experimental apparatus. In particular, the light intensity has been increased by utilizing a slit instead of a pinhole aperture in the optical system. This has allowed the decrease of exposure times to 16 seconds or less for all frequencies. This will also allow the exposure time to be held to a constant, and the modulation and average exposure to be varied by combinations of neutral density filters only. This will permit the generation of more accurate calibration data, plus reducing the required exposure times to values closer to those used in applications.

In addition to increasing the available light intensity, a detailed series of photometer measurements have been performed in order to insure that intensity measurements made in the Fourier transform plane can be correlated with those made in the film plane. The correlation between these measurements was good, with the expected error on the order of three percent or less. This indicates that intensity measurements can be made in the transform plane with the existing optical system with little loss of accuracy.

II. MENSURATION RESEARCH PROGRAM

A small amount of data is available from Westover in the mensuration research program. The measurements were performed on photographs that had a resolution in the range of 70-90 lines per millimeter as read from standard 3-Bar targets. The measurements were performed on a 3-Bar group with a spatial frequency of about 32 lines per millimeter. This was done in order to place the object size small enough to be significantly affected by the system performance. The measurements were made in two ways:

1. Visually, using cross hairs.

2. From a chart recording of a microdensitometer trace, using the average of maximum and minimum densities as the criteria for measurement.

Measurements have been made both on original negatives and duplicate positives. The total quantity of data is not large enough to run a complete statistical analysis, but some significant trends can be noted in the available data. These are:

1. The difference in means between visual and machine measurements is small, but the variance of visual measurements is considerably greater than that of the machine measurements.

2. The errors in the measurement on the duplicate negative are, in general, greater than the measurements made on the original negative. In addition, the errors appear to be biased in one direction; that is, the trend in the duplicate positive is for the measurements to be all larger (for bars) or smaller (for spaces) than the measurements on the original negative. This indicates that more research is required in methods of minimizing errors introduced in the duplicating process.

As previously indicated, the quantity of data available at this time is too limited

to allow a complete statistical analysis. When more data becomes available, a detailed analysis will be performed.

The in-house mensuration program is underway, with two targets with a reflectance density of 0.6 between the background and target objects. The objects range in size from 6 to 2000 microns (referenced to the film plane). The objects used are squares, circles, single lines, and 3-Bar targets. The photographs are to be run through three generations of duplication and the propagation of errors analyzed.

SECRET
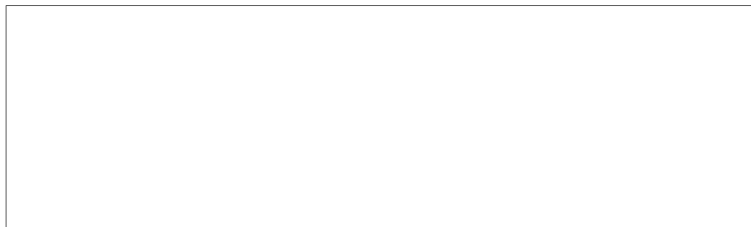
25X1

16 January 1967   25X1

IMAGE ANALYSIS PROGRAM
SIX MONTHS REPORT
January, 1967
Contract #62185

Submitted By

25X1

16 January 1967

SECRET

A Statistical Description of some Effects Produced
by Photographic Grain

In any complete theory of the statistical fluctuations for photographic emulsions one should be prepared to take into account at least the following items:

1.) The statistical fluctuations in the incident light. (Coherence and photon correlation effects)

2.) The average geometric photon flux density incident on the film. As examples of different geometric distributions producing well-known photographic curves we cite:

Incident photon flux	Associated photographic result
a.) thin slit of light	line spread function
b.) sharp discontinuity	edge gradient
c.) sinusoidal	transfer function
d.) three rectangular bars	resolution chart
e.) constant	H & D curve

3.) The statistical fluctuations in size, sensitivity and location of the unexposed grains.

4.) Scattering and diffusion of light during exposure.

5.) Chemical effects during processing.

6.) The statistical fluctuations in size and location of the blackened grains.

and

7.) The relation between the fluctuations in transmission and density actually existing on the developed film and the smoothed version of these when viewed by an equivalent scanning aperture; e.g. eye, projector, microdensitometer, etc.

The first and last (1 and 7) of these items do not present any new problems; both of them having been well investigated are reasonably well understood today. (See refs. 1 and 2.) This report does not consider items 4 and 5 although both are important factors that eventually must be considered. The main part of this report is concerned with item 6. However, insofar as the incident photon flux density (item 2) and statistical properties of the unexposed grain (item 3) are concerned, Appendix I describes a method for handling these problems whenever they are the major factors in reducing the quality of the image on film.

So far as item 6 is concerned we begin by assuming that the film has been exposed and developed. The

SECRET

resulting collection of blackened grains we characterize

by a population density of grain centers d(ξ, η) and a

probability density distribution of grain radii such

that p(r)dr is the fraction of grains whose radius lies

in the interval (r,r+dr). See Fig. 1.0
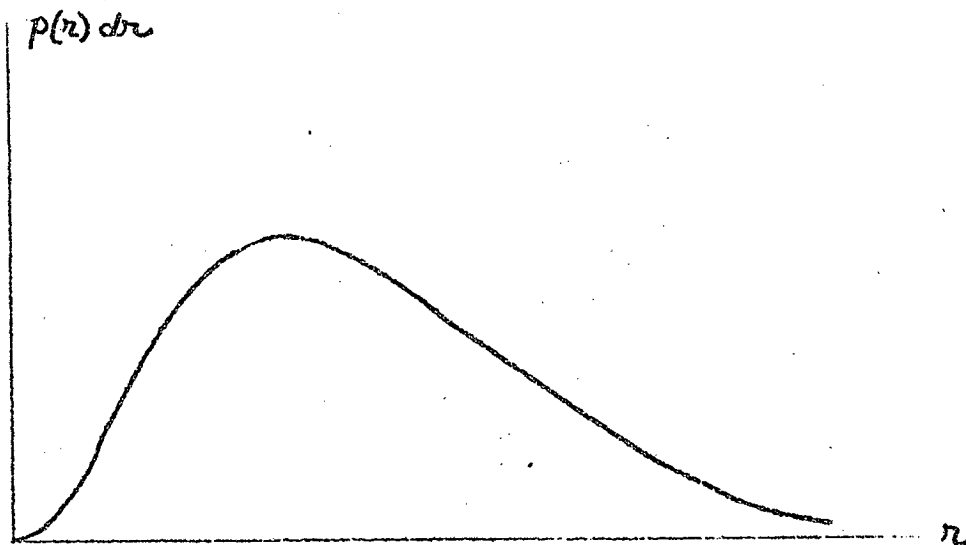
Fig. 1.0

It will turn out to be useful to introduce
the probability distribution function

1.) $$P(R) = \int_0^R p(r)\,dr$$

describing the fraction of grains whose radius is less
than R. Since $\int p(r)\,dr = 1$ we may also introduce

2.) $$Q(R) = 1 - P(R) = \int_R^\infty p(r)\,dr$$

to describe the probability that a grain has a radius
greater than R.

Now if, in the small, $d(\xi, \eta)$ describes the
average number $\bar{n}$ of blackened grains whose centers lie
in the region ΔA centered at (ξ, η) then we take for the
probability of finding n grains in ΔA the Poisson dis-
tribution*

3.) $$P_{\bar{n}}(\Delta A) = \frac{\bar{n}^n \, e^{-\bar{n}}}{n!} \quad ,$$

$$\bar{n} = d(\xi, \eta) \cdot \Delta A \quad .$$

*Later in our calculation we will choose the geometry
of ΔA to be a long thin strip of width Δ extending
in the n direction in order to contain a large enough
population to allow us to use the Poisson distribution.

Next (conceptually at least) we consider a large ensemble of films having the same statistical properties and each subject to the same (statistically speaking) rain of photons. On each we set up a carte-sian coordinate system in a plane and choosing a <u>point</u> (x,y) we examine each of these films to determine whether the point transmission $T(x,y)$ is 0 or 1. Counting the fraction of this ensemble whose transmission $T(x,y)$ is one, we determine $\overline{T}(x,y)$. With reference now to Fig. 2.0, we see that $\overline{T}(x,y)$ for a single member of the ensemble is simply the probability that the transmission at the point (x,y) is unity. That is

$$4.) \qquad \overline{T}(x,y) = \text{Prob}\left[T(x,y) = 1\right] \ .$$
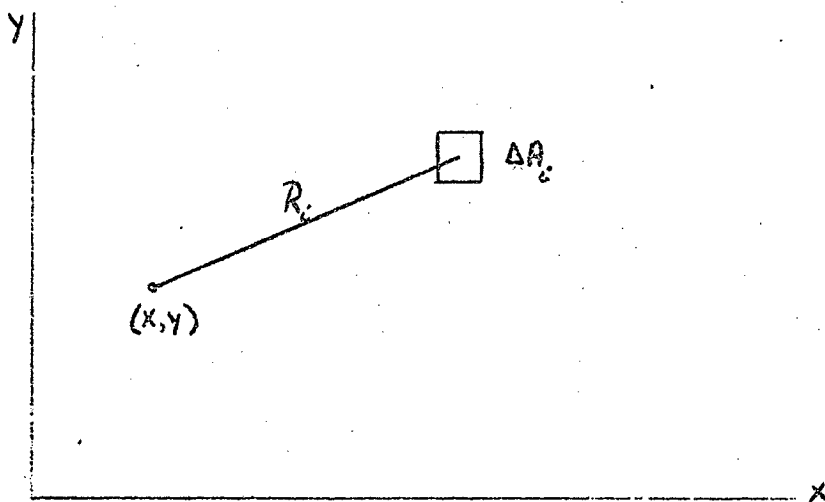
Fig. 2.0

SECRET

-6-

We now wish to calculate the right hand side
of this equation.   First we define:

$p_i \equiv$ probability that a cell ΔA_i surrounding
(x,y) has the property that it does <u>not</u>
contain the center of a grain which extends
to (x,y)

Then in order for (x,y) to have $T = 1$, all cells surround-
ing x,y must have this property.   That is

5.) $T(x,y) = \prod_i p_i$

In order to calculate p_i we note that ΔA_i may contain no
grain centers or it may contain one grain center which
does not extend to (x,y) or it may contain two grain centers,
neither of which extend to (x,y) or etc, etc.

Reasoning this way we can write

$$P_i = P_0(\Delta A_i) + P_1(\Delta A_i)P(R_i) + P_2(\Delta A_i)P^2(R_i) + \text{----}$$

6.)
$$= e^{-\bar{n}_i}\left[1 + \frac{\bar{n}_i P(R_i)}{1!} + \frac{[\bar{n}_i P(R_i)]^2}{2!} + \text{---}\right] \quad,$$

SECRET

or in more compact form

7.)
$$P_i = e^{-[1-P(R_i)]\,\bar{\pi}_i} \quad ;$$

$$\bar{\pi}_i = d(\xi,\eta)\,\Delta A_i \quad .$$

Substituting this into equ. 5 we have

8.)
$$\bar{T}(x,y) = \prod_i e^{-[1-P(R_i)]\,d(\xi,\eta)\,\Delta A_i}$$

$$= e^{-\sum_i [1-P(R_i)]\,d(\xi,\eta)\,\Delta A_i} \quad ,$$

and finally passing from the sum to the integral, we have

9.)
$$\bar{T}(x,y) = e^{-\iint d(\xi,\eta)[1-P(R)]\,d\xi\,d\eta} \quad .$$

Before proceeding it will be convenient to introduce the relationship between photographic density and transmission in the form

10.)
$$D = \log_{10} \frac{1}{T}$$

or inverting this equation

11.)
$$\overline{T} = e^{-\frac{D}{M}} \quad ,$$

where $M = \log_{10} e = 0.4343$. Comparing equs. 11 and 9 we can write

12.)
$$D(x,y) = M \int\!\!\int_{-\infty}^{+\infty} Q(\xi - x, \eta - y)\, d(\xi, \eta)\, d\xi\, d\eta \quad ,$$

where we have used the relations $Q = 1 - P$ and $R = \sqrt{(\xi - x)^2 + (\eta - y)^2}$.

Now equation 12 has all the features of a linear filter relation between the population density of grain centers (input) and the photographic density (output). In Appendix I we describe a method for calcu-lating the population density of activated grain centers themselves from the incident photon flux density and

statistical properties of the unexposed grains.

Let us attempt to illustrate the use of equ. 12 with several examples:

I. $d_0(\xi, \eta) = \dfrac{\bar{n}}{A} = $ const., and equal-sized grains $[p(r) = \delta(r-r_0)]$
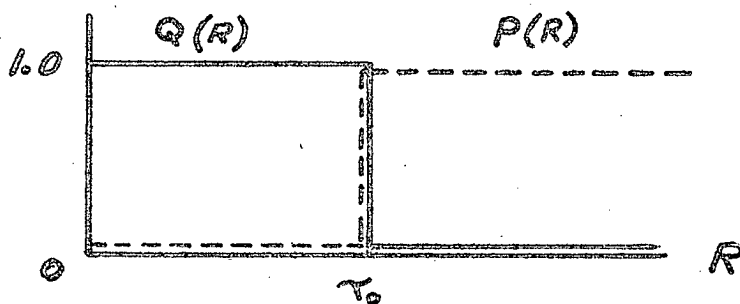
Fig. 3.0

SECRET

-10-

Under these simplifying assumptions $Q(R)$ takes on the simple form shown in Fig. 3.0 and we can write Equation 12 as

13.)
$$D = Md_0 \, 2 \int_0^{r_0} R \, dR$$
$$= Md_0 \, (\pi r_0)^2 = M \frac{\bar{n}}{A} a_0$$

where a_0 is the area of a single grain. Equation 13 verifies some earlier work (3) on simple models of photographic grain which demonstrates the linear relation between population density and photographic density.

II. $d_0\left(\begin{smallmatrix}?\\3\end{smallmatrix}, \eta\right) = \dfrac{\bar{n}}{A} = \text{const.}$, and $p(r) = 2\pi\lambda \eta \, e^{-\pi\lambda r^2}$

$\lambda = \dfrac{1}{\bar{a}}$
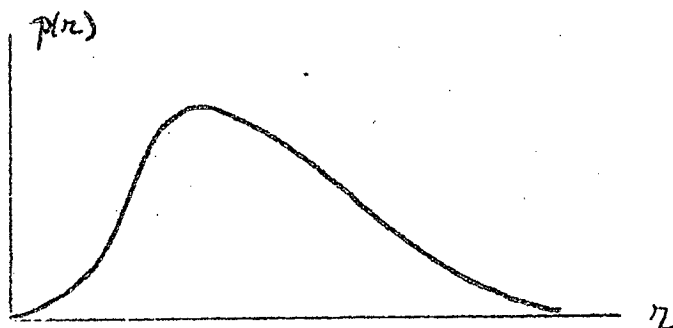
Fig. 4.0

SECRET

For this radius (area) distribution it is an
easy matter to show that

14.) $Q(R) = e^{-\pi \lambda R^2} = 1-P(R)$

Substituting these conditions back into equ. 12 we find
that even for a distribution of grain sizes the relation

15.) $D = M d_0 \, \bar{a} = \dfrac{M \bar{n} \, \bar{a}}{\bar{A}}$

still holds where $\bar{a}$ is the mean grain area.

III. For Q(R) arbitrary, let us take $d(\xi, \eta) = d_0 \, \delta(\xi)$.

Substituting this form of a thin line of
population centers into equ. 12 we have

16.) $D(x) = M d_0 \, L(x)$

where we now refer to

17.) $L(x) = \displaystyle\int_{-\infty}^{+\infty} Q(x, \eta-y) \, d\eta = \int_{-\infty}^{+\infty} Q(x, \eta') \, d\eta'$

as the line spread function.

From this point on the methods of linear filter theory can be applied in a straightforward way, and we now list with minimum comment how one proceeds.

IV. Edge Gradient: $\qquad d(\xi, \eta) = d_0\, \mu(\xi)$

Here μ is the Heaviside unit step function defined to be 0 for $\xi < 0$ and 1 for $\xi > 0$. Substituting this into equ. 12 we have

$$18.) \qquad D(x) = M d_0 \int_0^\infty d\xi \int_{-\infty}^{+\infty} Q(\xi - x, \eta - y)\, d\eta \;,$$

or using equ. 17 we can write

$$19.) \qquad D(x) = M d_0 \int_{-\infty}^{x} L(z)\, dz$$

In the table following and Fig. 5.0 we summarize the situation for the two grain size distributions treated earlier.

SECRET

Equal Size Grains   Exponential Area Distribution
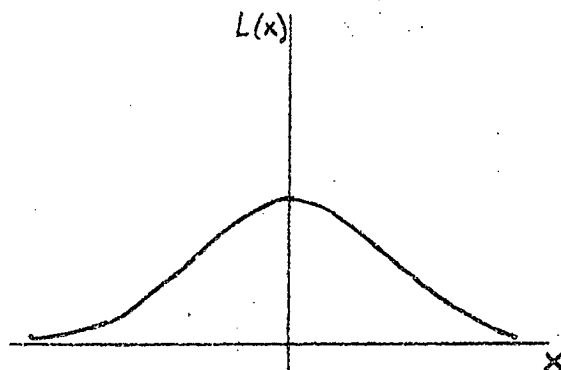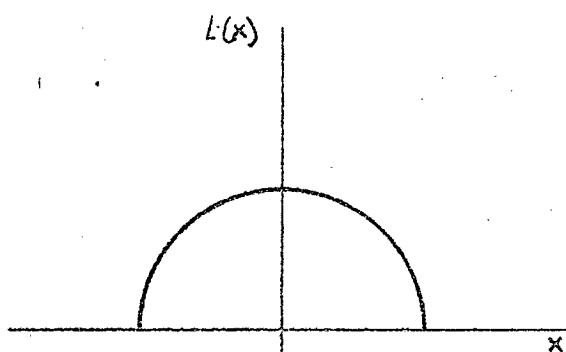
Line Spread Function

$$E(x) = \int_{-\infty}^{x} L(z)\,dz$$

$$E(x) = \int_{-\infty}^{x} L(z)\,dz$$
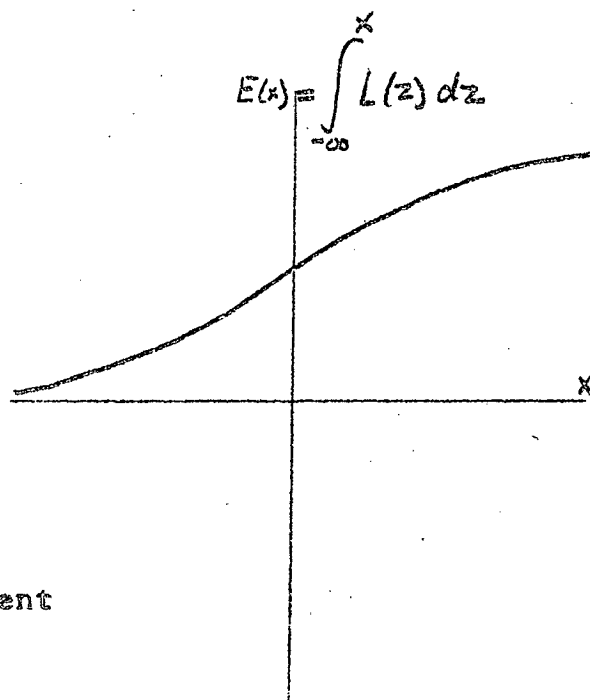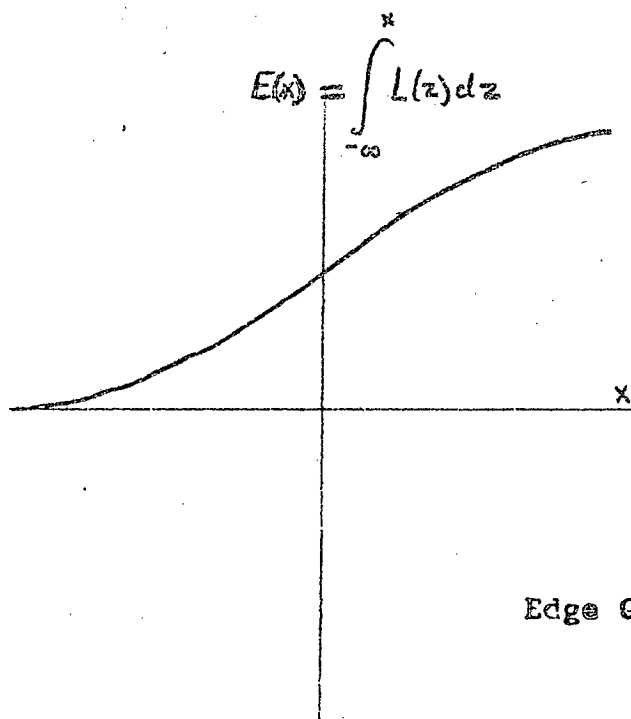
Edge Gradient

Fig. 5

Probability density p(r):	$\delta(r - r_o)$	$2\pi\lambda r\, e^{-\pi\lambda r^2}$; $\lambda = \frac{1}{a}$
Line spread function:	$2\sqrt{r_o^2 - x^2}$	$\frac{1}{\lambda}\, e^{-\pi\lambda x^2}$
Edge Gradient:	$\frac{\pi r_o^2}{2} + \frac{1}{2}\left(r_o^2 \sin^{-1}\frac{x}{r_o} + x\sqrt{r_o^2 - x^2}\right)$	$\int_{-\infty}^{x} \frac{e^{-\pi\lambda z^2}}{\lambda}\, dz .$

Table 1.0

V. Transfer function

Having established the form of the line spread function we can now return to equ. 12 and allow for the possible one dimensional variations in $d(\xi, \eta) = d(\xi)$. Under this condition equ. 12 takes the form

$$20.) \qquad D(x) = M \int_{-\infty}^{\infty} L(\xi - x)\, d(\xi)\, d\xi$$

In particular we can Fourier transform equ. 20 to write

$$21.) \qquad \tilde{D}(\omega) = T(\omega)\, \tilde{d}(\omega)$$

where τ (ω) the normalized transfer function is given by .

22.)

$$\tau(\omega) = \frac{\int_{-\infty}^{\infty} L(x) \, e^{i\omega x} \, dx}{\int_{-\infty}^{+\infty} L(x) \, dx}$$

 In summary then, while the grain size distribution and population density of grain centers determines the spatial filtering properties of the developed photographic film, it is clear that these considerations could be turned around to yield from measured data on edges, sine wave response, etc., the statistical variations in the grains which form the image. Finally we turn now from these considerations to Appendix I where an attempt is made to estimate how the variation in population density of grain centers comes about in the first place during the exposure.

Appendix I

The Variation in the Population Density of Activated Grains

with Incident Photon Flux Density

Consider Fig. I.A. Once again we assume
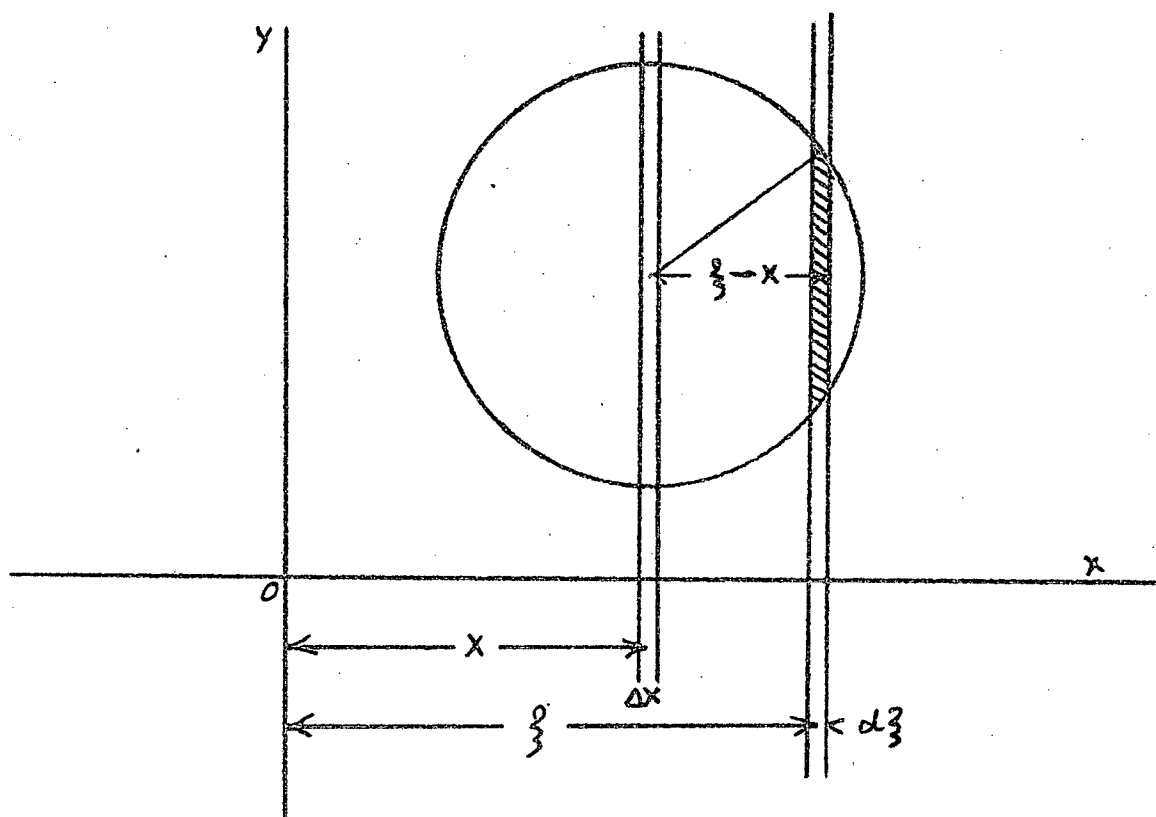
Fig. I.A

a large ensemble of statistically similar films all

subject to the same incident light intensity; in this

case a thin ribbon of light of width $\Delta\xi$ centered at ξ.
Now for any one film we consider a long thin strip of
width Δx containing a large number N_0 of centers of
potentially developable grains. We wish to calculate
$P(\xi,x)$, the probability that a grain whose center lies
in Δx centered on x will be rendered developable by a
thin slit of light of width $\Delta\xi$ at ξ. That is, we wish
to determine the fraction

I.1

$$P\left(\xi, x\right) \Delta\xi = \frac{N(\xi, x)}{N_0} = \frac{d(\xi, x)}{d_0} \quad ,$$

where N_0 and d_0 describe the total number and density of
grains centered in Δx that could be activated.

Now first we must estimate the fraction of
the grains lying in Δx that will extend to ξ, then of
that fraction we must calculate* the probability that

*Another factor describing the fact that different grains
require more quanta than others to be rendered develop-
able can be included and has been treated elsewhere (Refs.
3 and 4). Here we are stressing geometrical effects.

the photo-sensitive area of those grains (assumed uniformly distributed over the area of a grain) falls within $\Delta\xi$. In Fig. I.A we show a typical grain centered in Δx and extending beyond $\Delta\xi$. The probability that the photo-sensitive area of this grain is within the shaded region is just $\frac{2}{\pi \imath^2}\sqrt{\imath^2-(\xi-x)^2}\;\Delta\xi$. Adding these up for all grains extending to ξ and beyond we have

$$I.2 \qquad P(\xi,x)\,\Delta\xi = \int_{\xi-x}^{\infty} \frac{2\sqrt{\imath^2-(\xi-x)^2}}{\pi\imath^2}\, p(\imath)\, d\imath \;.$$

Now as in the main report the precise form of this probability distribution will depend upon the grain size distribution (as well as sensitivity and center location distribution). Nevertheless, here we put such questions aside and interpret equs. I.1 and I.2 to mean that for an incident intensity distribution of the form

I.3

$$I(\xi,\imath) = \delta(\xi) = \frac{1}{\Delta\xi}$$

SECRET

-19-

the line spread function in activated population density
of centers is given by

I.4 $L(\zeta - x) = d(\zeta - x) = d_o P(\zeta - x)$

so that for an arbitrary (one-dimensional) incident in-
tensity distribution we can sum up the contributions from
each strip $\Delta \zeta$ a distance $(\zeta - x)$ away by the laws of prob-
ability to determine

I.5 $d(x) = \int_{-\infty}^{\infty} L(\zeta - x) \, I(\zeta) \, d\zeta$,

again a linear filter theory relation between $I(\ )$ and $d(x)$
through the impulse response

I.6
$$L(\zeta - x) = \frac{2}{\pi} \int_{\zeta - x}^{\infty} \frac{\sqrt{r^2 - (\zeta - x)^2}}{r^2} \, p(r) \, dr \ .$$

Now from this point on it is not difficult to
show that if one inserts various probability density
functions p(r) and combines these results with those of
the main report, then the overall line spread function

SECRET

(due to geometrical considerations alone) is determined by the self-convolution of the probability density distribution for grain sizes. A simple order of magnitude argument shows then that the width of the line spread function, including only these effects, is approximately two average grain diameters wide. Since real films resolve far less than this, we conclude that these considerations, perhaps fine as far as they go, do not go far enough. One cannot simply combine the statistical and geometrical effects in items 2 and 3 with those of 6 and 7 without including the very important scattering, diffusing and chemical effects mentioned in items 4 and 5.

In particular, while the methods of the main report will handle the fluctuation problem once the population of developed grain centers is known, the considerations of this appendix are not sufficient to explain the fact that a thin slit of light apparently produces developable effects many grain diameters away. Perhaps it may be necessary to adopt a phenomenological approach to obtain effective scattering and chemical transfer functions, but given that items 1, 2 and 3 can be handled, one will not be able to proceed to items 6 and 7 in a complete theory without an understanding of the processes involved in items 4 and 5.

References

1.) Mandel, L., "Fluctuations in Light Beams", Progress
in Optics, Vol. II , Edit. by E. Wolf, North-Holland
Publishing Co.

2.) O'Neill, E. L., Introduction to Statistical Optics
Chap. VII, Addison-Wesley Publ. (1963)

3.) Silberstein, L. and Trivelli, A. P. H., J.O.S.A. 28
441-459, (1938)

25X1

PART II

Experimental Results

General Remarks

This part of the program was instituted to experimentally verify the results obtained in the theoretical approach described in Part I.

In our theoretical considerations we excluded the light-scattering in the emulsion during the exposure. Although a very important factor in the final image formation in commercial films, it was thought advisable to attack the complicated process of image formation in films one step at a time, and the statistical nature of the imaging process was worked out first.

One might hope that this scattering of the light in an emulsion consisting of a single layer of grains would be practically non-existent; as will be shown later, we strongly suspect that this is not the case.

Many measurements on the properties of film become extremely difficult when one works with small grain size. For example, microdensitometer traces of

FIG. 1

T.O. EXPERIMENTAL FILM

GRAIN SIZE IN MICRON
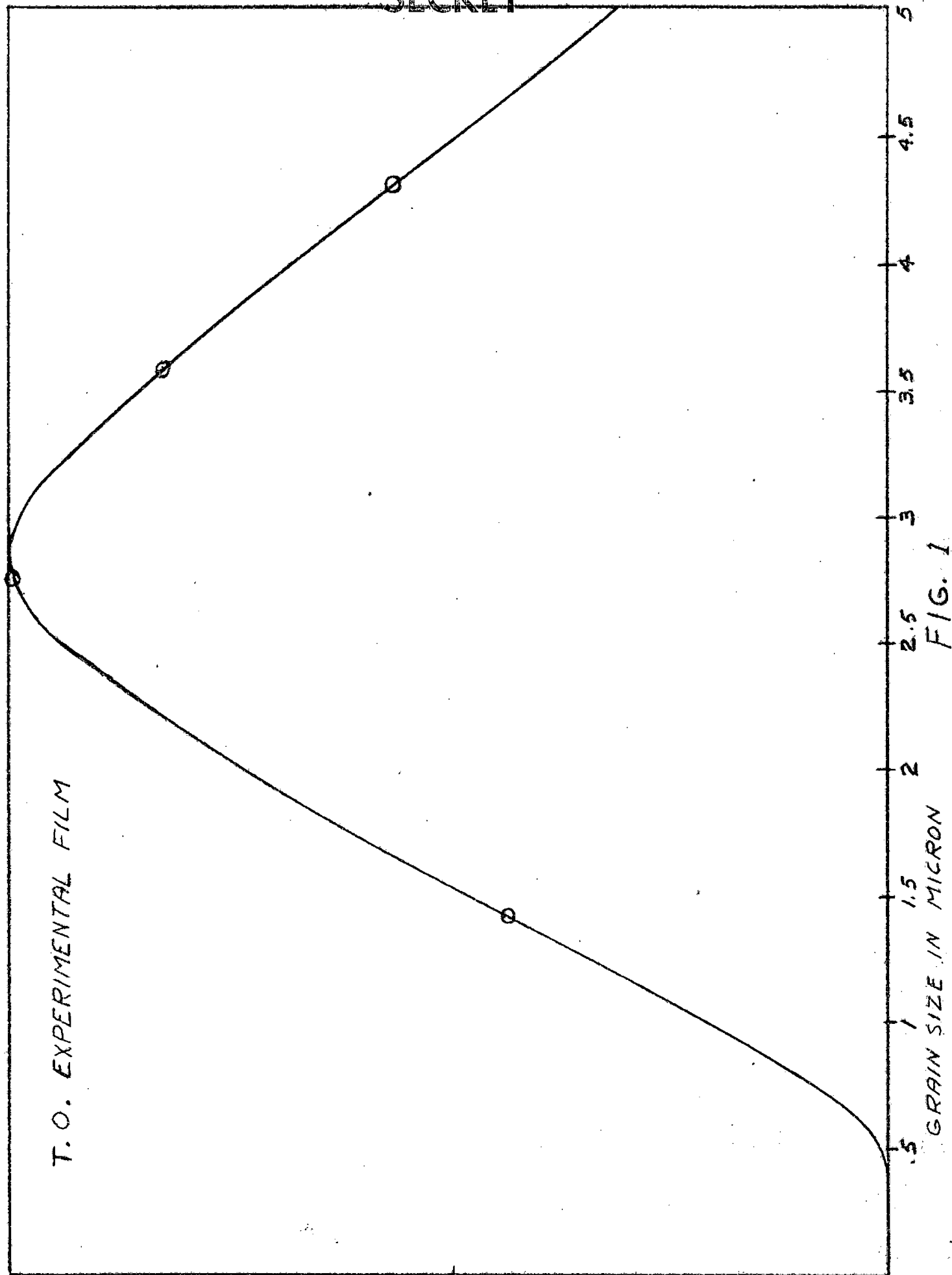
various images are then strongly influenced by the
properties of the microdensitometer. A large grain
size would make these difficulties minimal.

For these reasons [   ] 25X1
prepared special films for this program. These films
have a single layer of large grains. Only the coarsest
of their emulsions was used in the part of the program
reported on here.

Some Properties of the Experimental Film

The grain size distribution of this film, as
measured by [   ] is shown in Fig. 1. 25X1
This distribution is measured on undeveloped film.

The sensitive layer consists essentially of a
single layer of grains.

No protective coating was applied over the
sensitive layer. It was felt that this would make
possible closer contact between target and film during
exposures. We used contact printing for our exposures,
to eliminate the influence of the transfer function of
the lens used in a projective method.

The lack of this protective layer led to some
experimental difficulties, such as sensitivity to electro-
static charging of the film, and pressure sensitivity.
Techniques were developed to minimize the affects, and
we do not feel that they affect our results.

Experimental Equipment and Procedures

All our exposures were made with an Edgerton-Germeshausen and Grier sensitometer, Mark VI model. The exposure time was kept constant at 10^{-4} seconds throughout the experiments.

To print targets with different exposure levels, we inserted between the target and the glass plate carrying the target a neutral density filter.

All films were developed in D-19 for 5 minutes at 68°F. The films were continuously agitated to minimize adjacency affects.

All density measurements were made on a Joyce-Loebl microdensitometer. All slit sizes and slit areas reported, refer to the size of the slit projected in the film to be measured.

The H and D Curve

To measure the H and D curve a step-wedge was used. Since the exposure was made with diffuse light, the diffuse densities of the step-wedge was used in the computations. The density in the exposed strip was measured with the microdensitometer and is, therefore, the specular density. The density range is 0.5. The fog level is rather high and equals a density level of 0.098.

SECRET

D - LOG E CURVE
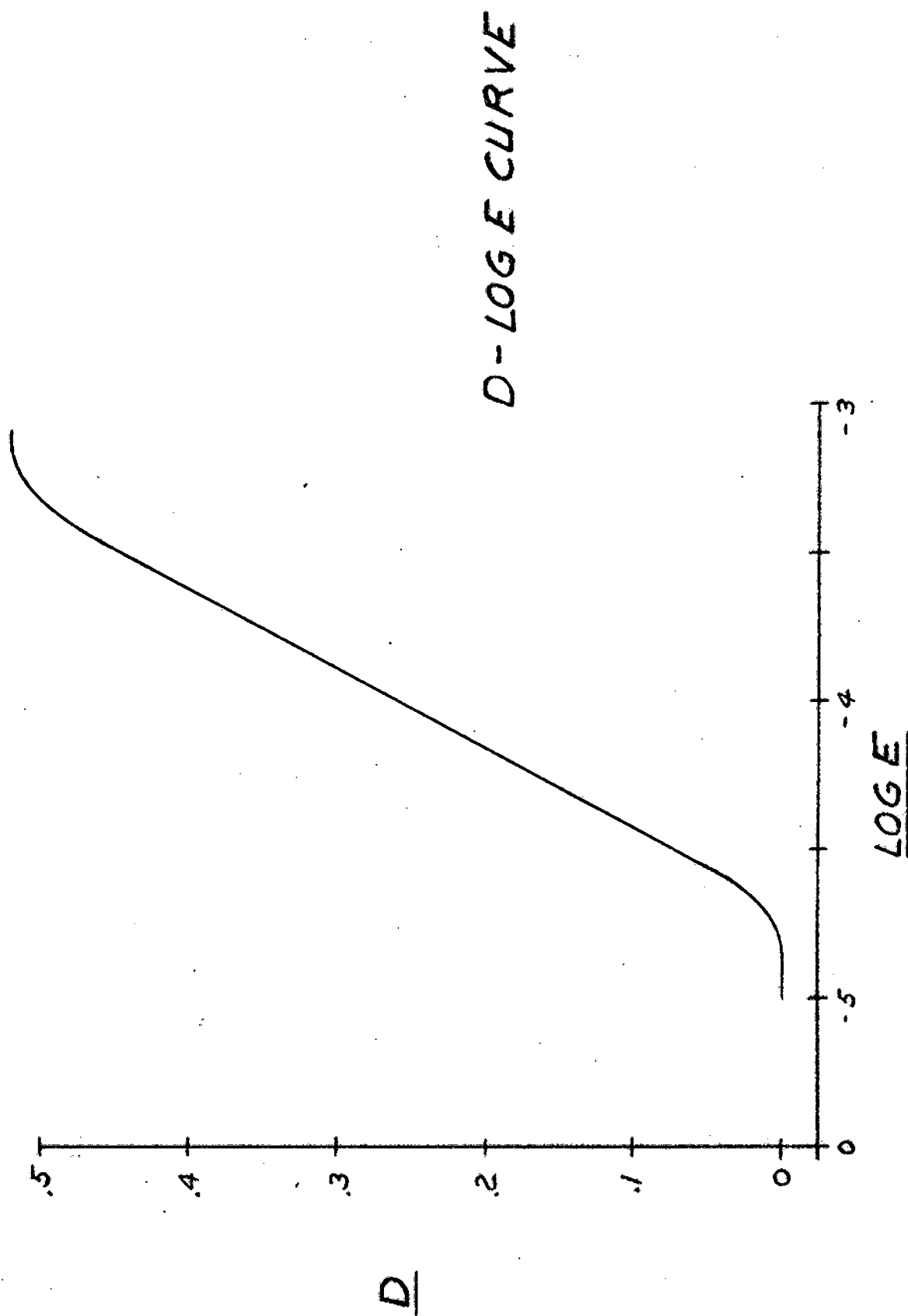
FIG. 2

Resolving Power Curves

In this experiment we printed targets consisting of 15 bars on the experimental films. The target array is shown in Fig. 3. The number of lines per millimeter for each target is shown in Table 4. The resolving power was determined as a function of the exposure for three targets with different contrasts.

In Fig. 6 we show a microdensitometer trace of a target that is just resolved. This trace was made with the microdensitometer; the scanning slit had a width of 3.3 microns and a length equal to the bars. A discussion of this curve will be given in the section "Some Remarks About the Experimental Results".

Due to these statistical effects, it is very difficult to have different readers read the same resolving power. The resolving power as a function of exposure and contrast of the target, as read by one reader, is shown in Fig. 5.

Edge Traces

For this experiment we prepared two edges with density differences of 0.71 and 1.13. These edges were printed on the experimental film and the resulting microdensitometer traces are shown in Figs. 8 and 9.
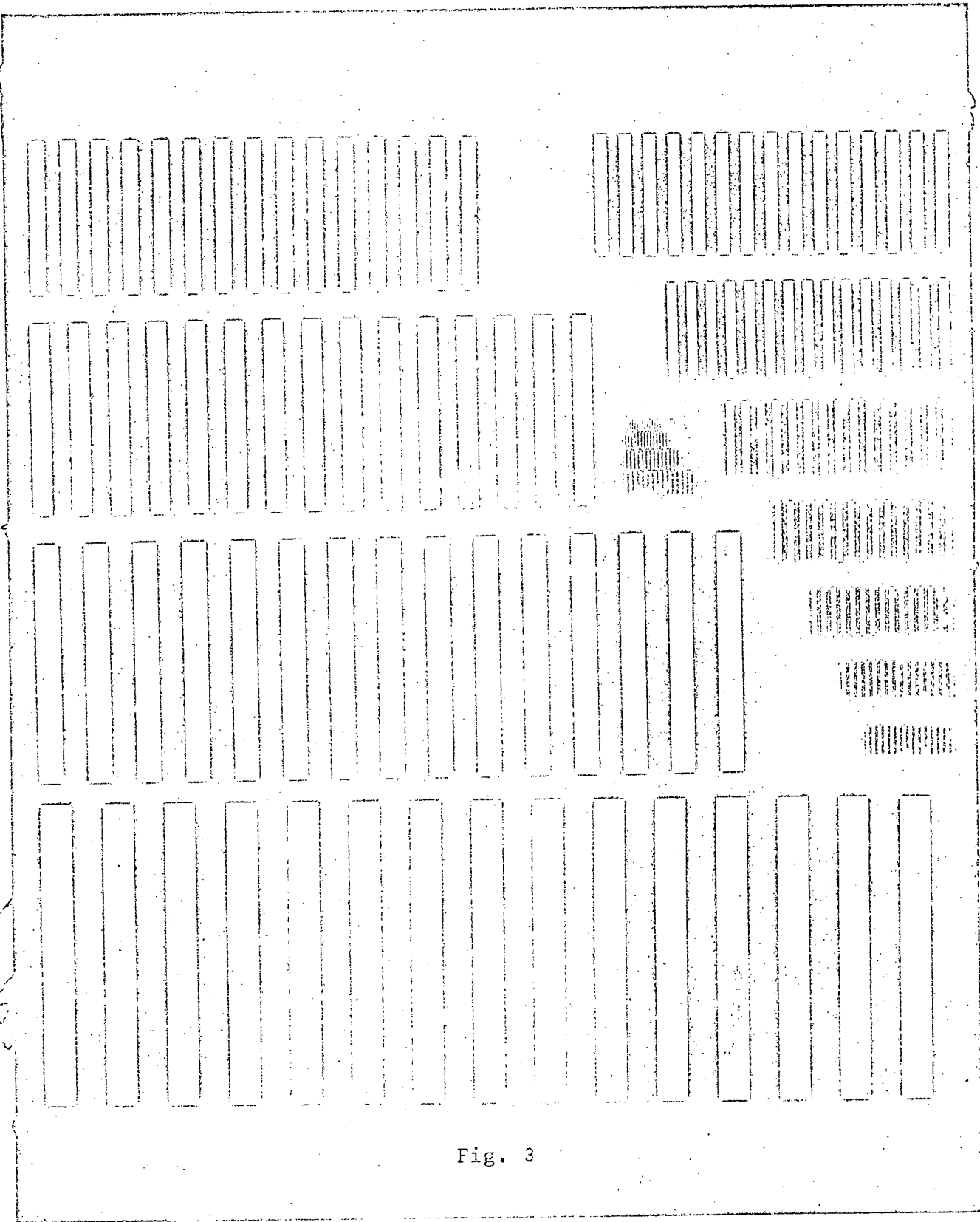
Fig. 3

GROUP I	GROUP II
1.00	10.00
1.26	12.59
1.58	15.85
2.00	19.96
2.51	25.12
3.16	31.63
3.98	39.82
5.01	50.14
6.31	63.13
7.95	79.48
10.00	100.00

TABLE IV

RESOLVING POWER CURVES
OBSERVATIONS BY L.R.

CONTRAST 2.3 △

CONTRAST 0.6 ☉

CONTRAST 0.14 ☉

RESOLVING POWER IN LINES/mm

RELATIVE LOG EXPOSURE
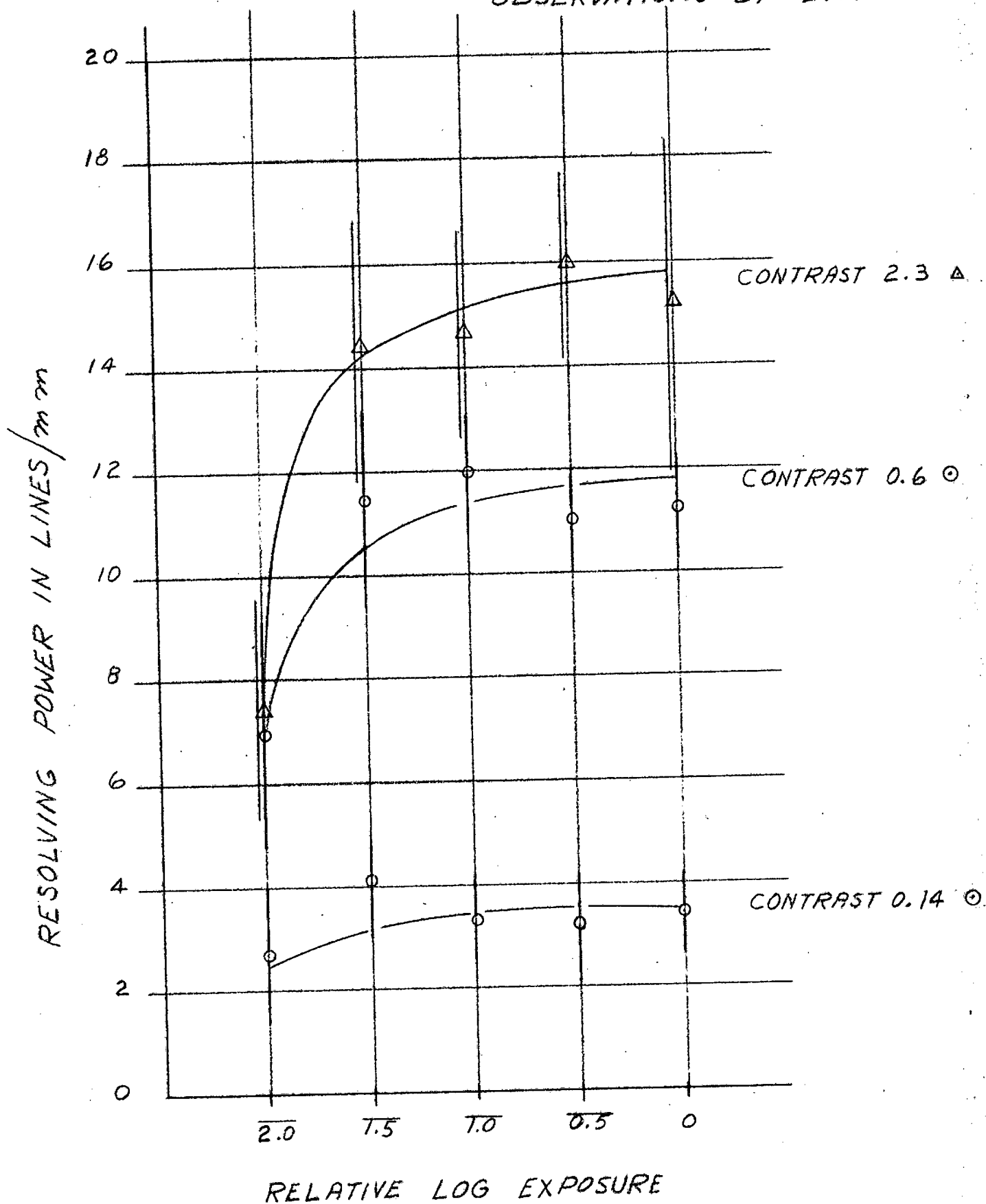
FIG. 5

From the theory based on the grain structure of the film, without taking scattering of the light in the emulsion during the exposure into account, the edge traces should extend at most over two grain diameters. In our curves we see that it spreads over almost a millimeter.

Therefore, other effects must come into play. A possible explanation is that image forming light is scattered by the grains. Our exposures were made in the sensitometer in which the light source is extremely diffuse. We plan to investigate the influence of the cone of light used in the image forming process, this time using a lens system to image the edge onto the film. In this way we can control the light cone entering the sensitive layer of the film to be exposed by stopping the lens down.

Another possible mechanism that would explain the shape of the edge trace is a chemical action by which, during development of the film, an exposed grain causes nearby grains to become developed. This effect can be studied by changing the developer used.

The extent over which the edge trace is broadened is, however, surprisingly large.

SECRET

10 e/mm TARGET
LEVER RATIO 50:1
MAGNIFICATION 10x
SLIT WIDTH .03mm
SLIT HEIGHT EQUALS
TARGET LENGTH
WEDGE : 0.021 d/cm

DENSITY
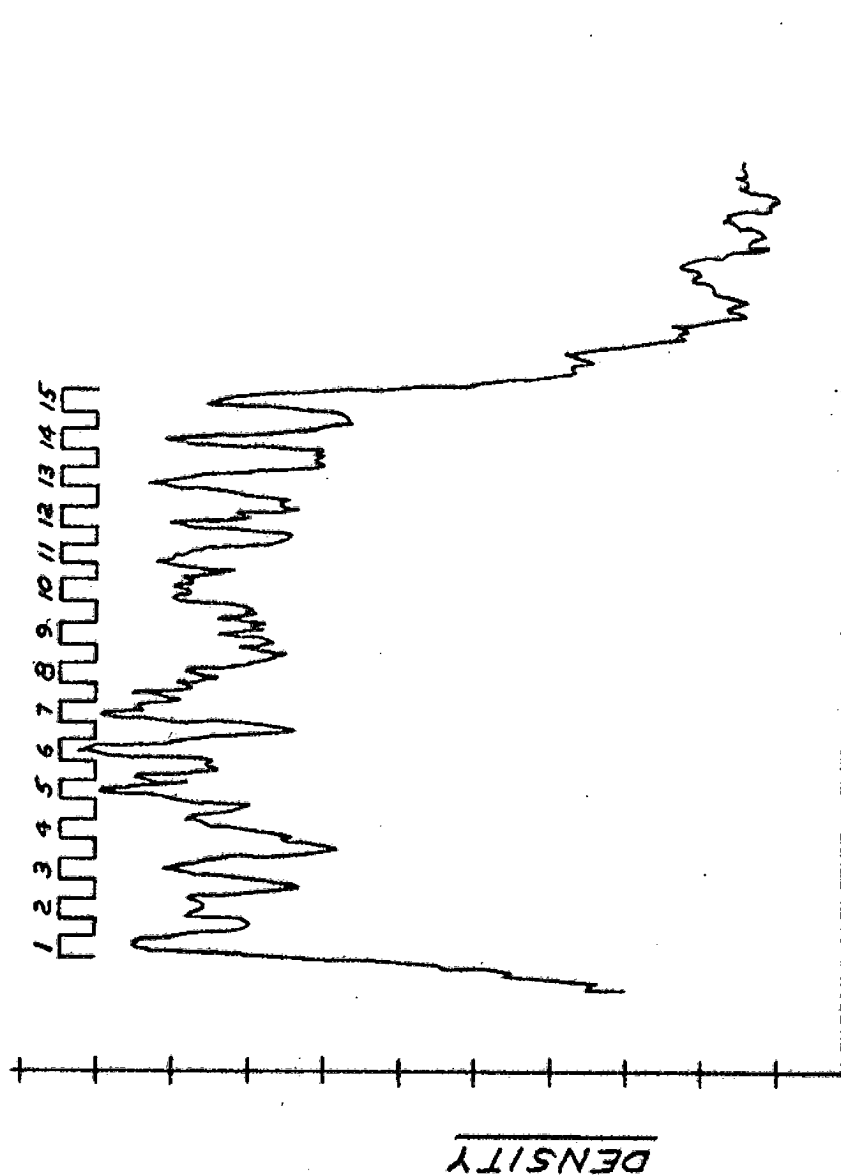
FIG. 6

SECRET

SECRET

FIG. 7

SECRET

KNIFE EDGE (CONTRAST 1.13)
LEVER RATIO 50:1
MAGNIFICATION 10X
SLIT WIDTH 0.03 mm
SLIT HEIGTH 3 cm
WEDGE 0.021 d/cm

200μ

FIG.8

DENSITY

FIG. 9

KNIFE EDGE (CONTRAST 0.7)
LEVER RATIO 50:1
MAGNIFICATION 10x
SLIT WIDTH 0.03 mm
SLIT HEIGHT 3 cm
WEDGE 0.021 d/cm

200μ

DENSITY
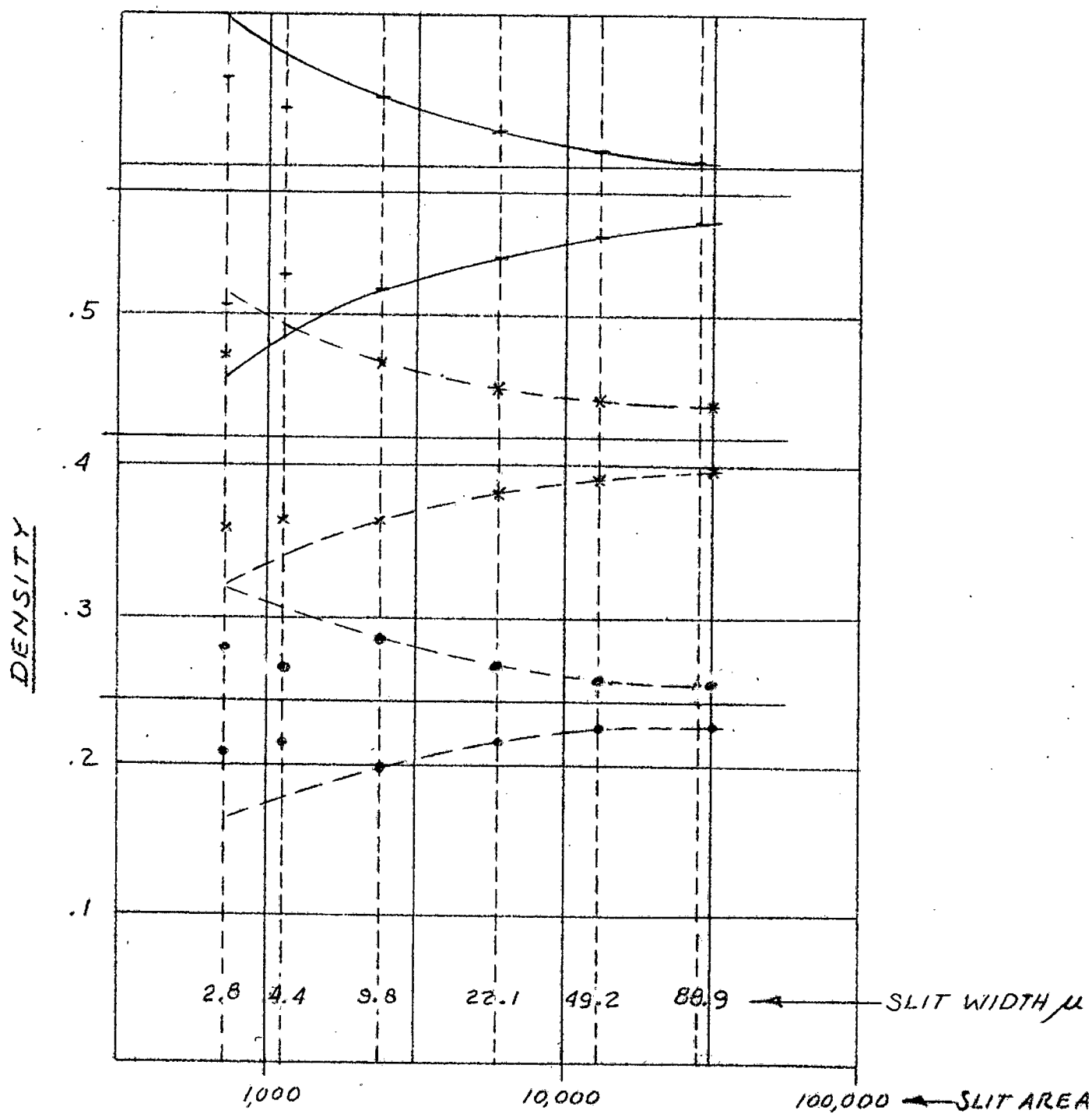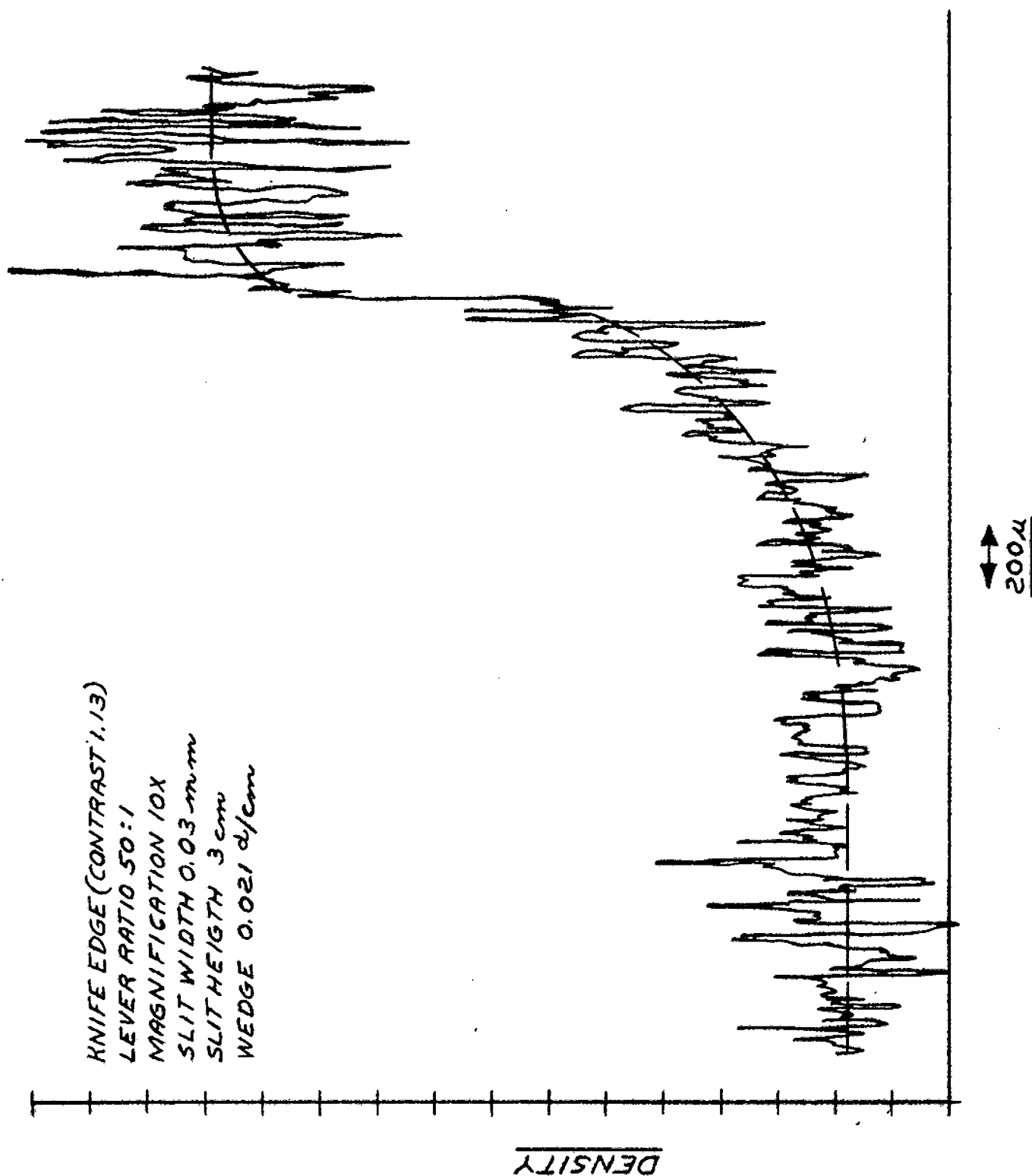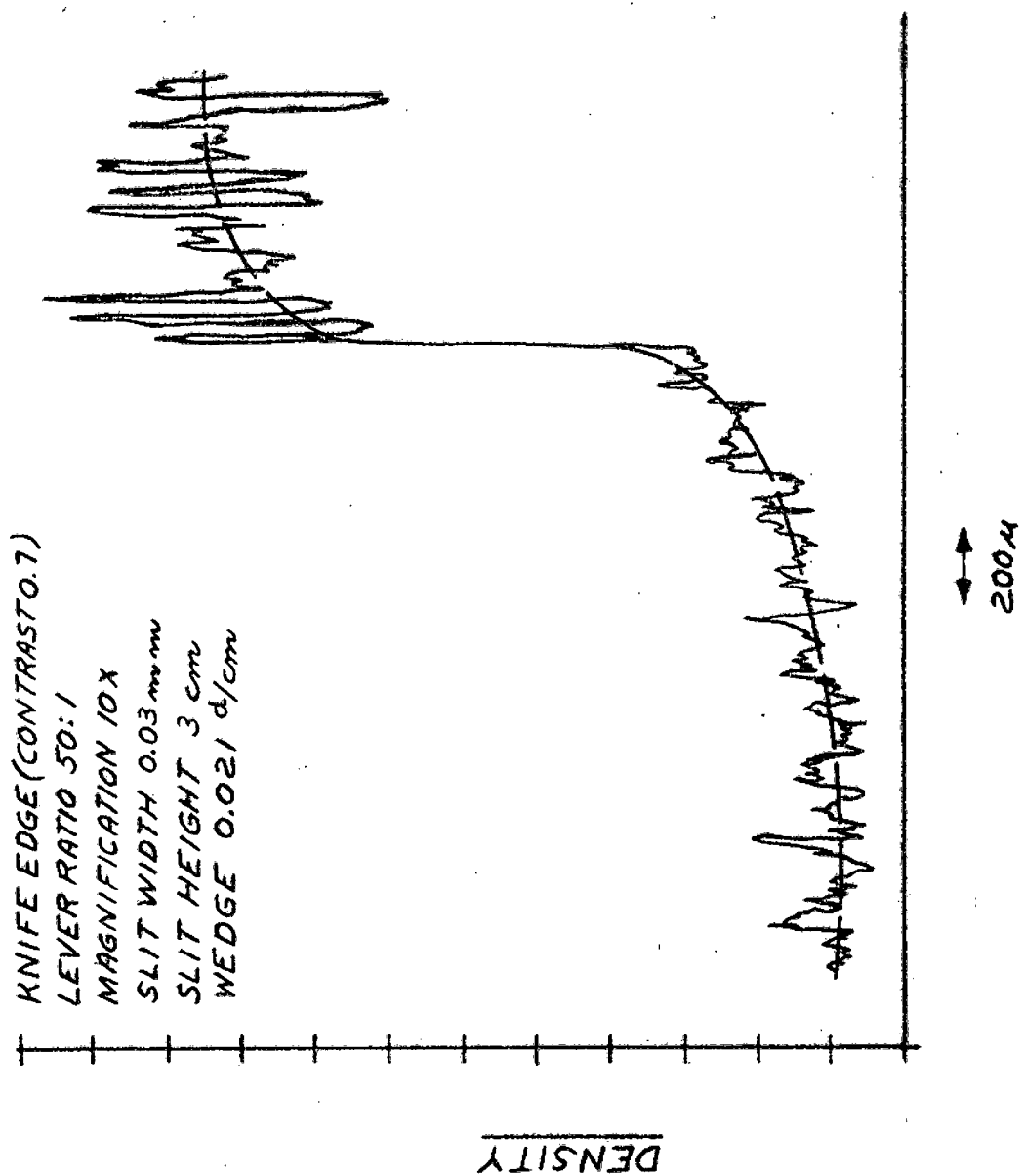
The Line-Spread-Function

An attempt was made to measure the line-spread-function directly, by exposing a very thin line on the film. For this purpose a line target with a line-width of one micron was prepared on high resolution film. The slit width was, however, so small that we could not get an exposure on the experimental film with our equipment. This slit width already represents one-third of a grain diameter. Larger slits would not give an image representing the line-spread-function. Altering the illuminating system would have made the results incomparable with all other measurements.

Since the future experiments call for equipment which uses a lens to put the targets on the film, imaging a fine line will not present a problem. It seemed, therefore, not advisable to change the illumination in our present program, and the attempt to measure the line-spread-function by contact printing was abandoned.

Granularity Measurements

To make the granularity measurements, the microdensitometer was modified in the following way. A separate chart-drive was placed in the rear of the microdensitometer. The pen of the densitometer was remounted on an extended arm so as to record on the

separate chart drive. The normal chart-holder was not
used. The arm driving the table, which held the film
to be measured, was driven by a separate drive, con-
sisting of a micrometer which was driven by a stepping
motor, thus moving the film in small increments. This
allowed the recorder to record the density of the film
in a sequence of isolated spots.

The density scale was divided into small
increments, and we counted the number of times that
a density was recorded in each interval. From this
frequency distribution the mean density and the
standard deviation was computed. The results are
shown in Fig. 7.

The theory predicts that the product of the
scanning area and the granularity is a constant,
provided that the scanning area is large compared to
the grain size. We have therefore computed this product
for the four largest slit sizes used; shown in Fig. 7
are the theoretical curves based on the average value
of this product.

For the smaller slits we find that the
measured values deviate considerably from the predicted
one. The slit widths here are, however, on the order
of one grain or smaller and deviations were to be
expected.

Some Remarks About the Experimental Results

From the experiments performed during these first six months it has become clear that our theoretical considerations, considering the role of the photographic grain, do not allow us to completely describe the image formation in films.

Light scattering and/or chemical effects must be taken into consideration and we plan to do this in the remaining time under the contract.

It is, however, clear from our experiments, that the statistical approach is important in describing the images on the film near the limit of resolution. In 15-bar targets, near the limit of resolution, one frequently finds some of the bars resolved. This is clearly shown in Fig. 6. In this microdensitometer trace of the image of a 10 lines/mm target, the first seven bars are clearly resolved, while the bars 8, 9, and 10 are unresolved. Bars 11 through 15 are again resolved.

Appendix II

Alternative Derivation of Some Grain Effects

The results derived in the previous sections can be arrived at by an alternative mathematical technique, which we shall describe briefly in this appendix. Disregarding three-dimensional effects, we consider flat, opaque grains which may or may not overlap. This implies that the local transmission T in any one point is always either zero or one. The average transmission $<T>$ in a point is defined as an ensemble average: an experiment is repeated many times, and $<T>$ is defined as the fraction of the number of experiments in which the point considered has a transmission one.

The incident light will be scattered by the undeveloped grains. This is a linear process that can be described by the common Fourier techniques. The light distribution E after this scattering process is considered to be known. Each grain is assumed to have one sensitive spot, which may be activated by the incident flux. The probability that it does get activated is S(E).

The sensitive spots will be Poisson distributed in the film plane, with mean density d_o. If a sensitive

spot at P is activated, the probability that, after development, its grain extends to a point P_1 will depend on the distance ℓ between P and P_1. This probability shall be denoted by $Q_1(P,P_1)$, and we assume it to be independent of the incident flux.

The probability that a surface element dxdy contains a sensitive spot P is:

$$d_o \, dxdy.$$

The probability that this sensitive spot is sensitized is

$$S(E) \, d_o \, dxdy,$$

and the probability that, after development, it causes the point P_1 to be covered is

$$Q_1(P,P_1) \, S(E) \, d_o \, dxdy.$$

If any of these three requirements is not fulfilled, the surface element dxdy will not cause P_1 to be opaque. So the probability that dxdy leaves P_1 transparent is

$$1 - Q_1(P,P_1) \, S(E) \, d_o \, dxdy.$$

The probability that all surface elements dxdy leave P_1 transparent is:

SECRET

-32-

$$\overline{\prod_{dxdy}} \left[1 - Q_1(P,P_1) S(E) \; d_o \; dxdy \right] \tag{1}$$

in which the product must be extended over all surface elements. This probability is, per definition, the mean transmission in P_1.

When $f(x)$ is integrable and bounded on (a,b) the following relation holds:

$$\lim_{\triangle x_i \to 0} \overline{\prod_{a,b}} (1-f(x_i) \triangle x_i) = \exp - \int_a^b f(x) dx.$$

Using this theorem to evaluate (1) we arrive at:

$$\langle T(P_1) \rangle = \exp - d_o \iint Q_1(P,P_1) S(E) dxdy,$$

the integral being extended over the film plane. Note that the incident flux E varies with P in the integration. In practice the range of integration will be limited by the finite reach of the covering probability $Q_1(P,P_1)$. The density in P_1 is defined by

$$D(P_1) = {}^{10}\log T(P_1),$$

so:

$$D(P_1) = \frac{d_o}{\log 10} \iint Q_1(P,P_1) S(E) dxdy. \tag{2}$$

Before we discuss this convolution we wish to bring it into a form more closely related to experiment. If the incident radiation has a uniform intensity over the film plane, Equation (2) reduces to:

$$D_u(P_1) = S(E) \cdot \frac{d_o}{\log 10} \iint Q_1(P,P_1) \, dxdy. \qquad (3)$$

The remaining integral is a constant which we may call the mean grain area $\bar{Q}_1$. Equation (3) then shows that the function $S(E)$ is, except for a constant, identical with the H and D curve for uniformly exposed film.

Substitution of (3) into (2) yields:

$$D(P_1) = \iint Q_1(P,P_1) \, D_u(E) \, dxdy \qquad (4)$$

This equation shows that, after the initial (linear) scattering process, the light distribution E can be converted point by point into density units by means of the H and D curve, where upon a convolution with the covering function $Q_1(P_1 P_1)$ yields the mean density distribution in the developed film.

Correlation functions in the film can be calculated by the same technique. Introducing a two-point covering function $Q_2(P,P_1 P_2)$, which represents the

probability that an activated sensitive spot at P

causes, after development, both P_1 and P_2 to be covered,

we find for a uniform exposure:

$$\langle T(P_1)T(P_2)\rangle \;=\; \langle T\rangle^2 10^{D_u(E)} \frac{\bar{Q}_2(P_1 P_2)}{\bar{Q}_1} \tag{5}$$

in which

$$\bar{Q}_2(P_1 P_2) \;=\; \iint Q_2(P,P_1,P_2)\;(dxdy)_P$$

Note that, if P_1 and P_2 coincide, $Q_2(P,P_1,P_1) = Q_1(P,P_1)$,

so that $\bar{Q}_2(P_1,P_1) = \bar{Q}_1$, whence

$$\langle T(P_1)T(P_1)\rangle \;=\; \langle T\rangle^2 10^{D_u(E)} \;=\; \langle T\rangle$$

which is correct because the local film transmission is

always either zero or one.

Equation (5) can be used to evaluate the Selwyn

granularity. For a scanning aperture specified by the

transmission function $s(x,y)$, normalized such that

$$\iint s(x,y)\,dxdy = 1$$

we find for the mean square observed transmission fluctuation:

$$\sigma_T^2 = \iint \langle T(P_1)T(P_2) \rangle \, \varphi_{ss}(x,y) \, dxdy,$$

where x and y are the components of the line segment connecting P_1 with P_2, and

$$\varphi_{ss}(x,y) = \iint s(\xi,\eta)\,s(x+\xi,y+\eta)\,d\xi d\eta .$$

(See: E. L. O'Neill, Introduction to Statistical Optics, Ch. 7, Addison Wesley, Reading, Massachusetts, 1963).

For a large scanning aperture with area A this leads to:

$$\sigma_T^2 = \langle T \rangle^2 \, \frac{1}{A} \iint dxdy \left[10^{D_u(E)\frac{\bar{Q}_2(x,y)}{\bar{Q}_1}} - 1 \right] \qquad (6)$$

This equation shows in a comprehensive manner the relation between the Selwyn granularity and the grain statistics.

SECRET

APPENDIX III

SECRET

Some Speculative Remarks Concerning the Statistical

Properties of Photographic Grain
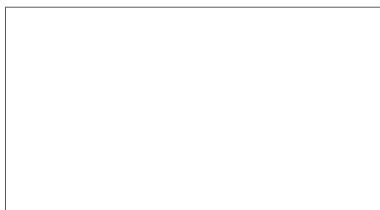
25X1

December 1965

25X1

Some Speculative Remarks Concerning the Statistical
Properties of Photographic Grain

Consider a whole ensemble of photographic plates of area A (assumed much larger than the average grain size) all of which possess the same statistical character and all of which were subject to the same (statistically speaking) photon rain. Moreover each member of the ensemble was subject to the same development process. Let us further consider setting up a Cartesian coordinate system on each member of the ensemble and recording the point transmission (0 or 1) at the same point (x y) on each. Finally we read the fraction out of the total for which we read $T(x\ y) = 1$ and denote this as the mean transmission $T(x\ y)$.

We now return to a typical member of this ensemble and calculate the expectation value of the transmission $T(x, y)$. If originally (that is, before development) the grain centers were distributed with a density $c_0 = \dfrac{N_G}{A}$ then in an area $\Delta S_i = \Delta x_i \cdot \Delta y_i$ we would expect to find $\overline{n_i} = d_0\,\Delta S_i$ grain centers. If we denote by P_{i_D} the probability* that a grain of any size whose center lies in ΔS_i has been rendered developable, then after exposure and development we would expect to find $\overline{m_i} = \overline{n_i}\,P_{i_D} = d\,\Delta S_i$ developed grain centers in ΔS_i, where $d = d_0\,P_{iD}$ is the new

*We shall soon attempt to calculate this.

SECRET

population density of grain centers.

Consider now Fig. 1.0. The probability that in
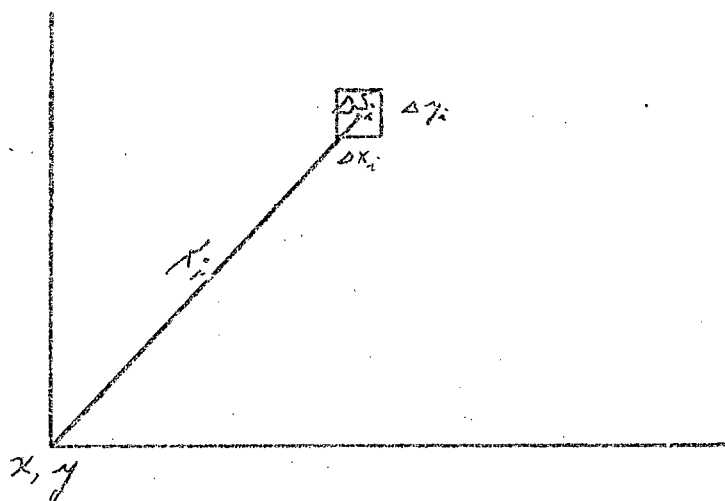
Fig. 1.0

ΔS_i we would find exactly m_i grain centers is given by the Bernoulli distribution

$$\text{1.)} \qquad P(m_i) = \frac{n_i!}{m_i!(n_i - m_i)!} \, P_{i_D}^{m_i} \left(1 - P_{i_D}\right)^{n_i - m_i}$$

with a mean and variance given by

$$\text{2.)} \qquad \overline{m_i} = n_i \, P_{i_D}$$

and

$$\sigma_{m_i}^2 = n_i \, P_{i_D} \left(1 - P_{i_D}\right)$$

Now if P_{i_D} is small and n_i large so that * $\overline{m_i}$ remains finite, then the Bernoulli distribution passes over to the Poisson distribution in the form

$$3.) \qquad P(m_i) = \frac{\overline{m_i}^{m_i}\, e^{-\overline{m_i}}}{m_i!}$$

with a mean and variance given by

$$4.) \qquad \overline{m_i} = d_0\, \Delta S_i\, \frac{P_i}{b}$$

and

$$\sigma_{m_i}^{2} = \overline{m_i}$$

Let us now describe the size of the grains (assumed circular here) through the distribution law $\rho(r_i) = Prob\,(r < r_i)$ We are now in a position to calculate $\overline{T}(x,y)$. With reference to Fig. 1.0 we now wish to calculate the probability that the element ΔS_i contains no grain centers $^{(1,2)}$ which extend to cover the point (x,y). We will denote this by P_i. It can come about a number of ways. Either ΔS_i contains no developed grain center or contains one which does not extend to $(x_1 y)$ or contains two, neither of which extends to $(x_1 y)$ etc., etc. In short we may write

$$5.) \qquad P_i = P(0) + P(1)\,\rho(r_i) + P(2)\,\rho^2(r_i) + \cdots P(m_i)\,\rho^{m_i}(r_i)$$

*This is a ticklish question. In the case where the assumptions cannot be made, see Appendix I.

-5-

Now inserting equ. 3 into equ. 5 we have

$$6.) \quad \bar{P}_i = e^{-\bar{m}_i} \sum_{m_i=0}^{\infty} \frac{[\bar{m}_i \, p(r_i)]^{m_i}}{m_i!} = e^{-\bar{m}_i[1 - p(r_i)]}$$

Recalling that $\bar{m}_i = d_0 \, P_{i_D} \Delta S_i$, we now conclude that the probability that (x, y) remains uncovered is the product of the probabilities that each cell ΔS_i does not contribute a grain center that extends to (x, y) so that we can write

$$7.) \quad \bar{T}(x,y) = \prod_i \bar{P}_i = e^{-d_0 \sum_i P_{i_D}[1 - p(r_i)] \Delta S_i}$$

Finally we recall that the macroscopic photographic density and transmission are related through the equation

$$8.) \quad \bar{D} = \log_{10} \frac{1}{\bar{T}}$$

Introducing $M = \log_{10} e$ we can invert equ. 8 to read

$$9.) \quad \bar{T} = e^{-\bar{D}/M}$$

We now compare equs. 7 and 9 and pass to the limit of infinitesimal cells ($\Delta S_i \Rightarrow \partial S$) and write finally

$$10.) \quad \bar{D}(x,y) = M d_0 \iint P_D [1 - p(r)] \, \partial S$$

SECRET

Let us now turn to the problem of calculating P_b.
With reference to Fig. 2.0 we let a = area of an unexposed
but potentially developable grain, ϵa = photosensitive area of
a grain and $dn_a = N_G \, f(a) \, da$ = number of grains[3] with areas
in the interval a to a + da.
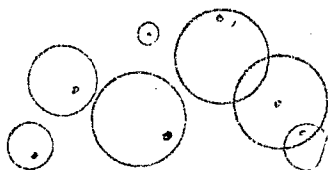
Fig. 2.0

Let us first consider the case of a uniform photon
rain of density $\frac{N_p}{A}$ over the plate. The probability of one
photon striking the photosensitive area of a grain of area
'a' is $\frac{\epsilon a}{A}$. For a rain of N, the probability that n strike
the photosensitive area is given by the Bernoulli distribution.

11.a)
$$P_N(n) = \frac{N!}{n!(N-n)!} \left(\frac{\epsilon a}{A}\right)^n \left(1 - \frac{\epsilon a}{A}\right)^{N-n}$$

with a mean and variance given by

11 b)
$$\overline{n} = p N = \frac{\epsilon a N}{A}$$

$$\sigma_n^2 = p q N = \frac{\epsilon a}{A}\left(1 - \frac{\epsilon a}{A}\right) N$$

Once again, if $\rho = \frac{\epsilon a}{A}$ is small and N large such that $\bar{n}$ is finite then this passes over to the Poisson distribution

$$12.) \qquad P_a(n) = \frac{\bar{n}^n e^{-\bar{n}}}{n!}$$

with a mean and variance given by

$$13.) \qquad \bar{n} = \frac{\epsilon a}{A} N$$

$$\text{and} \qquad \sigma_n^2 = \bar{n}$$

If now a grain of area 'a' requires n_1 quanta to render it developable then the probability that such a grain is struck by at least n_1 quanta is

$$14.) \qquad P_D(a) = \sum_{n=n_1}^{\infty} P_a(n) = 1 - \sum_{n=0}^{n-1} P_a(n)$$

and this is also equal to the ratio of the number of grains of size 'a' rendered developable to the total number of grains of size 'a'. Summing up over all grain sizes we have

$$15.) \qquad P_D = \frac{(N_G)_D}{N_G} = \int_0^{a_0} f(a)\, P_D(a)\, da$$

Now combining equs. 10, 14 and 15 we can write

16.) $$\bar{D} = M d_0 \iint P_b \left[1 - \rho(r) \right] \, dS$$

where $$P_b = 1 - \sum_{n=0}^{n_t - 1} \int_0^\infty \left(\frac{\bar{m}^n e^{-\bar{m}}}{n!} \right) f(a) \, da$$

and $$\bar{m} = \frac{\varepsilon a N}{A}$$

which can easily be transferred into a relationship between $\bar{D}$ and exposure $E = I\,T$ through the relations

17.) $$E = I\,T = \frac{N \hbar \omega T}{A}$$

so that the incident photon density can be written as

18.) $$\frac{N}{A} = \frac{E}{\hbar \omega T}$$

Let us now see if there is a grain of truth to these conjectures by examining some special (simplified) cases.

First we will assume that all grains have the same radius
R so that $f(a) = \delta(a-\bar{a}$ with $\bar{a} = \pi R^2$ and $[1-p(r)]$ is 1 for
$r \leq R$ and 0 for $r > R$. We wish now under these simplified
conditions to investigate some well known photographic
effects.

A.) $\bar{D}$ vs. $\angle_{og} E$

If the incident intensity is uniform over the
plate A, then we will choose to integrate on annular
rings (see Fig. 1.0) surrounding (x, y) and the integral
in equ. 10 becomes

19.)
$$\bar{D} = Md_0 \left[\int_0^{2\pi} d\theta \int_0^R [1-p(r)] r \, dr \right] P_b$$
$$= Md_0 \pi R^2 P_b = Md_0 \bar{a} P_b$$

where once more

$$P_b = 1 - \sum_{m=0}^{m-1} \frac{\bar{m}^m e^{-\bar{m}}}{m!}$$

with
$$\bar{m} = \frac{\epsilon \bar{a} N}{A}$$

It is instructive first to note that the maximum
density $\bar{D}_m$ occurs when $\frac{N}{A} \to \infty$ so that we can write

20.)
$$\frac{\bar{D}}{\bar{D}_m} = P_b = 1 - \sum_{m=0}^{m-1} \frac{\bar{m}^m e^{-\bar{m}}}{m!}$$

with now
$$\bar{D}_m = Md_0 \bar{a} = \frac{MN_b \bar{a}}{A}$$

corresponding to a minimum transmission $\bar{T}_m$ given by

21.)
$$\bar{T}_m = e^{-\frac{\bar{D}_x}{M}} = e^{-\frac{N_0\,\bar{a}}{A}}$$

which is just what we should expect if we consider a model
of of dropping black circles at random on a white background.
At first, with little overlapping the ratio of clear to
total area should decrease linearly and then as the popula-
tion density increases, the mean transmission should
asymptotically approach zero. . In fact the photographic
relation $\bar{D} = \log_{10}\frac{1}{\bar{T}}$ means physically that the photographic
density $\bar{D}$ and the population density of blackened grains
are simply related through the equation $\bar{D} = M d\,\bar{a}$.

Furthermore, since equ. 20 actually represents the
H & D curve, we can now interpret that curve to represent
the fraction (at a given exposure) of grains that are rendered
developable to those that could have been rendered developable
under infinite exposure.

Let us now look at equ. 20 a little more closely.
It turns out to be convenient to define an "effective exposure"
$$\mathcal{E}' = \bar{m} = \frac{\epsilon\,\bar{a}\,N}{A} = \left(\frac{\epsilon\,\bar{a}}{4\,\omega T}\right)\mathcal{E}$$
so that depending on how many quant : (n_1) are needed to render

ā developable we can write

$$\frac{\bar{D}}{\bar{D}_m} = 1 - e^{-\mathcal{E}'} \qquad m_1 = 1$$

22.)

$$= 1 - e^{-\mathcal{E}'}(1+\mathcal{E}') \qquad m_1 = 2$$

$$= 1 - e^{-\mathcal{E}'}\left(1+\mathcal{E}'+\frac{\mathcal{E}'^2}{2}\right) \qquad m_1 = 3$$

etc.

In Fig. 3.0 we show plots of $\bar{D}/\bar{D}_m$ vs. $\log_{10}\mathcal{E}'$ for $1 \leq m_1 \leq 4$. It is quite clear that there must be some truth to the model being considered here in that the gross features seem to agree with experimentally determined H & D curves. Of course one could not expect agreement in the fine details with all the simplications that have been assumed. Nevertheless, one might be able to come arbitraily close to the real curves by including size distribution curves and distribution functions for the photosensitive areas of the grains. Moreover, by assuming a more-than-one photon process together with a critical arrival time between photon arrivals it may very well be possible to predict the anomaly known as reciprocity failure. But these are subtler points that we leave for a later time. Instead, we turn now to a topic closely related to the determination of the H & D curve.

B.) Edge Gradients for Photographic Film

With reference to Fig. 4.0 let us now evaluate the integral in equ. 10 for the case where the incident intensity undergoes an abrupt discontinuity along $x = 0$, having a density $d_2 = N_2/A$ for $x < 0$ and $d_1 = N_1/A$ for $x > 0$. Once again assuming grains of equal size we can break up the region of integration into two parts and write

23.)
$$\bar{D}(x) = M d_0 \iint_{D_1} P_{D_1} [1 - p(r)] \, dS_1 + M d_0 \iint P_{D_2} [1 - p(r)] \, dS_2$$

where again
$$P_{D_j} = 1 - \sum_{m=0}^{m_j - 1} \frac{\bar{m}_j e^{-\bar{m}_j}}{m_j!}$$

with
$$\bar{m}_j = \frac{\epsilon \bar{a} N_j}{A} \qquad ; \quad j = L^2$$

Now since P_{D_j} is constant over each region dS_j we can pull it outside the integral and write for the population density of the developed grains

Let us now carry out the integrations. In the region $x > 0$ we can integrate first over the full circles up to $r = x$ then over the frustrated annular rings, being careful not to invade the region $x < 0$. That is, in
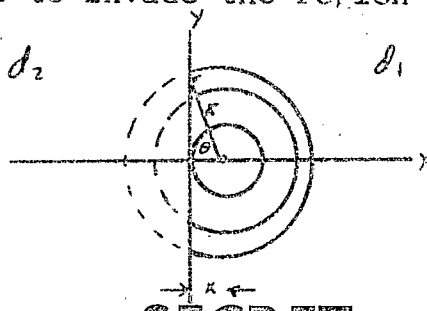
Fig 4.0

the region $x > 0$ we have

$$24.) \quad I_1 = \iint [\pi - \rho_{(r)}]\, dS_1 = \int_0^{2\pi} d\theta \int_0^x [\pi - \rho_{(r)}]\, r\, dr + 2\int_{\cos^{-1}\frac{x}{r}}^{\pi} d\theta \int_x^{\infty} [\pi - \rho_{(r)}]\, r\, dr$$

while in the region $x < 0$ we have

$$25.) \quad I_2 = 2\int_0^{\cos^{-1} x/r} d\theta \int_x^{\infty} [\pi - \rho_{(r)}]\, r\, dr$$

If we now insert the condition* that all the grains
have the same size (see Fig. 5.0)

Fig. 5.0

then we have for $x < R$

$$26.) \quad I_1 = \pi x^2 + \pi (R^2 - x^2) - 2\int_x^R \cos^{-1}\frac{x}{r}\, r\, dr$$

Making a slight change of variable to $u = R/r$; the integral
is easily evaluated and we have

*Note that this is for convenience in carrying out the
integration. In principle we could continue to include
the grain size distribution beyond this point.

-14-

27.) $$I_1 = \pi R^2 - \frac{\pi R^2}{2} \, c\ell(x/R)$$

where

$$c\ell\left(\frac{x}{R}\right) = \frac{2}{\pi}\left[\cos^{-1}\frac{x}{R} - \frac{x}{R}\sqrt{1-\left(\frac{x}{R}\right)^2}\right]$$
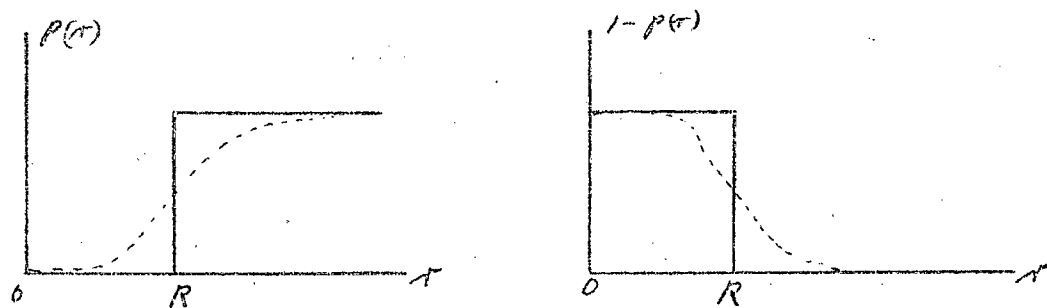
is the normalized convolution of a single grain with itself.

Proceeding along similar lines we have in the region $x < 0$

28.) $$I_2 = 2\int_x^R \cos^{-1}\left(\frac{x}{r}\right) r \, dr$$

$$= \frac{\pi R^2}{2} \, c\ell\left(\frac{x}{R}\right)$$

For $x > R$; $[1 - \rho(r)] = 0$ so that $I_1 = I_2 = 0$. Denoting by $\bar{D}_1 = M\bar{a}\, d_1$ and $\bar{D}_2 = M\bar{a}\, d_2$ the density on either side of the edge far from the discontinuity we can combine equs. 28, 27 and 23 to yield finally for the average density across an edge

29.) $$\bar{D}(x) = \bar{D}_2 \qquad\qquad x < -R$$

$$= \bar{D}_1 + \left(\frac{\bar{D}_2 - \bar{D}_1}{2}\right) c\ell\left(\frac{x}{R}\right) \qquad -R \le x \le R$$

$$= \bar{D}_1 \qquad\qquad x > R$$

The mean transmission across the edge of course is now given by

30.) $$\bar{T}(x) = e^{-\frac{\bar{D}(x)}{M}}$$

where in both equations

31.)

$$\bar{D}_i = M \bar{\sigma} \, d_j$$

$$d_j = d_0 \, P_{D_j} = d_0 \left[1 - \sum_{n=0}^{m_j-1} \frac{\overline{m_j}^{n_j} \, e^{-\overline{m_j}}}{m_j!} \right]$$

$$\overline{m_j} = \frac{\epsilon \bar{a} N_j}{A} \qquad j = 1, 2$$

Curves illustrating the transition across the edge in density and transmission are shown in Fig. 6.0 in several representative cases. It goes without saying, of course, that the derivative of this function yields directly the spread function or Green's function for the film. For the simple case treated here this amounts to each point being uniformly spread over the area of a single grain, but in the more general case this approach illustrates the role played by grain size distribution itself [$1 - \rho(\tau)$] in causing diffusion.

Fig. 6.0

-10-

C.) Fluctuations in D and T across an edge.

In addition to $\bar{T}$ and $\hat{D}$ one would also like to know σ_T and σ_D, the fluctuation from the mean across an edge. One round about way to determine this is to note that the auto-correlation in transmission defined as

32.) $$C(\xi,\eta) = T(x,y)\, T(x-\xi, y-\eta)$$

yields $\overline{T^2}$ directly when evaluated at the origin. From the relation

33.) $$\sigma_T^2 = \overline{(T - \bar{T})^2} = \overline{T^2} - (\bar{T})^2$$

one could then find σ_T. If we agree to consider equ. 32 in terms of an ensemble average in the form

34.) $$\overline{T_1 T_2} = \iint T_1\, T_2\, \rho(T_1, T_2; \rho)\, dT_1\, dT_2$$

then since the point by point transmission can only assume the values 0 or 1, only one of the four possible products of $T_1\, T_2$ will contribute; when they are both unity. Therefore the correlation function reduces to the problem of

finding the probability that both $T(x,y)$ and $T(x-\xi, y-\eta)$ are not covered by developed grains. This suggests the geometry shown in Fig. 7.0.
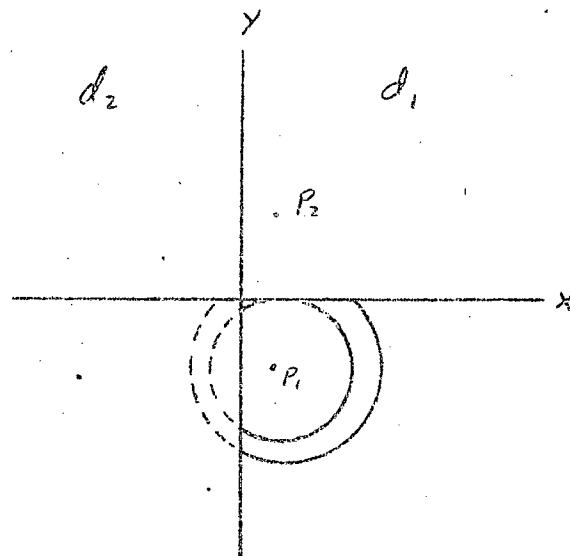
Fig. 7.0

With different densities on each side of the boundary $x = 0$, we surround $P_1(x, -y)$ with annular rings that never extend beyond the barrier $y = 0$. For then cells ΔS_x which contain grain centers that do not reach P_1, will similarly not contain grains that extend to P_2. The integration is straight-forward and might actually be interesting to do someday to calculate the correlation function. However, since we are interested here only in the variance there is a simpler way.

Consider the point by point transmission. It assumes the values either 0 or 1; therefore point by point $T^2 = T$. As a result we can write directly

35.)
$$\sigma_T{}^2 = \overline{T^2} - \overline{T}^2 = \overline{T}\left(1 - \overline{T}\right)$$

or
$$\sigma_T = \pm \sqrt{\overline{T\left(1 - \overline{T}\right)}}$$

And so, about an edge, we can now surround $\overline{T}(x)$ with envelopes $\overline{T} \pm \alpha\, \sigma_T$ within which we can be assured that $\overline{T}(x)$ lies with a level of confidence dictated by the parameter α. This becomes particularly significant, as W. Brouwer has already pointed out, when the incident intensity represents a sequence of edges. From the ratio of σ_T to $\overline{\Delta T}$ one can then predict resolution vs. density curves.

Finally we should like to relate the fluctuations in transmission to the fluctuations in density. Consider

36.)
$$\Delta D = D - \overline{D} = -\log_{10}\left(1 + \frac{(T - \overline{T})}{\overline{T}}\right)$$

$$= -\log_{10}\left(1 + \frac{\Delta T}{\overline{T}}\right)$$

$$= -0.4343\left[\frac{\Delta T}{\overline{T}} - \frac{1}{2}\left(\frac{\Delta T}{\overline{T}}\right)^2 + \frac{1}{3}\left(\frac{\Delta T}{\overline{T}}\right)^3 + \cdots\right]$$

Now if $\frac{\Delta T}{T} \ll 1$ then we can write

37.)
$$\sigma_D = \sqrt{(\Delta D)^2} \cong \frac{0.4343 \; \sigma_T}{T}$$

otherwise we must equ. 36.

So much for the statistical description of the fluctuations on the film. To see how these fluctuations vary with scanning aperture size (e.g. with visual inspection or scanning with a microdensitometer), see ref α

All of this, of course, is speculative at this time and awaits the ultimate test; numerical agreement with experiments.

Appendix I

In passing from equ. 1 to equ. 3 it was assumed that the conditions for a Poisson process were satisfied. If this turns out not to be the case, there is still some hope. Suppose later in the text that we substitute not equ. 3 but rather equ. 1 into equ. 5, then we would have

$$I.1 \qquad P_i = \sum_{m_i=0}^{m_i} \frac{m_i!}{m_i!(m_i-m_i)!} \left[\frac{P_i}{b} \, p(\tau_i) \right]^{m_i} \left(1 - \frac{P_i}{b} \right)^{m_i-m_i}$$

which represents the binomial expansion of

$$I.2 \qquad P_i = \left\{ 1 - \frac{P_i}{b} \left[1 - p(\tau_i) \right] \right\}^{m_i}$$

We can check this right away, for if $\frac{P_i}{b}$ is small, m_i large but $\overline{m_i} = m_i \frac{P_i}{b}$ finite this equation becomes

$$I.3 \qquad P_i \cong e^{-\overline{m_i}\left[1 - p(\tau_i) \right]}$$

agreeing with equ. 6. Let us however return to equ. I.2 and now take the product over all cells for the mean transmission

Declassified in Part - Sanitized Copy Approved for Release 2012/11/01 : CIA-RDP79B00873A000100010159-8

in the form

$$I.4 \qquad \bar{T}(x,y) = \prod_i P_i = \prod_i \left\{ 1 - P_D \left[1 - \rho(\tau_i) \right] \right\}^{n_i}$$

Now taking $\bar{D} = \log_{10} \frac{1}{\bar{T}}$ we have

$$I.5 \qquad \bar{D} = -M \sum_i n_i \log_e \left\{ 1 - P_D \left[1 - \rho(\tau_i) \right] \right\}$$

Once again we recall the relation $n_i = d_0 \, \Delta S_i$ and pass to the limit in the form

$$I.6 \qquad \bar{D} = -M d_0 \iint \log_e \left\{ 1 - P_D \left[1 - \rho(\tau) \right] \right\} dS$$

Again we can check this result by expanding to the first term in the series which yields

$$I.7 \qquad \bar{D} \cong M d_0 \iint P_D \left[1 - \rho(\tau) \right] dS$$

agreeing with equ. 16 in the main text. In the general case, however, we can expand I.6 in a series and write

$$I.8 \qquad \bar{D} = M d_0 \sum_{n=1}^{\infty} \frac{1}{n} \iint \left\{ P_D \left[1 - \rho(\tau) \right] \right\}^n dS$$

but for equal sized grains $\left[1 - \rho(\tau) \right]^n = \left[1 - \rho(\tau) \right]$ and we have

$$I.9 \qquad \bar{D} = M d_0 \bar{a} \sum_{n=1}^{\infty} \frac{P_D^n}{n}$$

$$= - M d_0 \bar{a} \log_e (1 - P_D)$$

Declassified in Part - Sanitized Copy Approved for Release 2012/11/01 : CIA-RDP79B00873A000100010159-8

References

1. Picinbono, B., Comptes Rendus $\underline{240}$ 2206 (1955)

2. O'Neill, E. L., Introduction to Statistical Optics, Addison Wesley, (1963)

3. Silberstein, L. and Trivelli, A.P.H., S.O.S.A. $\underline{28}$ 441 (1938)

4. Fry, T.C., Probability and its Engineering Uses, D. VanNostrand (1928)

Page Denied